Aus der Klinik und Poliklinik für Strahlentherapie und Radioonkologie
der Ludwig-Maximilians-Universität München
Direktor: Prof. Dr. med. Claus Belka

Immune-stimulatory effects induced by radiotherapy of breast cancer

Dissertation
zum Erwerb des Doktorgrades der Naturwissenschaften
an der Medizinischen Fakultät
der Ludwig-Maximilians-Universität München

vorgelegt von
Roman Hennel

aus Dachau

2016

Mit Genehmigung der Medizinischen Fakultät

der Ludwig-Maximilians-Universität München

Betreuerin: Prof. Dr. rer. nat. Kirsten Lauber

Zweitgutachter: Prof. Dr. rer. nat. Horst Zitzelsberger

Dekan: Prof. Dr. med. dent. Reinhard Hickel

Tag der mündlichen Prüfung: 02.12.2016

Für meine Familie

Table of contents

1 Abbreviations

A	Ampere
AM	Acetoxymethylester
AnxV	Annexin V
APC	Allophycocyanin or antigen-presenting cell
APC-Cy7	Allophycocyanin-cyanine 7
APS	Ammonium persulfate
Arm Ham	Armenian hamster
ATCC	American Type Culture Collection
ATP	Adenosine triphosphate
BRCA1	Breast cancer 1
BSA	Bovine serum albumin
BUV395	BD Horizon Brilliant™ Ultraviolet 395
C12-FDG	5-dodecanoylaminofluorescein-di-β-D-galactopyranoside
CD	Cluster of differentiation
CFSE	Carboxyfluorescein succinimidyl ester
cGAMP	Cyclic guanosine monophosphate-adenosine monophosphate
cGas	Cyclic GMP-AMP synthase
CTL	Cytotoxic T lymphocyte
CTLA-4	Cytotoxic T-lymphocyte-associated protein-4
δ-ALAS	δ-aminolevulinic acid synthase
Da	Dalton
DAMP	Damage-associated molecular pattern
ddH$_2$O	Double distilled water
dNTP	Deoxynucleoside triphosphate
EDTA	Ethylenediaminetetraacetic acid
e.g.	For example
EGF	Epidermal growth factor
Egr-1	Early growth response protein 1
EGTA	Ethyleneglycoltetraacetic acid
ELISA	Enzyme-linked immunosorbent assay
ER	Estrogen receptor α
ESL1	E-selectin ligand 1
T:E	Target to effector ratio
FCS	Fetal calf serum
FITC	Fluorescein isothiocyanate

FSC	Forward scatter
g	Gram or gravitational acceleration
GM-CSF	Granulocyte-macrophage colony-stimulating factor
Gy	Gray
h	Hour
HEPES	4-(2-hydroxyethyl)-1-piperazineethanesulfonic acid
Her2/neu	Human epidermal growth factor receptor 2
HRP	Horse radish peroxidase
HSP	Heat shock protein
HUVEC	Human umbilical vein endothelial cell
ICAM-1/-2	Intercellular adhesion molecule 1/2
i.e.	That is
IFN	Interferon
IGEPAL CA-630	Octylphenoxypolyethoxyethanol
IgG	Immunoglobulin G
IgM	Immunoglobulin M
IL	Interleukin
IORT	Intraoperative radiotherapy
IRF3	Interferon regulatory factor 3
l	Liter
k	Kilo (10^3)
LFA-1	Lymphocyte function-associated antigen 1
LPS	Lipopolysaccharides
m	Milli (10^{-3}) or meter
µ	Micro (10^{-6})
M	Molar (mol/l)
Mac-1	Macrophage receptor 1
MCP	Monocyte chemotactic protein
MDSC	Myeloid-derived suppressor cell
MHC	Major histocompatibility complex
MIF	Macrophage migration inhibitory factor
min	Minute
MOMP	Mitochondrial outer membrane potential
M_w	Molecular weight
n	Nano (10^{-9})
n.d.	Not detected

NKC	Natural killer cell
Nlrp3	NOD-like receptor family pyrin domain containing-3 protein
NOD-like	Nucleotide-binding oligomerization domain-like
p	Piko (10^{-12})
PAMP	Pathogen-associated molecular pattern
PARP	Poly(ADP-ribose)polymerase
PBMC	Peripheral blood mononuclear cell
PBS	Phosphate-buffered saline
PCR	Polymerase chain reaction
PD1	Programmed cell death receptor 1
PDL-1	Programmed death ligand 1
PE	Phycoerythrin
PECAM-1	Platelet endothelial cell adhesion molecule 1
PE-Cy5/7	Phycoerythrin-cyanine 5/7
PerCP-Cy5.5	Peridinin-chlorophyll-cyanine 5.5
PI	Propidium iodide
PP	Polypropylene
PR	Progesterone receptor
PRR	Pattern recognition receptor
PS	Phosphatidylserine
PSGL1	P-selectin glycoprotein ligand 1
PVDF	Polyvinylidene difluoride
RAGE	Receptor for advanced glycation endproducts
RIPK1	Receptor-interacting protein kinase 1
rpm	Rotations per minute
s	Second
SA-β-gal	Senescence-associated β-galactosidase
SASP	Senescence-associated secretory phenotype
SDS-PAGE	Sodium dodecyl sulfate polyacrylamide gel electrophoresis
SSC	Sideward scatter
SDF-1α	Stromal cell-derived factor 1α
STING	Stimulator of interferon genes
TAM	Tumor-associated macrophage
TBS	Tris-buffered saline
TEMED	Tetramethylethylenediamine
TGF-β	Transforming growth factor β

TLR	Toll-like receptor
TNF	Tumor necrosis factor
U	Unit
UTP	Uridine triphosphate
V	Volt
VCAM-1	Vascular cell adhesion molecule 1
VLA-4	Very late antigen 4
vs.	versus
yFMI	Forward migration index in y-direction
zVAD-fmk	Carbobenzoxy-valyl-alanyl-aspartyl-[O-methyl]-fluoromethylketone

2 Zusammenfassung

Neben Chirurgie und Chemotherapie ist die Strahlentherapie ein zentraler Bestandteil bei der Behandlung von Brustkrebs. Brustkrebs-Patientinnen werden klassischer Weise adjuvant fraktioniert bestrahlt, d.h. mit täglichen Dosen zwischen 1,8 und 2 Gy bis zu einer Gesamtdosis von 50-60 Gy nach brusterhaltender Operation. Aktuell sind hypofraktionierte Schemata mit täglich 2,66 Gy und mehr auf dem Vormarsch und in einigen Ländern bereits Standard. Zusätzlich zur fraktionierten Bestrahlung werden auch ablative Ansätze, z.B. in Form einer intra-operativen Bestrahlung (IORT), angeboten. Hierbei wird direkt nach der chirurgischen Resektion eine hohe Einzeldosis von bis zu 20 Gy in das ehemalige Tumorbett appliziert. Die Wirkung der Strahlentherapie beruht im Wesentlichen auf der Induktion von Tumorzelltod durch irreparable Schädigung der DNA. Es gibt jedoch zunehmend Hinweise für einen relevanten Beitrag des Immunsystems zum strahlentherapeutischen Erfolg. In verschiedenen Mausmodellen konnte gezeigt werden, dass vor allem ablative Bestrahlungsschemata in der Lage sind, adaptive Immunmechanismen nicht nur gegen den lokal bestrahlten Tumor, sondern auch gegen Fernmetastasen außerhalb des Bestrahlungsfeldes (sog. abskopale Effekte), auszulösen. Die genauen Mechanismen, die diesen immunologischen Vorgängen zu Grunde liegen, sind nur rudimentär verstanden. Vor allem die Eigenheiten verschiedener Bestrahlungsschemata im Hinblick auf die Induktion systemischer Anti-Tumor-Immunantworten konnten bisher nur unvollständig geklärt werden. Allerdings scheint die durch die unterschiedlichen Bestrahlungsregime hervorgerufene Art des Tumorzelltods eine entscheidende Rolle zu spielen. Um diese Hypothese zu überprüfen, wurden in der vorliegenden Dissertation verschiedene Brustkrebszelllinien verschiedenen Bestrahlungsschemata unterzogen und die daraus resultierenden immunologischen Effekte untersucht. Es konnte gezeigt werden, dass ablative Bestrahlung besser als jedes andere der getesteten Regimes sehr stark primäre Nekrose auslöst, insbesondere in schnell proliferierenden, tripel-negativen Brustkrebs-Zelllinien. Diese nekrotischen Brustkrebszellen setzen in der Folge Attraktionssignale frei, die in vitro Transwell-Migration und ungerichtete Chemokinese von Monozyten stimulierten. In vivo wurde die ungerichtete Chemokinese in gerichtete Leukozyten-Rekrutierung umgewandelt. Zentrale Vermittler in diesem Zusammenhang scheinen Endothelzellen zu sein, die

nach Exposition mit Überständen bestrahlter Brustkrebszellen stark aktiviert wurden. Die Endothelzell-Aktivierung war gekennzeichnet durch eine gesteigerte Expression von Adhäsionsmolekülen auf der Endotheloberfläche sowie durch die Freisetzung von Zytokinen und Chemokinen. Bemerkenswerterweise war das Endothelzell-mRNA-Profil von Adhäsionsmolekülen und pro-inflammatorischen Zytokinen nach Inkubation mit Überständen ablativ bestrahlter Brustkrebszellen einzigartig und unterschied sich klar von den Profilen, die mit anderen Bestrahlungsschemata beobachtet wurden. Für die beschriebenen Effekte auf Endothelzellen waren proteinartige Gefahrensignale (DAMPs) von sterbenden Brustkrebszellen verantwortlich. Des Weiteren waren diese Protein-DAMPs dafür verantwortlich, dass die Differenzierung und Maturierung Antigen-präsentierender Zellen aus Peripherblut-Monozyten verbessert wurde, was sich durch eine verstärkte Expression ko-stimulatorischer Moleküle auf ihrer Oberfläche darstellte. Diese dendritischen Zellen waren dadurch signifikant besser in der Lage, die Proliferation von CD8^{+} T-Zellen zu stimulieren. Die beschriebenen immunologischen Vorgänge zeigten ein einheitlich wiederkehrendes Schema: Die stärksten Effekte wurden beobachtet, wenn Überstände ablativ bestrahlter Brustkrebszellen eingesetzt wurden. Tatsächlich wurden auch die höchsten Konzentrationen von Protein-DAMPs in den Überständen der ablativ bestrahlten Brustkrebszellen gefunden. Zusammenfassend lässt sich festhalten, dass vor allem eine ablative Bestrahlung von Brustkrebszellen und der dadurch ausgelöste immunogene Zelltod das Potential haben, systemische Anti-Tumor-Immunmechanismen auszulösen.

3   Abstract

Besides surgery and chemotherapy, radiotherapy is a central component of breast cancer therapy. Classically, the treatment comprises an adjuvant, fractionated radiation regimen, i.e. patients receive daily doses of 1.8-2 Gy up to a total dose of 50-60 Gy, after breast conserving surgery, but hypofractionated regimens of daily 2.66 Gy or more are being on the rise. In addition to fractionated radiotherapy, ablative settings are also clinically available, for instance during intra-operative radiotherapy (IORT). Here, high single doses of up to 20 Gy are applied into the former tumor bed directly after surgery. The main effect of radiotherapy is the induction of tumor cell death as a consequence of excessive DNA damage. However, accumulating evidence suggests a relevant contribution of the immune system to the radiotherapeutic success. In different mouse models, radiotherapy was shown to induce adaptive anti-tumor immune mechanisms (so-called abscopal effects) not only against the locally irradiated tumor but also against distant out-of-field metastases – particularly when applied in ablative settings. The mechanisms underlying these immunological effects remain poorly understood, and little is known about the characteristics of different irradiation regimens with regard to their potential to induce systemic anti-tumor immunity. Nevertheless, the quality of tumor cell death induced by different irradiation regimens appears to be of crucial importance in this scenario. To evaluate this hypothesis, a panel of breast cancer cell lines was subjected to different irradiation regimens, and the resulting immunological effects were investigated. Ablative irradiation induced primary necrosis more potently than all other irradiation regimens tested, and this was most obvious in fast-proliferating breast cancer cells. Necrotically dying breast cancer cells, in turn, released attraction signals, which stimulated trans-well migration and undirected chemokinesis of monocytic cells in vitro. Importantly, this undirected chemokinesis was converted into directional leukocyte recruitment in vivo. Key players in this regard appear to be endothelial cells, which were strongly activated upon exposure to releasates of irradiated breast cancer cells in vitro, thus expressing high levels of adhesion molecules on their surface and releasing various cytokines and chemokines. Notably, for supernatants of ablatively irradiated breast cancer cells, the endothelial mRNA profile of adhesion molecules and pro-inflammatory cytokines was unique and clearly distinct from the ones observed with other irradiation regimens. The effects on

endothelial cells were exerted by proteinaceous damage-associated molecular patterns (DAMPs) derived from dying breast cancer cells. Furthermore, dying breast cancer cell-derived protein DAMPs enforced differentiation and maturation of antigen-presenting cells from peripheral blood monocytes as characterized by elevated expression of co-stimulatory molecules. In consequence, the CD8$^+$ T cell-stimulating capacity of these dendritic cells was significantly increased. Consistently, the observed immunological processes revealed a recurring pattern: The strongest effects were obtained with supernatants of ablatively irradiated breast cancer cells, in which the highest concentrations of DAMPs were found. In summary, these results indicate that irradiation-induced immunogenic cell death of breast cancer cells has the potential to provoke systemic anti-tumor immune mechanisms – especially upon ablative irradiation.

4 Introduction

4.1 Immune-stimulatory effects of radiotherapy

In 1953, R.H. Mole was the first describing 'abscopal' effects of radiotherapy [1]. Abscopal (from Latin 'ab' and Greek 'scopus': 'away from target') effects are systemic bystander effects of local irradiation which do not only lead to regression of the irradiated tumor but also of distant metastases outside the radiation field. Ever since Mole's observations, an emerging number of case reports were published, observing abscopal effects in a variety of tumor types, including lymphoma, metastatic melanoma, and metastatic non-small cell lung cancer [2,3,4,5].

Seminal studies from Demaria et al. demonstrated that abscopal effects of radiotherapy derive from systemic anti-tumor immune responses [6]. These were pioneering findings, since according to the concept of tumor immuno-editing, clinically occurring tumors are the result of a selection process of neoplastic cells that have escaped from immune destruction [7] (Figure 1): During cancer development, transformed cells are recognized, attacked, and eliminated by the host's innate and adaptive immune system (elimination phase). However, ongoing pressure of the immune system may select tumor cells that survive the elimination phase. In the course of this this equilibrium phase, novel tumor cell subclones with acquired non-immunogenic phenotypes can emerge and contribute to increased resistance to immune attack. Due to immune cell exhaustion, the equilibrium phase finally transits into the escape phase, which is characterized by accumulation of suppressive immune cells, such as $CD4^+$ regulatory T cells (T_{regs}) and myeloid-derived suppressor cells (MDSCs), and the development of poorly immunogenic or even immune-inhibitory tumor cells, for instance by upregulation of the $CD8^+$ T cell-inhibitory ligand PDL-1 and downregulation of MHC class I molecules. At this stage, tumor cells have successfully evaded elimination by the immune system, resulting in uncontrolled expansion, finally manifesting in clinically detectable, progressively growing tumors.

In order to elicit systemic anti-tumor mechanisms, escaped tumor cells need to be unmasked for the host's immune system. In principle, radiotherapy appears to have the capacity to provoke such a change in tumor cell immunogenicity. Formenti and Demaria coined the concept that radiotherapy is a powerful means of in situ vaccination, because it reinforces the host's immune system against local tumors as well as distant – i.e. abscopal – metastases [8].
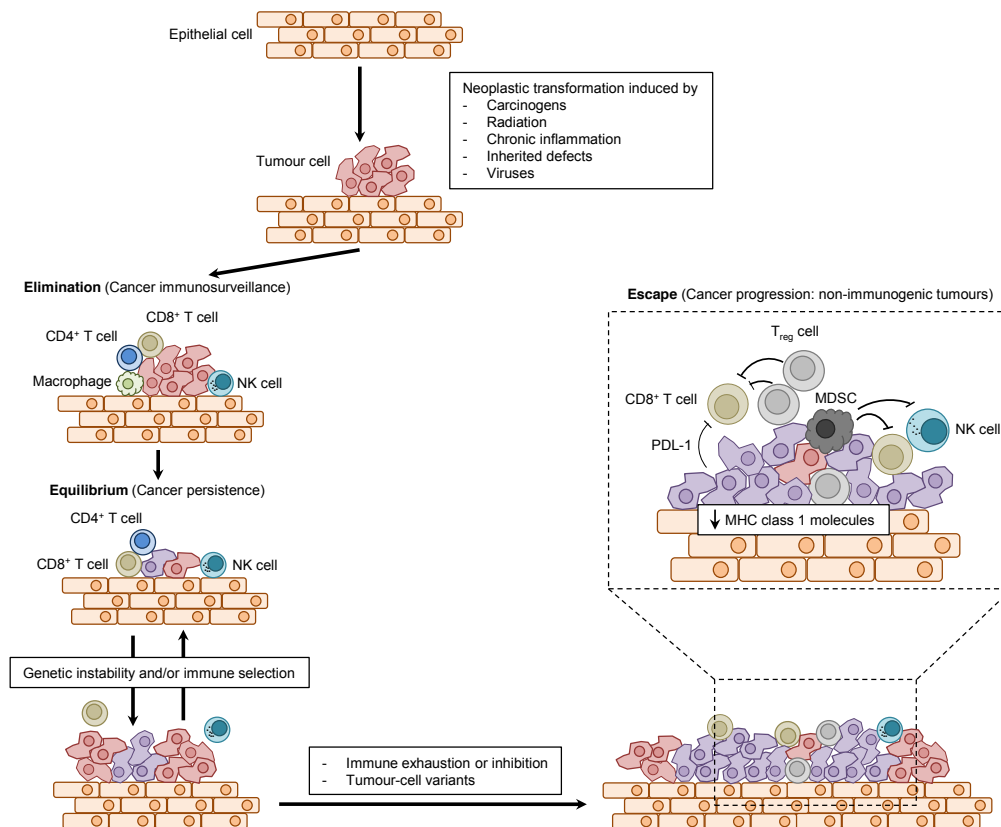
Figure 1 The process of tumor immuno-editing is a three-step process (adapted from [7]).

Tumor immuno-editing is divided into three phases: Elimination, equilibrium, and escape. The transformation of normal cells into tumor cells is induced by various stimuli. These include carcinogens, radiation, chronic inflammation, activation of proto-oncogens, and oncoviruses. Usually, transformed tumor cells are recognized and rapidly eliminated by cells of the innate and adaptive immune system, such as macrophages, NK cells, and effector CD4$^+$/CD8$^+$ T cells (elimination phase). Incomplete elimination of tumor cells results in equilibrium, where immune cells prevent the tumor from further expansion but at the same time are unable to remove the tumor entirely (equilibrium phase). In turn, tumor cell variants with immune-evasive and immune-suppressive features emerge, and the constant pressure of the immune system selects these aggressive, poorly immunogenic tumor cells. Tumor escape mechanisms include downregulation of MHC class I molecules and upregulation of the T cell-inhibiting molecule PDL-1. Furthermore, immune cell exhaustion supports the transition from the equilibrium phase to the tumor escape phase. Here, the immune system is no longer able to control the tumor cell variants. Distinct immune subpopulations are polarized into tumor-supporting cells (e.g. myeloid-derived suppressor cells). Finally, the escape phase results in progressively growing, clinically manifesting tumors. CD, cluster of differentiation; IFN, interferon; NKC, natural killer cell; MHC, major histocompatibility complex; MDSC, myeloid-derived suppressor cell; PD1, programmed cell death receptor 1; PDL-1, programmed death ligand 1; T$_{reg}$, regulatory T cell.

Since the first publication in 2004, several groups have strived to elucidate the mechanisms underlying radiation-induced anti-tumor immunity. On the basis of the corresponding observations, a model of an irradiation-induced cascade of type I (IFNα/β) and type II (IFNγ) interferons with the involvement of dendritic cells and CD8$^+$ T cells has been proposed (Figure 2).
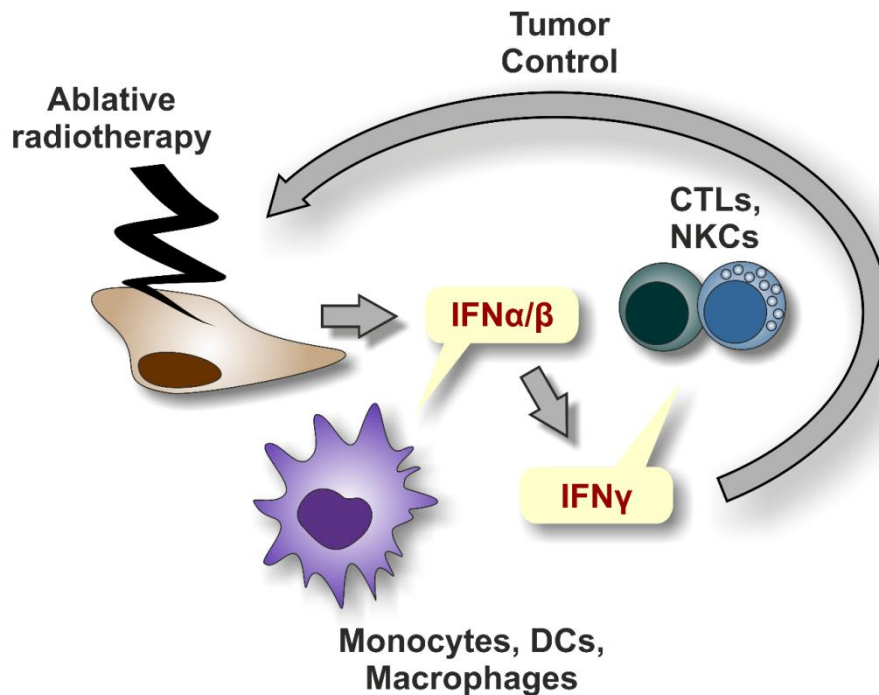
Figure 2 A cascade of type I and II interferons induced by ablative irradiation contributes to tumor control (adapted from [9]).

In different mouse models, it was shown that ablative irradiation of tumor cells leads to production of type I interferons (IFNα/β) from tumor-infiltrating monocytic cells, such as dendritic cells and macrophages. These type I interferons enhance cross-presentation of tumor-antigens by dendritic cells to CD8^{+} T cells in the lymph nodes. Upon activation, cytotoxic CD8^{+} T cells (and NK cells) produce IFNγ, which not only promotes anti-tumor functions of immune cells but also increases the immunogenicity of tumor cells, and inhibits tumor growth, finally resulting in local and systemic tumor control. CTL, cytotoxic T lymphocyte; DC, dendritic cell; IFN, interferon; NKC, natural killer cell.

In 2005, Lugade and colleagues could show that ablative radiation, i.e. one single dose of 15 Gy, of B16 murine melanomas induces the generation of tumor-specific, IFNγ-producing effector T cells and enhances their intra-tumoral accumulation [10]. The same group described later that IFNγ produced by anti-tumor effector T cells elevates the immunogenicity of irradiated tumor cells by enhancing MHC class I expression on melanoma cells and shaping the tumor's vasculature for leukocyte trafficking [11]. Moreover, the important role of IFNγ not only in increasing the immunogenicity of tumor cells but also for CD8^{+} T cell effector function after ablative radiation was confirmed by Gerber and colleagues [12]. Lee and colleagues highlighted the indispensability of CD8^{+} T cells for the control of the local tumor as well as distant, out-of-field (abscopal) metastases after ablative irradiation [13]. Another study of Burnette and colleagues revealed that, besides IFNγ, type I IFNs (IFNα/β) produced by tumor-infiltrating dendritic cells upon ablative radiation are crucial for the induction

of potent anti-tumor immune responses. They could show that type I IFNs strongly enhance the cross-priming activity of dendritic cells and CD8^{+} T cells in tumor-draining lymph nodes [14] via autocrine mechanisms [15]. In accordance, Diamond et al. and Fuertes et al. showed that type I IFNs have functions distinct from those of IFNγ in anti-tumor immunity: while IFNγ mainly enhances the immunogenicity of tumor cells themselves, type I IFNs elevate the immune-stimulatory effects of cells of the innate immune system [16] [17]. Moreover, it was recently shown that type I IFNs also support the intra-tumoral recruitment of effector CD8^{+} T cells by inducing chemokine release from intra-tumoral macrophages after ablative radiotherapy [18]. The mechanisms behind the production of type I IFNs by tumor-infiltrating dendritic cells upon radiation are currently still being investigated. So far, a pathway known from pathogen defense was brought into focus: Cytosolic sensing of tumor DNA by dendritic cells can lead to the production of cyclic guanosine monophosphate-adenosine monophosphate (cGAMP) by cyclic GMP-AMP synthase (cGAS). cGAMP acts as a second messenger, thereby activating the adaptor protein stimulator of interferon genes (STING), which in turn enables the production of type I IFNs by the transcription factor interferon regulatory factor 3 (IRF3) [19] [20]. Interestingly, in the context of anti-viral immunity, Ablasser and colleagues could show that cGAMP-producing cells are able to transfer cGAMP to neighboring cells, which activates STING-dependent production of type I IFNs, thus inducing 'bystander immunity' [21].

It should be noted that irradiation-induced anti-tumor immune responses seem to rely predominantly on dendritic cells and CD8^{+} T cells, while CD4^{+} T cells (and macrophages) appear to be dispensable – at least in certain settings [22]. However, the role of CD4^{+} T cells in anti-tumor immunity is dependent on the CD4^{+} T cell subset: CD4^{+} helper 1 T cells (T_{h1}) can augment the generation of anti-tumor CD8^{+} T cells after radiotherapy, and the ablation of intra-tumoral immune-suppressive CD4^{+} T_{regs} greatly enhances the immunogenicity of established tumors and improves the outcome of radiotherapy [14] [23] [24]. Furthermore, Filatenkov and colleagues showed that IFNγ-producing CD8^{+} T cells generated upon ablative irradiation do not only eliminate tumor cells but also intra-tumoral suppressor cells (e.g. MDSCs), thereby shifting the immune-suppressive tumor microenvironment into an immune-supportive one [25].

In addition, radiotherapy itself improves the immunogenicity of tumor cells, e.g. it increases MHC class I surface expression [26] and induces Fas-receptor upregulation

[27] on tumor cells, thus improving their recognition and elimination by cytotoxic CD8^{+} T cells.

Notably, most studies describing induction of anti-tumor immunity by radiotherapy were performed using ablative settings, i.e. single doses of 10 Gy and more. However, in clinical practice, the application of ablative irradiation is limited to accessible, small tumor volumes, whereas fractionated irradiation regimens, i.e. daily doses of approximately 2 Gy over several weeks, are most commonly applied [28] [29] [30]. Induction of anti-tumor immunity, as described above, is rarely seen when using fractionated radiation regimens [13] [25]. Only extremely hypofractionated settings, i.e. doses of 7.5 Gy in two fractions were also able to induce anti-tumor immunity [31]. The mechanisms behind the differences between ablative and fractionated irradiation in inducing adaptive anti-tumor immunity are poorly understood. A relevant cancer entity to investigate these mechanisms is breast cancer, because here fractionated, hypofractionated, and ablative regimens are used in parallel without hard-wired stratification markers at hand. Moreover, the infiltration of CD8^{+} T cells was shown to be predictive for the clinical outcome in breast cancer [32], emphasizing the clinical relevance of immunological studies in the context of breast cancer radiotherapy.

4.2 Epidemiology and treatment of breast cancer

Breast cancer is the most frequent cancer entity in women with about 70,000 new cases per year in Germany (according to the Robert Koch-Institute, see www.krebsdaten.de). These tumors commonly develop from transformed cells of the milk ducts and lobules. In most cases, breast cancers are reliant on the female sexual hormones estrogen and progesterone, and/or on epidermal growth factor (EGF). The overexpression of the corresponding receptors defines the therapeutic treatment regimen and is of prognostic value. Stratification is based on histopathological examination of estrogen-receptor α (ER), progesterone receptor (PR), and human epidermal growth factor receptor 2 (Her2/neu). Since ER and PR are steroid hormone receptors, they are mainly found in the cytosol. Upon ligand binding, they translocate into the nucleus, where they act as transcription factors. In contrast, Her2/neu is a plasma membrane-bound receptor tyrosine kinase which activates downstream pathways by phosphorylation of adaptor proteins upon ligation. Treatment of ER-positive breast cancer is based on the neutralization of the activating ligand estrogen. This can be achieved either by inhibiting ER with small

molecules, such as tamoxifen or raloxifen, or by inhibiting the synthesis of estrogens. Aromatase inhibitors, such as anastrozol, block a key enzyme in the estrogen synthesis pathway, thereby decreasing endogenous estrogen levels. Breast cancer cells overexpressing Her2/neu are commonly treated with the monoclonal antibody trastuzumab, blocking Her2/neu itself [33]. However, no specific therapy is available for breast cancers overexpressing neither hormone receptors nor Her2/neu. These so called triple-negative breast cancers are the most malignant subtype [34]. They develop particularly in younger women (<40 years) and are associated with specifically poor prognosis in comparison to other breast cancer subtypes [35]. In addition to classical histopathological stratification, molecular subtypes of breast cancer were defined on the basis of gene expression patterns [36] [37]. Although no generally accepted classification has been proposed yet, three molecular subtypes seem to be of importance: The luminal, the basal, and the Her2-enriched subtype. The luminal molecular subtype occurs mainly as ER-overexpressing breast cancer, while the basal and the Her2/neu subtype mainly reflect triple-negative or Her2/neu-overexpressing breast cancers, respectively [38].

Mutations in several genes of the DNA damage response involved in DNA repair are clearly linked to the development of breast cancer. For instance, women carrying mutations in one allele of the Breast cancer 1 (BRCA1) gene have a 60% risk to develop breast cancer by the age of 70 [39] [40]. The risk for ovarian cancer is also elevated for BRCA1 mutation carriers. Of note, BRCA1 mutations are inherited. Besides BRCA1, other genes have been identified as potential breast cancer driving genes. These include BRCA2, PALB2, ATM, and PTEN [41]. Interestingly, the mutation status of the well-known tumor suppressor p53 differs between the breast cancer subtypes: Mutations of p53 are found less often in ER overexpressing breast cancers than in triple-negative breast cancers [38]. Mechanistically, this might be explained by the observation that in ER-overexpressing breast cancer ER is able to bind p53, thus abrogating its tumor suppressing functions [42] [43].

Standard treatment of breast cancer includes fractionated radiotherapy in an adjuvant setting i.e. after breast conserving surgery. Patients receive daily fractions of 1.8 – 2 Gy over several weeks up to a total dose of about 50-60 Gy. The benefits of fractionated radiotherapy on tumor burden and tolerability are well described in the literature [44]: Fractionated radiotherapy leads to tumor cell elimination with concurrent

reduced normal tissue reactions, since tumor cells and normal tissue differ with regard to their DNA damage repair efficiency: Normal tissue cells can repair DNA damage between the fractions due to functional DNA repair mechanisms, while most tumor cells show deficiencies in DNA repair. Furthermore, tumor reoxygenation and redistribution of tumor cells into more radiosensitive phases of the cell cycle can occur between the fractions. Hypofractionated regimes with less but higher daily doses currently find their way into the clinical routine. Especially in Canada and the UK, hypofractionation with 2.66 Gy per day and shortened overall treatment time is already standard, and ongoing trials will elucidate whether even higher single doses (5.7-6 Gy) may define a new optimum [45]. In addition, ablative irradiation using intraoperative radiotherapy (IORT) is clinically available. In IORT, single high doses of up to 20 Gy are applied into the former tumor bed directly after tumor resection [46]. Notably, the 5-year local recurrence as well as breast cancer mortality of IORT-treated patients is similar to those treated with classically fractionated regimens [47].

4.3 Triggering adaptive anti-tumor immunity by radiotherapy

Figure 3 summarizes the essential steps for the induction of adaptive anti-tumor immunity by radiotherapy, which will be outlined in the following sections.

4.3.1 DAMP release is a hallmark of immunogenic cell death and can be induced by ionizing irradiation

Induction of immunogenic cancer cell death has been reported as a powerful first step for the stimulation of systemic anti-tumor immunity [49] (Figure 3). It is characterized by release of DAMPs [50]. DAMPs are evolutionarily conserved intracellular molecules, which have distinct roles within the cell under normal conditions. Upon release into the extracellular space, these molecules exert important pro-inflammatory functions. Cells of the innate immune system recognize DAMPs via pattern recognition receptors (PRRs), including toll-like receptors (TLRs), C-type lectin receptors, nucleotide-binding oligomerization domain-like receptors (NOD-like receptors), retinoic acid-inducible gene I-like receptors (RIG-I-like receptors), and others. Upon receptor binding, DAMPs modulate multiple functions of the cell. For example, they stimulate dendritic cell maturation by upregulation of MHC molecules and co-stimulatory receptors and induce lymph node homing of dendritic

cells, resulting in enhanced (cross-) priming of naïve T cells [26]. Beside others, nucleotides, HSP70, HMGB1, and S100 proteins are well-known DAMPs.
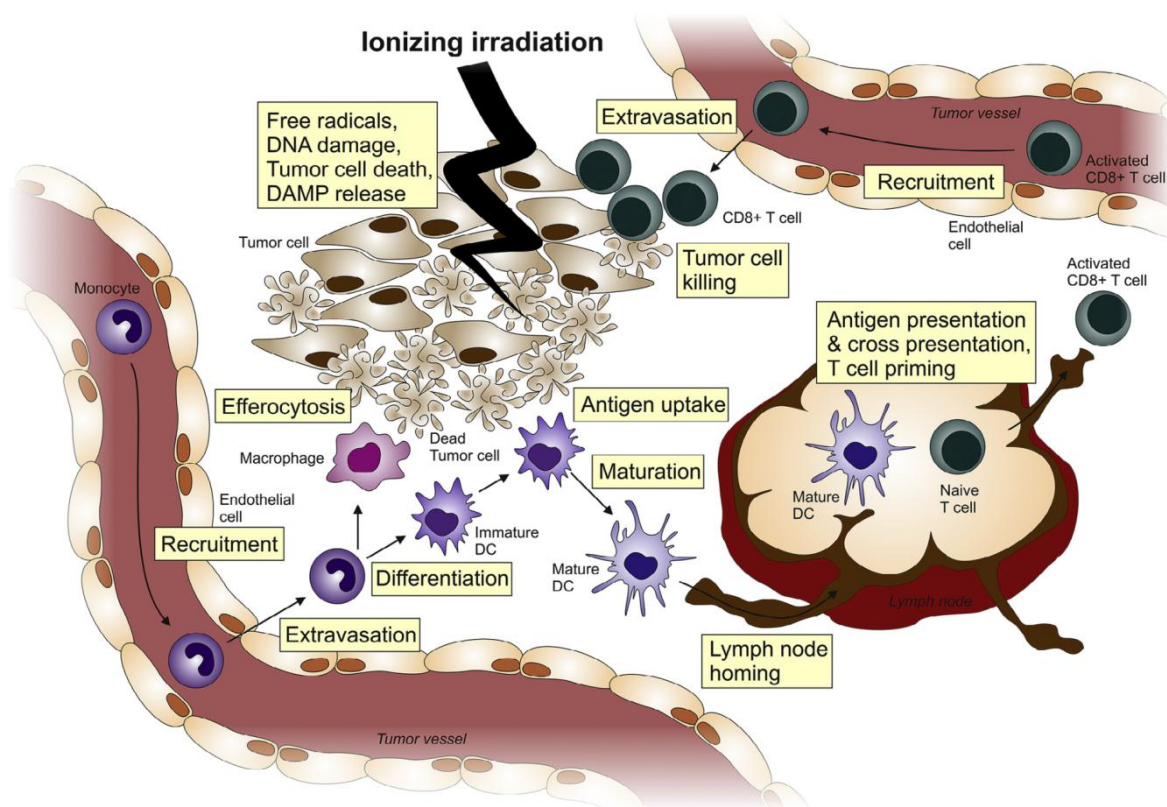
Figure 3 The concept of irradiation-induced anti-tumor immunity (adapted from [48]).

Ionizing irradiation can induce immunogenic forms of tumor cell death, which are characterized by release of DAMPs. These DAMPs activate endothelial cells resulting in recruitment and extravasation of monocytic cells to sites of tumor cell death. Monocytes differentiate into dendritic cells and macrophages, engulf dying tumor cell-derived material and mature. Mature dendritic cells leave the tumor and enter the draining lymph nodes. There, they cross-present tumor antigens to naïve CD8$^+$ T cells, which proliferate and differentiate into cytotoxic T cells upon stimulation. Cytotoxic T cells leave the lymph nodes and eliminate not only primary tumor cells but also distant metastases outside the irradiation field (abscopal effects) upon recognition of their cognate tumor antigen. CD, cluster of differentiation; DC, dendritic cell; DAMP, damage-associated molecular pattern.

Nucleotides, such as adenosine triphosphate (ATP) and uridine triphosphate (UTP), exert at least two different immune functions, depending on the type of purinergic receptor they are interacting with: Binding to the purinergic receptor P2RX$_7$ leads to activation of the NOD-like receptor family pyrin domain containing-3 protein (Nlrp3) inflammasome of dendritic cells and tissue-resident monocytes, resulting in production and secretion of pro-inflammatory interleukin (IL)-1β [51] [52] [53]. Additionally, ATP and UTP were identified as attraction signals for P2RY$_2$-expressing cells [54]. Therefore, nucleotides can also act as 'find-me' signals of dying cells for phagocytes.

However, instead of directly stimulating chemotaxis in target cells, ATP and UTP rather function as autocrine amplifiers of monocyte chemotaxis and paracrine stimulators of cytokine and chemokine production in monocytes and endothelial cells [52] [55]. ATP can either be actively secreted during apoptosis via a caspase-3 dependent opening of pannexin1 channels or passively released during necrosis [56].

As mentioned before, not only nucleotides but also intracellular proteins are well-known DAMPs. One of those is the chaperone HSP70. Since tumor cells are highly dependent on the stabilization and overexpression of oncogenic proteins, the basal expression levels of chaperones, such as HSP70 and HSP90, are higher than in non-malignant cells. HSP70 is a stress-inducible protein, which can be released in response to ionizing irradiation, especially in combination with hyperthermia [57]. Released HSP70 stimulates the upregulation of the co-stimulatory molecule CD80 as well as the lymph node homing receptor CCR7 on dendritic cells. Furthermore, membrane-bound HSP70 on tumor cells was shown to support natural killer cell (NKC)-dependent tumor elimination [58] [59].

Another well-known DAMP is High mobility group box protein 1 (HMGB1). Under physiological conditions, HMGB1 is bound to DNA in the nucleus. During necrosis, it is passively released and acts as a highly immunogenic signal [60] [61], especially for dendritic cells: It activates TLR4 leading to enhanced cross-presentation of tumor antigens to CD8$^+$ T cells [62]. Interestingly, the immunogenic potential of HMGB1 is dependent on its oxidation status: Completely reduced HMGB1 promotes leukocyte recruitment, while disulfide-HMGB1 is highly pro-inflammatory In contrast, oxidized HMGB1 is important for the resolution of inflammation [63]. Apart from TLR4, HMGB1 also interacts with other PRRs, such as TLR2 and RAGE [64] [65].

S100 proteins also play important roles as DAMPs. More than 20 members of the S100 family have been identified so far [66]. They comprise a family of calcium sensing proteins which regulate intracellular calcium-dependent pathways [67]. Many cancer types, such as breast cancer, melanoma, and colorectal cancer, show overexpression of S100 proteins [66]. Particularly the S100A8/A9 heterodimer is of interest in the context of immune-activating signals. S100A8/A9 was shown to bind to TLR4 and the receptor for advanced glycation endproducts (RAGE), thereby stimulating the release of pro-inflammatory cytokines from monocytic cells and

favoring the extravasation of monocytes and neutrophils by upregulation of the integrin Mac-1 [68] [69] [70] [71].

The main source of DAMPs are necrotic cells (primary and secondary necrotic ones), whose disintegrated plasma membrane allows passive release of intracellular material. Primary necrosis is referred to as an uncontrolled, accidental form of cell death, which is induced by extreme cell stress, for instance upon high doses of ionizing irradiation [72].
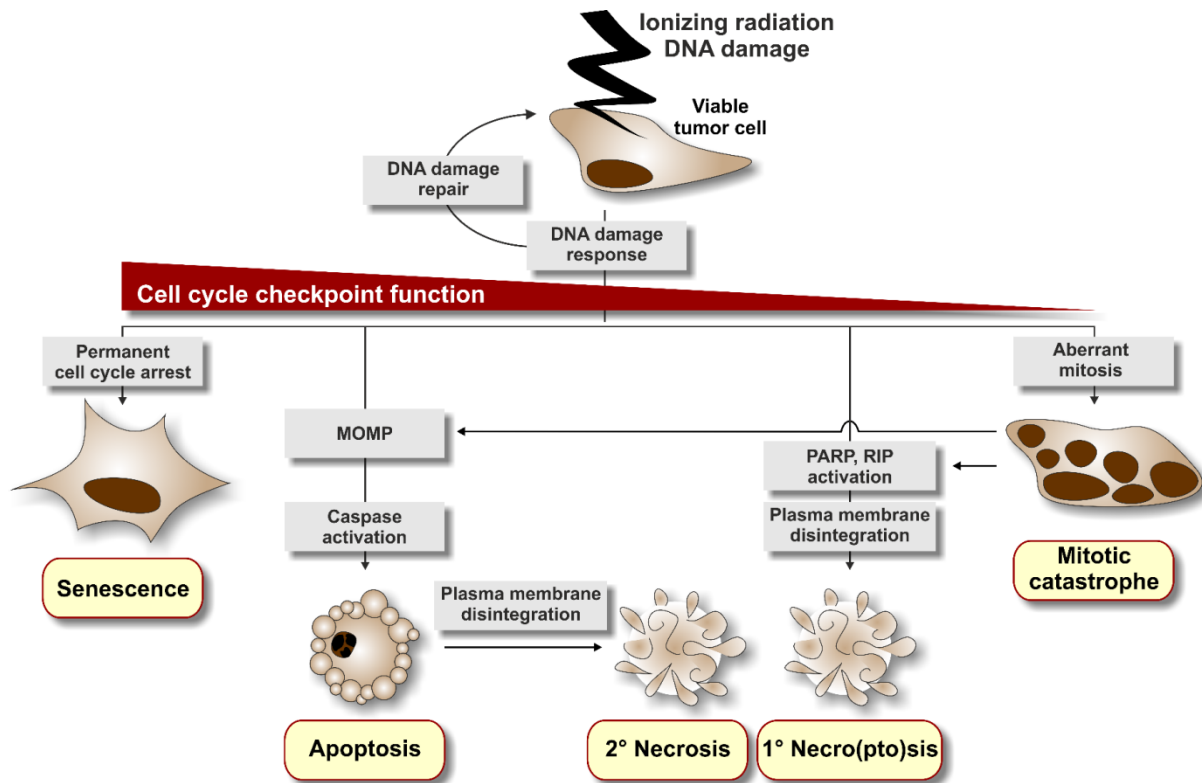
Figure 4 Irradiation-induced cell death modalities (adapted from [9]).

Excessive irradiation-induced DNA damage which cannot be repaired, leads to various cell death modalities in tumor cells. Which type of cell death mode is executed, depends on multiple factors, such as the tumor cell's origin, its genetic repertoire, the radiation dose, and the functionality of cell cycle checkpoints. Cells of the hematopoietic system primarily undergo apoptosis via the intrinsic (mitochondrial) pathway in response to ionizing radiation. Apoptosis is a strictly controlled mode of cell death. A key feature of apoptosis is the maintenance of plasma membrane integrity. If not removed in time by amateur or professional phagocytes, apoptotic cells can transit into secondary necrosis. In contrast, primary necrosis is an uncontrolled, accidental type of cell death, which is characterized by early loss of cell integrity and subsequent release of intracellular contents. Necroptosis is a controlled form of necrosis, which is regulated by RIPK1 and -3. Cells of epithelial origin mainly undergo mitotic catastrophe in response to ionizing radiation, when cell cycle checkpoints are defective. After several aberrant cell divisions, these cells commonly undergo a very chaotic, mainly necrotic form of cell death. However, also apoptotic phenotypes have been observed upon mitotic catastrophy. If cell cycle checkpoint functionality is preserved, cells may become senescent after radiation. They irreversibly exit the cell cycle, but remain metabolically active. MOMP, mitochondrial outer membrane potential; PARP, poly(ADP-ribose)polymerase; RIP, receptor-interacting protein kinase.

In addition to primary necrosis, irreparable DNA damage induced by irradiation leads to apoptosis, mitotic catastrophe, or senescence, respectively, depending on the cell's origin, its genetic repertoire, and the functionality of cell cycle checkpoints (Figure 4). Notably, these modes of cell death clearly differ in their immunogenic potential. In contrast to necrosis, apoptosis is a highly organized form of cell death. Cells of the hematopoietic system mainly undergo apoptosis in response to ionizing radiation via the intrinsic apoptotic pathway [73]. During intrinsic apoptosis, breakdown of the mitochondrial outer membrane potential is followed by release of pro-apoptotic factors, such as cytochrome c, which leads to activation of pro-caspase-9, in turn activating downstream effector caspases [74]. Apoptotic cells are characterized by membrane blebbing, chromatin condensation and DNA fragmentation. During this strictly controlled process of cell death, the membrane integrity stays intact. As such, apoptosis is an immunogenically silent form of cell death, which induces the production of anti-inflammatory cytokines, including transforming growth factor β (TGF-β) and IL-10, by phagocytes [75]. However, apoptotic cells which are not removed in time by neighboring cells or professional phagocytes, might transit into secondary necrosis, thereby losing plasma membrane integrity and releasing their intracellular contents [76].

Cells of epithelial origin, as is the case for most solid cancers, rarely undergo apoptosis in response to ionizing irradiation. If cell cycle checkpoint functions are lost, these cells experience mitotic catastrophe as characterized by several aberrant cell divisions, resulting in giant cells with abnormal nuclear morphology, which finally die in a highly chaotic, necrotic way.

If cell cycle checkpoint function is still preserved, cells with excessive DNA damage can irreversibly exit the cell cycle and undergo cellular senescence. This is hallmarked by an upregulation of cyclin-dependent kinase inhibitors, such as p21, p27, and p16. Furthermore, activity of senescence-associated β-galactosidase is upregulated and commonly used for the detection of senescence [77]. Senescent cells remain metabolically active and secrete various factors, such as chemokines, growth factors, and proteases. As a whole, these factors represent the senescence-associated secretory phenotype (SASP) [78]. On the one hand, DNA damage-induced senescence by irradiation can result in permanent and irreversible growth arrest of tumor cells, thus inhibiting tumor progression. On the other hand, Angelini and

colleagues showed that the SASP can promote breast cancer metastasis [79]. To add complexity, Pribluda et al. described a p53-dependent mechanism, which switches the senescent environment from a cancer-suppressive to a cancer-promoting one [80].

Since DAMP release by dying tumor cells is a prerequisite to alert the immune system, the induction of immunogenic cell death can be an essential step at the very beginning of the anti-tumor immune response. In contrast, large numbers of tumor cells undergoing non-immunogenic forms of tumor cell death might attenuate or even prevent effective immune reactions against cancer cells.

Importantly, the mere existence of a pro-inflammatory milieu inside the tumor is not sufficient to induce potent anti-tumor immunity: The factors released from immunogenically dying cells must also be converted and amplified in order to attract immune cells to sites of tumor cell death and danger (Figure 3). This process – the leukocyte recruitment cascade – has been studied extensively as discussed in the following section.

4.3.2 Leukocyte recruitment to sites of danger and cell death

As one of the first steps in the induction of adaptive anti-tumor immune responses after irradiation, monocytes are recruited to sites of tumor cell death, were they subsequently differentiate into dendritic cells, which take up tumor material and (cross-) present it to naïve T cells in the draining lymph nodes (Figure 3).
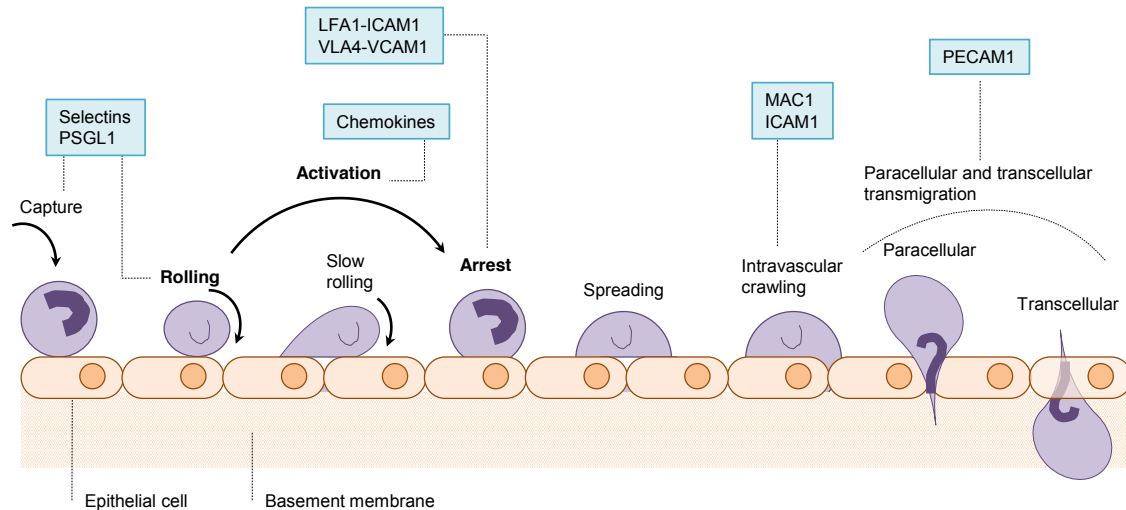
Figure 5 The leukocyte adhesion cascade (adapted from [81]).

Leukocytes extravasate from the blood to sites of infection or damage. They are captured by activated endothelial cells and roll on their luminal surface. Both steps are mediated by the interaction between E- and P-selectins expressed on activated endothelial cells and their corresponding receptors on leukocytes (e.g. PSGL1). Subsequently, leukocytes are activated by chemokines released from endothelial cells, followed by arrest, spreading, and intravascular crawling. These steps are dependent on the interaction between integrins (e.g. LFA-1, Mac-1) expressed on leukocytes and adhesion molecules (e.g. ICAM-1, VCAM-1) on the surface of activated endothelial cells. Finally, leukocytes extravasate through the endothelial cell layer into the tissue via para- or transcellular mechanisms in a PECAM-1-dependent manner. ICAM-1, Intercellular adhesion molecule 1; LFA-1, Lymphocyte function-associated antigen 1; Mac-1, Macrophage receptor 1; PECAM-1, Platelet endothelial cell adhesion molecule 1; PSGL1, P-selectin glycoprotein ligand 1; VCAM-1, vascular cell adhesion molecule 1.

The leukocyte adhesion cascade summarizes the steps necessary for leukocyte recruitment from the blood stream to sites of infection and/or tissue damage (Figure 5). This extravasation process into the tissue is typically observed in postcapillary venules. It is initiated by the capture or tethering of leukocytes from the blood stream to the surface of endothelial cells and subsequent rolling of leukocytes on the endothelium. Both processes are dependent on selectins [82] of which three types have been described: L-selectin, E-selectin, and P-selectin. The latter two are mainly expressed on endothelial cells and are strongly upregulated by inflammatory signals: DAMPs and pro-inflammatory cytokines, induce the synthesis and surface expression of E-selectin as well as the translocation of P-selectin, which is stored in Weibel-Palade bodies, to the luminal side of endothelial cells. In contrast, L-selectin is not expressed on the endothelium but on leukocytes. All three selectins bind to P-selectin glycoprotein ligand 1 (PSGL1) expressed by all leukocytes. E-selectin additionally binds to CD44 and E-selectin ligand 1 (ESL1) [83]. Temporal, reversible interaction of

E- and P-selectin on the activated endothelium with their cognate leukocyte ligands leads to capture and rolling of leukocytes on the endothelium. Recently, Zuchtriegel and colleagues demonstrated that rolling of neutrophils is predominantly mediated by P- and L-selectin interacting with PSGL1 and CD44, while inflammatory monocytes additionally require E-selectin [84].

Upon rolling, leukocytes are activated and arrest on the endothelium. This is triggered by endothelial cell-derived chemokines and depends on the interaction between leukocyte integrins and adhesion molecules of the immunoglobulin superfamily on the activated endothelium [85]. The most important integrins found on myeloid cells are the β_2-integrins lymphocyte function-associated antigen (LFA-1; CD11a/CD18), macrophage receptor 1 (Mac-1; CD11b/CD18), and the β_1-integrin very late antigen 4 (VLA-4; CD49d/CD29). Monocytes express β_2- as well as β_1-integrins, whereas neutrophils express mainly β_2-integrins [86]. The integrin-interacting adhesion molecules of activated endothelial cells include ICAM-1, ICAM-2 and VCAM-1. Whereas β_2-integrins LFA-1 and Mac-1 bind to ICAM-1 and ICAM-2, the β_1-integrin VLA-4 binds to VCAM-1 [87] [88]. Integrins occur in three different conformations, which display different affinities to their corresponding ligands [89] [90]. However, the integrin activation pathways are very complex and have been reviewed elsewhere [81].

Leukocyte arrest is followed by spreading and crawling on the endothelium. Crawling is also integrin-mediated, and the interaction between Mac-1 and ICAM-1/-2 is of crucial importance [91] [92] [93]. The last step in leukocyte recruitment is the extravasation through the endothelial wall into the tissue. In principle, two ways have been described: The paracellular and the transcellular migration route. Both are fine-tuned processes, which depend on many interactions between the extravasating leukocyte and the endothelial cell [94]. Notably, platelet endothelial cell adhesion molecule 1 (PECAM-1; CD31), which is part of the inter-endothelial cell junctions, appears to play a central role in both transmigration pathways [95] [96]. Once the leukocyte has extravasated, it is guided to the site of infection or damage. In this context, pericytes have been shown to promote neutrophil migration after extravasation by acting as 'speedways' to sites of sterile inflammation [97].

Apart from cell adhesion molecules, recruitment of leukocytes into inflamed tissue requires chemokines. Several chemokines released by activated endothelial cells or immobilized on their surface, have been identified as potent inducers of chemotaxis

(i.e. directional migration towards the chemokine gradient). Based on the localization of cystein residues in their secondary structure, they are categorized into four main classes, containing the C, the CC, the CXC, or the CX3C motif, respectively. CXC chemokines, such as IL-8, CXCL1, and MIP-2a, are described as preferential chemotactic stimuli for neutrophils, while CC chemokines such as monocyte chemotactic protein (MCP)-1, -2, and -3 mainly attract monocytes [98] [99]. However, overlapping effects have been demonstrated [100] [101]. Chemokines are recognized by specific G-protein-coupled receptors on leukocytes guiding them along the concentration gradient on the endothelium. Once a leukocyte has extravasated into the tissue, it has to be navigated closer to the sites of danger. To this end, chemokine-mediated guidance as provided by endothelial cells is outcompeted by stronger chemotactic stimuli. For neutrophils, it was shown that dying cell-derived DAMPs released from mitochondria, such as formylated peptides and mitochondrial DNA, are hierarchically superior to endothelial chemokines, thus directing neutrophils to the origin of tissue damage [102] [103].

4.3.3 Dendritic cells as key players in adaptive anti-tumor immunity

Once recruited to the site of radiation-induced tumor cell death, monocytic cells can differentiate into dendritic cells which are of crucial importance for the induction of T cell-dependent anti-tumor immunity (Figure 3). As a first step, immature dendritic cells derived from recruited monocytes engulf dying tumor cell material and receive maturation signals. The maturation process is characterized by upregulation of different surface molecules on dendritic cells. These include the maturation marker CD83 as well as the co-stimulatory molecules CD80, CD86, and CD40, as well as MHC class II receptors. In addition, the lymph node homing receptor CCR7 is upregulated on mature dendritic cells. CCR7 is essential to guide dendritic cells (as well as T and B cells) into the draining lymph node [104]. Due to strong upregulation of these markers, mature dendritic cells are highly potent antigen-presenting cells (APCs). As mentioned in chapter 4.3.1, the maturation process of dendritic cells is strongly influenced by DAMPs, such as HMGB1, ATP, and HSPs [62] [51] [57]. Mature dendritic cells that have captured tumor antigens enter the draining lymph nodes where they interact with naïve T cells. The interface between T cells and dendritic cells is characterized by a plethora of receptors and their corresponding ligands as well as various cytokines involved. Therefore, the term 'immunological synapse' has

been established [105] (Figure 6). To get into close proximity and to maintain antigen presentation, T cells bind ICAM-1 on dendritic cells by the integrin LFA-1 [107]. The interaction between T cells and dendritic cells is stable for several minutes [108]. In principle, three signals are necessary for T cell stimulation by dendritic cells: (i) (cross-) presentation of antigens on MHC receptors to the T cell receptor, (ii) interaction of co-stimulatory receptors with co-stimulatory ligands, and (iii) release of cytokines supporting T cell differentiation and proliferation. Two classes of MHC molecules are found on dendritic cells for (cross-) presentation of antigens to T cells: Antigens presented on MHC class II receptors are recognized by CD4$^+$ T cells, while antigens on MHC class I receptors are cross-presented to CD8$^+$ T cells. In order to generate the second activating signal, the interaction between CD28 (expressed on T cells) and CD80 or CD86 (expressed on dendritic cells) is essential. To maintain clonal T cell expansion, stimulated T cells release IL-2 in an autocrine manner and for further differentiation dendritic cells release cytokines such as IL-12.
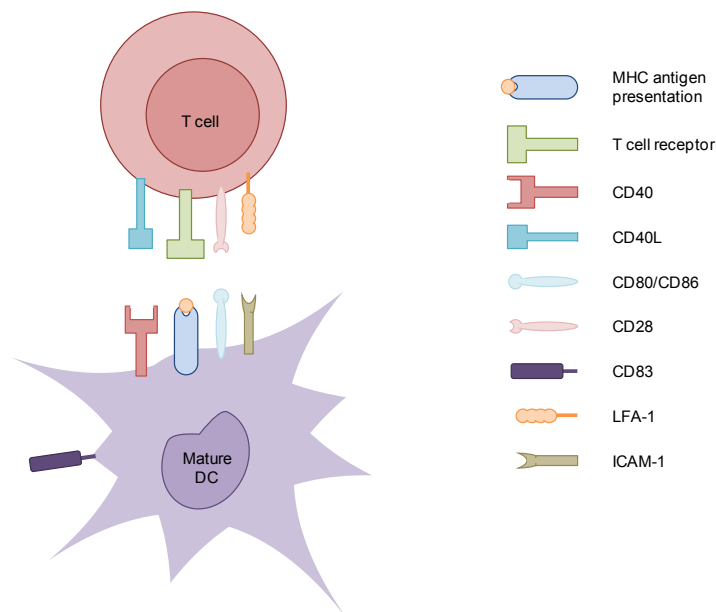
Figure 6 Representative scheme of the immunological synapse (adapted from [106]).

The interface between a T cell and a mature dendritic cell is termed the 'immunological synapse'. It is built up by multiple interacting molecules on both cells. To establish and stabilize the contact, the integrin LFA-1 on the T cell binds ICAM-1 on the dendritic cell. T cell activation by the dendritic cell requires the (cross-) presentation of an antigen on MHC molecules to the specific T cell receptor. Furthermore, co-stimulatory ligands, such as CD80/CD86 bind to CD28, delivering the second activating signal for the T cell. Vice versa, the interaction between CD40 and CD40L delivers an activating signal to the dendritic cell. CD83 is a common marker for dendritic cell maturation. DC, dendritic cell; ICAM-1, intercellular adhesion molecule 1; LFA-1, lymphocyte function-associated antigen 1; MHC, major histocompatibility complex.

In the following, the expanding T cells differentiate into effector T cells and leave the lymph node. Upon recognition of antigens by the specific T cell receptor, effector T cells are activated without a second signal. Therefore, they are potentially able to eliminate not only the primary tumor, but also distant metastases. As mentioned in chapter 4.1, cytotoxic CD8$^+$ T cells are the most important effector T cells in adaptive anti-tumor immunity. They kill target cells via several cytotoxic mechanisms. For instance, CD8$^+$ T cells express FasL, which induces apoptosis of target cells upon binding to the death receptor Fas expressed on their plasma membrane. Another example is the release of the serine protease granzyme B in combination with perforin, which may also induce cell death in the target cell. Furthermore, they produce IFNγ, thereby enforcing the immune response (e.g. activation of macrophages, dendritic cells and T cell differentiation) and enhancing tumor immunogenicity (e.g. upregulation of MHC class I molecules).

In addition to the aforementioned co-stimulatory molecules, various interacting proteins expressed on T cells and APCs have been identified [109]. Among those, activation of CD40 on dendritic cells by CD40L on T cells is noteworthy, because this interaction delivers a co-stimulatory signal from the T cell to the APC, resulting in increased APC activation [110]. Moreover, interactions between CD80/CD86 and PDL-1 with their corresponding receptors on the T cells – cytotoxic T-lymphocyte-associated protein-4 (CTLA-4) and programmed cell death receptor 1 (PD1), respectively – are of special interest, since both cause T cell inhibition, thereby limiting effector T cell activity. These mechanisms lead to attenuation of immune responses, and therefore protect against autoimmunity and excessive immune responses [111] [112]. Interestingly, both the inhibitory as well as the activating function of CTLA-4 and CD28 are dependent on binding to CD80/CD86 on APCs. Ipilimumab, a monoclonal antibody directed against CTLA-4, was one of the first immunotherapeutic drugs approved by the FDA for the treatment of metastatic melanoma to resolve this endogenous T cell inhibition and to strengthen adaptive anti-tumor responses [113]. Notably, abscopal effects of radiotherapy appear to be more pronounced and more frequent under ipilimumab treatment [3]. Enhanced surface expression of PDL-1 is not only found on regulator APCs, but is also a common mechanism how tumor cells escape destruction by effector T cells through binding of PD1 [114] [115] [116]. Two monoclonal antibodies, nivolumab and pembrolizumab (both approved by the FDA for metastatic

melanoma and NSCLC [117] [118], interfere with this tumor escape mechanism by binding PD1 on T cells. However, ipilimumab as well as nivolumab and pembrolizumab have severe side effects such as excessive inflammatory reactions, which need to be carefully monitored.

5 Objective

Radiotherapy efficiently induces tumor cell death and, thus, is a mainstay in cancer treatment. However, accumulating evidence suggests a contribution of the immune system to the radiotherapeutic outcome: Particularly when applied in ablative settings (i.e. in high single doses of 10-20 Gy), radiotherapy appears to induce systemic anti-tumor mechanisms, which are much less frequently observed with classically fractionated irradiation regimens (i.e. daily doses of 2 Gy). Yet, the mechanisms behind these immunological phenomena remain poorly understood.

In the present study, central steps governing radiation-induced anti-tumor immunity were investigated in the context of fractionated and ablative radiotherapy of breast cancer in vitro and in vivo: Induction of tumor cell death, recruitment of monocytes, maturation of monocyte-derived antigen-presenting cells, and stimulation of adaptive T cell responses were examined in order to understand key elements of radiation-induced anti-tumor immunity.

6 Materials and Methods

6.1 Materials

6.1.1 Suppliers

Table 1. List of suppliers

Supplier	Headquarter of supplier
ATCC	Manassas, VA, USA
Bachem	Bubendorf, Switzerland
BD Biosciences	Heidelberg, Germany
Biochrom	Berlin, Germany
BioLegend	San Diego, CA, USA
Bio-Rad	Hercules, CA, USA
BioTek Instruments GmbH	Bad Friedrichshall, Germany
Carl Roth	Karlsruhe, Germany
Corning	Corning, NY, USA
eBioscience	San Diego, CA, USA
Enzo Life Sciences	Loerrach, Germany
Eppendorf	Hamburg, Germany
Fermentas	St. Leon-Roth, Germany
GE Healthcare	Munich, Germany
Glaswarenfabrik Karl Hecht	Sondheim, Germany
Greiner BIO-ONE	Kremsmuenster, Austria
ibidi	Martinsried, Germany
IBL International	Hamburg, Germany
Leica Microsystems	Wetzlar, Germany
LI-COR	Lincoln, NE, USA
Life Technologies	Karlsruhe, Germany
Lonza	Basel, Switzerland
New England Biolabs	Frankfurt, Germany
Merck	Darmstadt, Germany
Macherey-Nagel	Dueren, Germany
Microsoft	Richmond, WA, USA
Miltenyi Biotec	Bergisch Gladbach, Germany
Philips	Amsterdam, Netherlands
PromoCell	Heidelberg, Germany
R&D Systems	Minneapolis, MN, USA
ratiopharm	Ulm, Germany
Roche Applied Science	Penzberg, Germany
Sarstedt	Nuembrecht, Germany
Sigma-Aldrich	Taufkirchen, Germany
Thermo Fisher Scientific	Waltham, MA, USA

Supplier	Headquarter of supplier
Tree Star Inc.	Ashland, OR, USA
Xstrahl	Camberley, UK
Zeiss	Goettingen, Germany

6.1.2 Cell lines and culture media

Table 2. Cell lines

Cell line	Origin	Supplier
BT-474	Human breast cancer	ATCC
BT-549	Human breast cancer	ATCC
HCC1806	Human breast cancer	ATCC
HCC1937	Human breast cancer	ATCC
MCF7	Human breast cancer	ATCC
MDA-MB-468	Human breast cancer	ATCC
THP-1	Human acute monocytic leukemia	ATCC
HUVECs	Primary human endothelial cells	PromoCell

Table 3. Cell culture media and supplements

Medium/Supplement	Supplier
RPMI-1640	Life Technologies
DMEM	Life Technologies
DMEM/F12 1+1	Life Technologies
Fetal calf serum (FCS)	Life Technologies
Penicillin/Streptomycin	Life Technologies
HEPES buffer	Life Technologies
Phosphate-buffered saline (PBS)	Life Technologies
Trypsin/EDTA	Life Technologies
Endothelial Cell Growth Medium	PromoCell
Supplement Mix	PromoCell
DetachKit	PromoCell
X-Vivo 15	Lonza
Human AB-serum	Sigma-Aldrich

6.1.3 Reagents, buffers and commercial kits

Table 4. Reagents and solutions

Reagent/Solution	Supplier
ATP	Sigma-Aldrich
Annexin V-FITC	BD Biosciences
Annexin staining buffer	BD Biosciences
APS	Sigma-Aldrich
Apyrase	New England Biolabs
ARL-67156	R&D Systems
Bafilomycin A1	R&D Systems
Biocoll Separating Solution (1.077 g/ml)	Biochrom
Bradford Reagent	Bio-Rad
BSA	Sigma-Aldrich
C12-FDG	Life Technologies
Calcein-AM	Merck
Anti-CD3 magnetic beads	Miltenyi
Anti-CD14 magnetic beads	Miltenyi
cOmplete™ULTRA Tablets, Mini, EASYpack	Roche Applied Science
Bromophenol blue	Sigma-Aldrich
CFSE	Life Technologies
Cytochalasin D	Sigma-Aldrich
Diluent C	Sigma-Aldrich
dNTPs	Fermentas
EDTA	Sigma-Aldrich
EGTA	Sigma-Aldrich
Ethanol	Merck
FACS staining buffer	BD Biosciences
Fluoromount	Sigma-Aldrich
Formaldehyde	Merck
Glycine	Sigma-Aldrich
Glycoblue	Thermo Fisher Scientific
GM-CSF	R&D Systems
Heparin-Natrium 5000	rathiopharm
HEPES	Sigma-Aldrich
Hoechst-33342	Sigma-Aldrich
IGEPAL CA-630	Sigma-Aldrich
IL-4	R&D Systems
Isopropanol	Merck
KCl	Sigma-Aldrich
LPS	Sigma-Aldrich
Maxima SYBR Green qPCR Master Mix	Thermo Fisher Scientific

Reagent/Solution	Supplier
2-Mercaptoethanol	Sigma-Aldrich
Methanol	Merck
$MgCl_2$	Sigma-Aldrich
Milk powder	Carl Roth
NaCl	Sigma-Aldrich
Nail polish	Maybelline
NaN_3	Sigma-Aldrich
Necrostatin-1	Enzo Life Sciences
Oligo(dT)$_{18}$	Fermentas
PageRuler™	Thermo Fisher Scientific
Paraformaldehyde	Sigma-Aldrich
Phalloidin-Alexa Fluor568	Thermo Fisher Scientific
PhosSTOP™	Roche Applied Science
PKH26	Sigma-Aldrich
PKH67	Sigma-Aldrich
2-Propanol	Merck
Propidium iodide (PI)	Sigma-Aldrich
Proteinase K	New England Biolabs
Random hexamers	Fermentas
Revert Aid H Minus M-MuLV reverse transcriptase	Fermentas
Ribolock RNase inhibitor	Fermentas
Rotiphorese® Gel 30 (37.5:1)	Carl Roth
SDS	Sigma-Aldrich
SDF-1α	R&D Systems
TEMED	Carl Roth
TNF	R&D Systems
Tris	Sigma-Aldrich
Triton-X 100	Sigma-Aldrich
zVAD-fmk	Bachem

Table 5. Buffers and gels

Buffer	Reagent	Concentration
Annexin staining buffer (10×)	HEPES pH 7.4 NaCl $CaCl_2$ in ddH_2O	0.1 M 1.4 M 25 mM
Caspase lysis buffer	HEPES-K pH 7.4 KCl $MgCl_2$ EDTA EGTA IGEPAL CA-630 in ddH_2O	20 mM 84 mM 10 mM 0.2 mM 0.2 mM 0.5%
FACS stain buffer	BSA Sodium azide in PBS pH 7.4	2% 0.09%
Laemmli buffer (4×)	Tris-HCl pH 6.8 Glycerol SDS Bromophenol blue 2-Mercaptoethanol in ddH_2O	250 mM 25% 8% 0.04% 4%
SDS-PAGE running buffer (10×)	Tris Glycine SDS in ddH_2O	250 mM 1.9 M 1%
Separation gel	Rotiphorese® Gel 30 (30% acrylamide, 0.8% bis-acrylamide) Separation gel buffer APS TEMED ddH_2O	6-15% 26% 0.1% 0.08% ad 100%
Separation gel buffer	Tris-HCl pH 8.8 SDS in ddH_2O	1.5 M 0.384%

Buffer	Reagent	Concentration
Stacking gel	Rotiphorese® Gel 30 (30% acrylamide, 0.8% bis-acrylamide)	5%
	Stacking gel buffer	13.5%
	APS	0.1%
	TEMED	0.08%
	ddH$_2$O	ad 100%
Stacking gel buffer	Tris-HCl pH 8.8	1.5 M
	SDS	0.384%
	in ddH$_2$O	
Western blot blocking buffer	Milk powder	5%
	in 1× Western blot washing buffer	
Western blot lysis buffer	Tris pH 7.6	50 mM
	NaCl	150 mM
	Triton-X 100	1%
	in ddH$_2$O	
	cOmplete™ULTRA tablet	1 tablet per 10 ml buffer
	PhosSTOP™ tablet	1 tablet per 10 ml buffer
Western blot transfer buffer	Tris	44 mM
	Glycine	40 mM
	Methanol	20%
	in ddH$_2$O	
Western blot washing buffer	Tris pH 7.5	13 mM
	NaCl	150 mM
	Triton-X 100	0.02%
	in ddH$_2$O	

Table 6. Commercial kits

Kit	Supplier
Bio-Plex Pro Human Chemokine Assay (40-Plex Panel)	Bio-Rad
DuoSet® IC ELISA	R&D Systems
HMGB1-ELISA	IBL International
NucleoSpin® RNA kit II	Macherey-Nagel
TMB Peroxidase EIA Substrate Kit	Bio-Rad

6.1.4 Antibodies

Table 7. Antibodies for flow cytometric analyses of human blood cells

Antibody	Color	Isotype	Supplier	Dilution
CD3	PE-Cy7	Mouse IgG1, κ	BD Biosciences	1:50
CD4	PE	Mouse IgG1, κ	BD Biosciences	1:25
CD8	APC	Mouse IgG1, κ	BD Biosciences	1:25
CD39	PE	Mouse IgG2b, κ	BD Biosciences	1:25
CD40	PE-Cy5	Mouse IgG1, κ	BD Biosciences	1:25
CD73	FITC	Mouse IgG1, κ	BD Biosciences	1:25
CD80	PE	Mouse IgG1, κ	BD Biosciences	1:25
CD83	PE-Cy7	Mouse IgG1, κ	BD Biosciences	1:100
CD86	Alexa Fluor700	Mouse IgG1, κ	BD Biosciences	1:100
CD203c	APC	Mouse IgG1, κ	BD Biosciences	1:25
Isotype IgG1	Alexa Fluor700	Mouse IgG1, κ	BD Biosciences	1:25
Isotype IgG1	APC	Mouse IgG1, κ	BD Biosciences	1:25
Isotype IgG1	FITC	Mouse IgG1, κ	BD Biosciences	1:25
Isotype IgG1	PE	Mouse IgG1, κ	BD Biosciences	1:25
Isotype IgG1	PE-Cy7	Mouse IgG1, κ	BD Biosciences	1:50/1:100
Isotype IgG1	PE-Cy5	Mouse IgG1, κ	BD Biosciences	1:25
Isotype IgG2b	PE	Mouse IgG2b, κ	BD Biosciences	1:25

Table 8. Antibodies for flow cytometric analyses of mouse blood cells

Antibody	Color	Isotype	Supplier	Dilution
CD11b	FITC	Rat IgG2b, κ	eBioscience	1:100
CD11c	PerCP-Cy5.5	Arm Ham IgG	eBioscience	1:100
CD45	APC-Cy7	Rat IgG2b, κ	BD Biosciences	1:100
F4/80	eFluor450	Rat IgG2a, κ	eBioscience	1:100
H-2	Alexa Fluor700	Rat IgG2b, κ	eBioscience	1:100
Ly6C	PE-Cy7	Rat IgM	BD Biosciences	1:100
Ly6G	BUV395	Rat IgG2a, κ	BD Biosciences	1:100
PDCA1	APC	Rat IgG2b, κ	eBioscience	1:100
Siglec-H	PE	Rat IgG2b, κ	eBioscience	1:100
Isotype IgG	PerCP-Cy5.5	Arm Ham IgG	eBioscience	1:100
Isotype IgG2a	BUV395	Rat IgG2a, κ	BD Biosciences	1:100
Isotype IgG2a	eFluor450	Rat IgG2a, κ	eBioscience	1:100
Isotype IgG2b	Alexa Fluor700	Rat IgG2b, κ	eBioscience	1:100
Isotype IgG2b	APC	Rat IgG2b, κ	eBioscience	1:100
Isotype IgG2b	APC-Cy7	Rat IgG2b, κ	BD Biosciences	1:100
Isotype IgG2b	FITC	Rat IgG2b, κ	eBioscience	1:100

Antibody	Color	Isotype	Supplier	Dilution
Isotype IgG2b	PE	Rat IgG2b, κ	eBioscience	1:100
Isotype IgM	PE-Cy7	Rat IgM	BD Biosciences	1:100

Table 9. Primary antibodies for western blot analyses

Antibody	Isotype	Clonicity	Supplier	Dilution
p21^{WAF1}	Mouse IgG1, κ	monoclonal	BD Biosciences	1:1000
Vinculin	Mouse IgG1, κ	monoclonal	Sigma-Aldrich	1:1000

Table 10. Secondary antibodies for western blot analyses

Antibody	Reactivity	Clonicity	Species	Supplier	Dilution
IgG-IRDye® 680LT	Mouse	polyclonal	Goat	LI-COR	1:20,000
IgG-IRDye® 800CW	Mouse	polyclonal	Goat	LI-COR	1:20,000

Table 11. Antibodies for immunofluorescence staining of human cells

Antibody	Color	Isotype	Reactivity	Supplier	Dilution
E-selectin	PE	Mouse IgG1, κ	Human	BD Biosciences	1:25
ICAM-1	PE	Mouse IgG1, κ	Human	BD Biosciences	1:25
VCAM-1	PE	Mouse IgG1, κ	Human	BD Biosciences	1:25

Table 12. Antibodies for confocal microscopy of air pouch skins

Antibody	Color	Isotype	Supplier	Dilution
CD31 (PECAM-1)	Alexa Fluor647	Rat IgG2a, κ	BioLegend	1:100
F4/80	Alexa Fluor488	Rat IgG2a, κ	Thermo Fisher Scientific	1:100
Ly6G	-	Rat IgG2a, κ	BioLegend	1:100
Anti-Rat IgG	Alexa Fluor546	Goat IgG	Thermo Fisher Scientific	1:400

6.1.5 Primers

Table 13. Primer sequences for quantitative real-time PCR of human samples

All primers were synthesized by Sigma-Aldrich.

Gene	Primer	Sequence 5'-3'
18S rDNA	Forward	CGGCTACCACATCCAAGGAA
	Reverse	GCTGGAATTACCGCGGCT
β_2-microglobulin	Forward	TGCTCGCGCTCATCTCTCTTTC
	Reverse	TCTCTGCTGGATGACGTGAGTAAAC
CX3CL1	Forward	ACAGAACCAGGCATCATGCG
	Reverse	CGGGTCGGCACAGAACAG
CXCL1	Forward	AAGCTTGCCTCAATCCTGCAT
	Reverse	TGGATTTGTCACTGTTCAGCATCT
δ-ALAS	Forward	TCCACTGCAGCAGTACACTACCA
	Reverse	ACGGAAGCTGTGTGCCATCT
Egr-1	Forward	GAGCACCTGACCGCAGAGTC
	Reverse	CCAGCACCTTCTCGTTGTTCA
E-selectin	Forward	CCTACCTGTGAAGCTCCCACTG
	Reverse	AGGAGGGAGAGTCCAGCAGC
HCC1&2	Forward	GCGTCAGCGGATTATGGATTAC
	Reverse	ACGGAATGGCCCCTTTTG
I-309	Forward	GCTTGCTGCTAGCTGGGATGT
	Reverse	CTCCGCAAATGAGAAGCAACA
ICAM-1	Forward	GGAACAACCGGAAGGTGTATGA
	Reverse	GTTCTGGAGTCCAGTACACGGTG
IL-1α	Forward	GCTTCCTGAGCAATGTGAAATACA
	Reverse	CAAATTTCACTGCTTCATCCAGATT
IL-6	Forward	GGTACATCCTCGACGGCATCT
	Reverse	AGTGCCTCTTTGCTGCTTTCAC
IL-8	Forward	TGGCAGCCTTCCTGATTTCT
	Reverse	TGCACTGACATCTAAGTTCTTTAGCA
IP-10	Forward	TGGCATTCAAGGAGTACCTCTCT
	Reverse	GTAGCAATGATCTCAACACGTGG
I-TAC	Forward	TGTTCAAGGCTTCCCCATGT
	Reverse	GAGGCTTTCTCAATATCTGCCACT
MCP-1	Forward	CAGCAAGTGTCCCAAAGAAGCT
	Reverse	TGGAATCCTGAACCCACTTCTG
MCP-2	Forward	GCTGGAGAGCTACACAAGAATCAC
	Reverse	GCCCCGTTTGGTCTTGAA
MCP-3	Forward	GAGAGCTACAGAAGGACCACCAGT
	Reverse	GGGTCAGCACAGATCTCCTTGT

Gene	Primer	Sequence 5'-3'
MCP-4	Forward	AGGCTGAAGAGCTATGTGATCACC
	Reverse	CCTTGCCCAGTTTGGTTCTG
MIP-2a	Forward	CGCATCGCCCATGGTTAA
	Reverse	CAGTTGGATTTGCCATTTTTCAG
MIP-2b	Forward	CCCATGGTTCAGAAAATCATCG
	Reverse	GTTGGTGCTCCCCTTGTTCA
p21^{WAF1}	Forward	CTGGAGACTCTCAGGGTCGAAA
	Reverse	AGTGGTAGAAATCTGTCATGCTGGT
p53	Forward	ATGGAGGAGCCGCAGTCAG
	Reverse	TCAGTCTGAGTCAGGCCCTTCT
P-selectin	Forward	CCACCAATGTGTGAAGCCATC
	Reverse	TCAGAACAATCCAGGCTGCC
RANTES	Forward	CTCTGCGCTCCTGCATCTG
	Reverse	GCGGGCAATGTAGGCAAA
SDF-1α	Forward	TGCTGGTCCTCGTGCTGAC
	Reverse	TGGCAACATGGCTTTCGAA
TNF	Forward	TCTTCTCGAACCCCGAGTGA
	Reverse	GGAGCTGCCCCTCAGCTT
VCAM-1	Forward	ACGCAAACACTTTATGTCAATGTTG
	Reverse	AGCTGCCTGCTCCACAGG

6.1.6 Consumables

Table 14. Consumables

Consumable	Supplier
1.5 ml, 2 ml safe-lock tubes	Eppendorf
2 ml, 5 ml, 10 ml, 25 ml, 50 ml stripettes	Corning
6-, 24-, 96-(f/v-bottom) well plates	Corning
15 ml, 50 ml tubes, conical base, PP	Sarstedt
96-well f-bottom solid white plate	Thermo Fisher Scientific
Cell culture dish, standard, 100 × 12 mm	Sarstedt
Combitips advanced	Eppendorf
epT.I.P.S.	Eppendorf
FACS tubes, 1.3 ml, PP	Greiner BIO-ONE
Glass tubes, 100 × 12 mm, heavy walled	Glaswarenfabrik Karl Hecht
Immobilon-FL PVDF membrane	Merck
LightCycler 480 Multiwell Plates 96-well	Roche Applied Science
MultiScreen 96-well Transport Receiver Plate	Merck
MultiScreen-MIC Plate 5 μm	Merck
T-75-, T-175-cell culture flasks	Corning

6.1.7 Equipment and devices

Table 15. Equipment and devices

Device	Supplier
AxioObserver Z1 inverted microscope	Zeiss
Bio-Plex 200	Bio-Rad
LC480 qPCR cycler	Roche Applied Science
Leica TCS SP5 Confocal microscope	Leica Microsystems
LSR II flow cytometer	BD Biosciences
Mueller RT-250	Philips
NanoDrop 2000c	Thermo Fisher Scientific
Odyssey® CLx infrared imaging system	LI-COR
RS225 X-Ray research irradiator	Xstrahl
SE 400 Vertical Unit for SDS-PAGE	GE Healthcare
Synergy MX fluorescence reader	BioTek Instruments GmbH
Thermomix comfort	Eppendorf
Trans-Blot transfer cell for western blotting	Bio-Rad

6.1.8 Software

Table 16. Software

Software	Version	Supplier
AliBaba	2.1	Niels Grabe
Excel	2010	Microsoft
FACSDiva	6.1.3	BD Biosciences
FlowJo	7.6.3	Tree Star Inc.
Chemotaxis and Migration Tool	2.0	ibidi
ImageJ	1.47	Open source
Origin	9.1	Microcal
Word	2010	Microsoft

6.2 Methods

6.2.1 Cell culture

6.2.1.1 Cultivation of cancer cell lines

BT-474, HCC1806, HCC1937, MCF7 and THP-1 cells were cultured in RPMI-1640 medium supplemented with 10% heat-inactivated FCS, 100 U/ml penicillin, 0.1 mg/ml streptomycin and 10mM HEPES buffer at 37°C and 5% CO_2. BT-549 and MDA-MB-468 cells were cultivated in DMEM and 1+1 DMEM/F12 medium, respectively, supplemented with 10% FCS, 100 U/ml penicillin, and 0.1 mg/ml streptomycin at 37°C and 7.5% CO_2. For sub-cultivation and seeding for experiments, cells were washed once in PBS and trypsinized at 37°C until a single cell suspension was obtained. The trypsinization process was stopped by adding serum-containing cell culture medium to the cell suspension in excess. The cells were collected and pelleted at 314 g for 5 min. The supernatant was removed, the pellet re-suspended in culture medium and the cells were sub-cultivated or used for experiments.

6.2.1.2 Primary cells

6.2.1.2.1 Human umbilical vein endothelial cells (HUVECs)

HUVECs were cultivated in full endothelial growth medium, consisting of Endothelial Cell Growth Medium and SupplementMix at 37°C and 5% CO_2. Sub-cultivation and seeding for experiments was performed as described for the cancer cell lines. However, the special DetachKit, containing of HEPES-BSS, Trypsin/EDTA and Trypsin Neutralizing Solution, was used for cell detachment: HUVECs were washed in HEPES-BSS buffer before trypsinization. The trypsinization process was stopped by adding equal amounts of Trypsin Neutralizing Solution to the cell suspension, and the centrifugation was performed at 220 g for 3 min.

6.2.1.2.2 Isolation of human peripheral blood monocytes and T cells

Primary human peripheral blood monocytes and T cells were isolated from heparinized blood from healthy donors by positive selection of CD14$^+$ or CD3$^+$ cells, respectively. Heparinized blood was carefully layered on top of the Biocoll Separating Solution and centrifuged continuously for 20 min at 787 g with reduced acceleration and without brake. Afterwards, the cell layer of peripheral blood mononuclear cells (PBMCs) above the Biocoll Separating Solution was collected and washed twice with

PBS. The PBMCs were re-suspended to a concentration of 10^8 cells/ml in ice-cold MACS buffer containing 0.5% bovine serum albumin (BSA, Miltenyi). The re-suspended PBMNCs were incubated with 1× anti-CD14 or anti-CD3 magnetic beads (200 µl beads per 10^8 total cells) on ice for 15 min. Afterwards, cells were washed in BSA MACS buffer and loaded onto a pre-washed MACS Column in the magnetic field of a MACS Separator. After three washing steps with ice-cold BSA MACS buffer, the column was removed from the magnetic field and $CD14^+$ or $CD3^+$ cells were eluted with BSA MACS buffer into a glass tube. The eluted cells were washed in X-Vivo 15 medium, counted, and used for further experiments.

6.2.2 Cell number determination

All cell numbers were determined with a Neubauer improved counting chamber. Single cell suspensions were pipetted into the chamber, and the cells in the four large squares were counted. The mean number of cells within one large square was multiplied with the chamber factor 10,000 in order to obtain the density of the cell suspension in cells/ml.

6.2.3 Growth curve analyses and calculation of doubling times

Cells were seeded into 24-well plates (2.5×10^4 cells per well) in culture medium containing 10% FCS and allowed to adhere for 5 h. Medium was replaced by medium supplemented with 10% or 2.5% FCS, respectively, and cells were grown for up to 4 days. On each day, cells were harvested by trypsin treatment and counted. Growth curves were generated by plotting log cell number (y-axis) versus time in hours (x-axis). The slopes of the corresponding regression lines allowed the calculation of doubling times according to the formula

$$\text{Doubling time [h]} = \log(2)\frac{\Delta\text{time [h]}}{\Delta\log(\text{cells})}$$

6.2.4 X-ray treatment and production of cell-free culture supernatants

Cells were seeded into 6-well ($0.5\text{-}1 \times 10^6$ cells per well) or 24-well plates ($0.3\text{-}1 \times 10^5$ cells per well) in culture medium containing 10% FCS and allowed to adhere overnight. Immediately prior to irradiation, the culture medium was replaced by medium containing 2.5% FCS. For initial experiments, X-ray treatment was performed on a Mueller RT-250 γ-ray tube. After decommissioning of this device, an RS225 X-Ray research irradiator was employed. Both X-ray sources were operated

at 200 kV and 10 mA with a Thoraeus filter (0.38 mm Sn, 0.23 mm Cu, 0.99 mm Al). The dose rates were 1 min 52 s for 1 Gy using the Mueller RT-250 and 1 min 4 s for 1 Gy using the RS225. Fractionated irradiation was carried out every 24 h for up to four days.

For the production of cell-free supernatants, culture supernatants were collected from the 6-well plates at the indicated time points. In order to remove cell debris, supernatants were centrifuged at 10,000 g for 5 min at 4°C and immediately transferred into a fresh tube and stored at -80°C for further use. Thawing of supernatants for experiments was performed in a ThermoMix at 30°C, 1400 rpm for 10 min.

6.2.5 Cell migration analyses

6.2.5.1 Trans-well migration assay

The attraction of monocytic cells by irradiated tumor cells and their releasate was analyzed by trans-well migration assays with THP-1 cells and cell-free culture supernatants of irradiated breast cancer cells. The assays were performed in 96-well MultiScreen-MIC trans-well chambers with 5µm pore size. THP-1 cells in log phase were adjusted to a concentration of 2×10^6 cells/ml in RPMI-1640 supplemented with 10% FCS, and labeled with 1 µM Calcein-AM for 20 min at 37°C and 5% CO_2. The labeled THP-1 cells were washed once in RPMI-1640 supplemented with 10% FCS. 1×10^5 labeled THP-1 cells per well were seeded in a final volume of 80 µl onto the 96-well MultiScreen-MIC filter plate. The filter plate was mounted onto the receiver plate containing 320 µl of cell-free culture supernatants, 200 nM ATP, or 200 ng/ml stromal cell-derived factor 1α (SDF-1α) in serum-free RPMI-1640, respectively. Transmigration was allowed for 90 min at 37°C and 5% CO_2. Subsequently, the filter plate was removed and the transmigrated THP-1 cells in the receiver plate were collected at 314 g for 5 min. After discarding 220 µl of supernatant, THP-1 cells were re-suspended in the remaining medium and transferred into a 96-well v-bottom plate. The v-bottom plate was centrifuged at 314 g for 5 min. The remaining supernatants were discarded entirely and the sedimented THP-1 cells were lysed in 100µl caspase lysis buffer (see Table 5) for 5 min. The lysates were transferred into a 96-well f-bottom plate and green Calcein fluorescence was quantified with a Synergy MX

fluorescence reader (wavelength=Ex. 480+/- 20 nm, Em. 508+/- 20 nm). Transmigrated cells were calculated as percentage of total cells deployed.

For biochemical characterization of the released monocytic attraction signals, cell-free culture supernatants were subjected to ultracentrifugation with VivaSpin 2 centrifuge tubes with an exclusion limit of 10 kDa. Cell-free culture supernatants, 200 nM ATP and 200 ng/ml SDF-1α were centrifuged at 872 g until the entire liquid phase had passed the filter membrane. The filter membrane was rinsed very well with culture medium and both fractions (substances smaller or larger than 10 kDa) were readjusted to the initial volumes employed. Both fractions were applied to a trans-well migration assay.

For further biochemical characterization, cell-free culture supernatants were treated with ATP-diphosphohydrolase (apyrase). Therefore, 500 mU apyrase were added to 1.5 ml cell-free culture supernatants, 200 nM ATP, or 200 ng/ml SDF-1α, respectively. Nucleotide degradation was allowed for 30-50 min at 37°C. Heat-inactivated apyrase (95°C, 40 min) served as control. After apyrase treatment, samples were applied to trans-well migration assays.

The ectonucleotidase CD39 on MCF7 cells was pharmacologically blocked with 100 µM ARL-67156. The MCF7 cells were seeded and irradiated with indicated doses. Then ARL-67156 was added at a final concentration of 100 µM and refreshed daily. Cell-free culture supernatants were produced as described (see chapter 6.2.4) and subjected to transmigration assays.

6.2.5.2 2D chemotaxis assay

To investigate if the induced trans-well migration behavior of monocytic cells to cell-free culture supernatants is directed (chemotaxis) or not (chemokinesis), 2D chemotaxis assays were set up. Therefore, primary monocytes were isolated as described in chapter 6.2.1.2.2 one day before the experiment. After preparation, monocytes were seeded in 6-well plates (1×10^6 cells per well) in 2 ml X-Vivo 15 medium supplemented with 10% autologous serum and incubated overnight at 37°C and 5% CO_2. The next day, monocytes were collected and re-suspended in X-Vivo 15 supplemented with 5% autologous serum. 2.5×10^4 monocytes were seeded into the observation area of a humidified µ-slide 2D chemotaxis chamber and allowed to adhere for 15 min at 37°C and 5% CO_2. Non-adherent monocytes were washed away and both reservoirs of the chamber were filled with X-Vivo 15 supplemented

with 5% autologous serum. Cell-free culture supernatants, 1 μM ATP or 1 μg/ml WKYMVm were added into the upper reservoir. The 2D chemotaxis chamber was mounted onto the heated stage of the AxioObserver Z1 inverted microscope and time-lapse video microscopy was performed at 37°C and 5% CO_2 for 3 h at 5× magnification. Pictures were taken every 2 min and 40 randomly picked cells were tracked with the ImageJ manual tracking plug-in. Analysis window was set from 10 min to 2 h 10 min (2 h time frame). Accumulated distance, Euclidean distance and y forward migration index (yFMI=mean of endpoint y direction/accumulated distance of all tracked cells) were determined with the ibidi chemotaxis and migration tool.

Apyrase treatment of cell-free culture supernatants was performed as described for the trans-well migration assays (see chapter 6.2.5.1).

6.2.6 Flow cytometry

All flow cytometry measurements were performed with an LSR II flow cytometer and data were analyzed with FACSDiva or FlowJo 7.6.3 Software, respectively.

6.2.6.1 PS externalization and plasma membrane integrity

During apoptosis, the phospholipid phosphatidylserine (PS) is exposed on the outer plasma membrane surface. By interaction of Annexin V-FITC (AnxV-FITC) and PS, apoptotic cells can be identified. Loss of plasma membrane integrity is a major event during necrosis. Propidium iodide (PI) is a fluorescent DNA intercalator, which does not penetrate an intact plasma membrane. Hence, PI can only intercalate into DNA in necrotic cells, which have lost plasma membrane integrity. To analyze apoptosis and necrosis, cells were seeded into 24-well plates (0.5-1 × 10^5 cells per well), irradiated with the indicated doses (see chapter 6.2.4), and incubated for up to 4 days. Culture supernatants were collected, and cells were harvested by trypsinization. After pooling both fractions, samples were washed in 1× Annexin staining buffer (diluted in ddH$_2$O). Each sample was incubated in 50 μl 1× Annexin staining buffer containing 5 μl AnxV-FITC and 2 μg/ml PI at 4°C for 15 min. After washing in 1× Annexin staining buffer, cells were analyzed by flow cytometry. Cells positive for AnxV-FITC were considered as apoptotic and cells double positive for AnxV-FITC and PI as necrotic. To distinguish between primary and secondary necrosis, cells were treated with 50 μM of the poly-caspase inhibitor carbobenzoxy-valyl-alanyl-aspartyl-[O-methyl]-fluoromethylketone (zVAD-fmk) 30 min prior to irradiation. Necroptosis was excluded

by inhibiting the receptor-interacting protein kinase 1 (RIPK1), a central kinase in the necroptotic pathway, with 50 µM necrostatin-1 30 min prior to irradiation.

6.2.6.2 Senescence-associated β-galactosidase activity

Upregulation of senescence-associated β-galactosidase (SA-β-gal) and increase in granularity are common markers, which can be employed for the identification of senescent cells [119]. Cells were seeded in 24-well plates ($0.5\text{-}1 \times 10^5$ cells per well) and irradiated as described. At the indicated time points after irradiation, cells were incubated with 100 nM bafilomycin A1 in serum-free medium for 1 h at 37°C for lysosomal alkalization. Subsequently, the green fluorogenic SA-β-gal substrate 5-dodecanoylamino-fluorescein-di-β-galactopyranoside (C12-FDG) was added at a final concentration of 50 µM, and substrate conversion was allowed for 1 h at 37°C. After two washing steps with PBS, cells were collected by trypsinization, re-suspended in PBS and analyzed by flow cytometry. Cells with high FITC and high sideward scatter (SSC) signals were considered senescent.

6.2.6.3 Ectonucleotidase surface expression

For the detection of ectonucleotidases on the outer cell surface, cells were seeded in 6-well plates (5×10^5 cells per well) and irradiated as described (see chapter 6.2.4). Cells were harvested by trypsinization at the indicated time points, and 2 µl anti-CD39-PE, anti-CD73-FITC, anti-CD203c-APC or isotype controls were added to 1×10^5 cells in 50 µl FACS staining buffer. After incubation for 30 min on ice, cells were washed twice in FACS staining buffer, and fluorescence of PE, FITC, and APC was analyzed by flow cytometry. Relative surface expression was calculated as the median fluorescence intensities of anti-ectonucleotidase staining subtracted by the corresponding isotype controls.

6.2.6.4 Dendritic cell surface markers

To investigate the influence of tumor-derived signals on the differentiation of monocytes to dendritic cells, the expression of characteristic dendritic cell surface markers (CD40, CD80, CD83, CD86, and HLA-DR) was measured by flow cytometry. Primary human peripheral blood monocytes were isolated as described in chapter 6.2.1.2.2. After isolation, 2×10^5 monocytes per well were seeded into 24-well plates in 400 µl serum-free X-Vivo 15 and incubated for 1 h at 37°C and 5% CO_2. The medium was removed, and monocytes were incubated in 300 µl of conditioned cell-

free culture supernatants (see chapter 6.2.4) or 200 ng/ml Lipopolysaccharides (LPS) (in serum-free X-Vivo 15) for 4 h at 37°C and 5% CO_2. Subsequently, 300 μl X-Vivo 15 supplemented with 20% autologous serum and GM-CSF and IL-4 at final concentrations of 20 ng/ml and 40 ng/ml, respectively, were added. Monocytes were incubated for 5 days at 37°C and 5% CO_2. On day 3 after isolation, GM-CSF and IL-4 were renewed. Dendritic cells were harvested by trypsinization on day 5. After trypsinization, dendritic cells were washed with ice-cold FACS staining buffer and transferred into a 96-well v-bottom plate on ice. 2 μl of anti-CD40-PE-Cy5, anti-CD80-PE, and 0.5 μl of anti-CD83-PE-Cy7, anti-CD86-Alexa Fluor700 or isotype controls for a total volume of 50 μl in FACS staining buffer were added followed by incubation for 30 min on ice in the dark. Thereafter, dendritic cells were washed twice in FACS staining buffer, and fluorescence of PE-Cy5, PE, PE-Cy7, and Alexa Fluor700 was analyzed by flow cytometry. Relative surface marker expression was calculated as described for ectonucleotidase expression (see chapter 6.2.6.3). The fold increase was calibrated on the 0 Gy sample.

Biochemical characterization of tumor-derived signals influencing CD80 expression was carried out as described for the trans-well migration assays (see chapter 6.2.5.1). LPS was used as a positive control. Instead of apyrase, the cell-free culture supernatants were digested with the protein-degrading enzyme Proteinase K (20 μg/ml) for 30 min at 37°C.

Furthermore, the influence of tumor-derived signals on the maturation of differentiated dendritic cells was investigated. Therefore, monocytes were isolated as described before in the differentiation assay. However, monocytes were first differentiated to dendritic cells for 5 days in X-Vivo 15 supplemented with 10% autologous serum and 20 ng/ml GM-CSF and 40 ng/ml IL-4, before cell-free culture supernatants or 100 nM TNF (in serum-free X-Vivo 15) were added, respectively. The treatment protocol and the FACS analysis were performed analogously to the differentiation assay.

6.2.6.5 Phagocytosis assay

Phagocytosis of irradiated HCC1937 breast cancer cells by dendritic cells was analyzed by co-incubation of both cell types stained with different fluorescent dyes. Human peripheral blood monocytes were isolated as described in chapter 6.2.1.2.2. After isolation, monocytes were stained with the green membrane labeling dye

PKH67. Therefore, monocytes were diluted in Diluent C to a concentration of 4×10^7 cells/ml in a glass tube and PKH67 was added at a final concentration of 1 μM. Monocytes were stained for 1.5 min. The staining process was stopped by diluting the reaction 1 + 1 with 100% FCS.

After 1 min, monocytes were washed in X-Vivo 15 supplemented with 10% autologous serum and seeded into a T75 flask. For the differentiation of monocytes to dendritic cells, 20 ng/ml GM-CSF and 40 ng/ml IL-4 were added. Monocytes were incubated for 5 days at 37°C and 5% CO_2, whereby GM-CSF and IL-4 were renewed 3 days after isolation. On the day of monocyte isolation, HCC1937 cells were stained with the orange cell membrane labeling dye PKH26 according to the PKH67 staining protocol for monocytes. However, HCC1937 cells were diluted to a concentration of 2×10^7 cells/ml, PKH26 was added at a final concentration of 2 μM, and staining was allowed for 5 min. The stained HCC1937 cells were seeded into 24-well plates (3-10 $\times 10^4$ cells per well) in RPMI-1640 medium supplemented with 10% FCS. On the next day, labeled HCC1937 were irradiated with the indicated doses (see chapter 6.2.4). On day 5 after monocyte isolation and HCC1937 seeding, dendritic cells were collected and co-incubated with the irradiated HCC1937 cells at the indicated ratios (target to effector cells T:E) for 2 h at 37°C and 5% CO_2. After co-incubation, cells were collected by trypsinization and analyzed by flow cytometry. Percentage of phagocytosis was calculated as the percentage of PKH67/PKH26 double-positive dendritic cells on the basis of all dendritic cells deployed (positive for PKH67). Active phagocytosis of HCC1937 cells by dendritic cells was confirmed by treatment with cytochalasin D, an inhibitor of actin filament polymerization. Dendritic cells were treated with 20 μM cytochalasin D 1 h before co-incubation with HCC1937 cells.

6.2.6.6 Allogeneic mixed leukocyte reaction

Apart from dendritic cell differentiation and phagocytosis, the influence of tumor-derived signals on the induction of T cell proliferation by dendritic cells was studied. To this end, human peripheral blood monocytes and T cells were isolated as described in chapter 6.2.1.2.2 from two allogeneic blood donors. After isolation, monocytes were allowed to adhere in 6-well plates (1×10^6 cells per well) for 1 h in 2 ml serum-free X-Vivo 15 at 37°C and 5% CO_2. The medium was removed, and monocytes were incubated in 1.5 ml cell-free culture supernatants, 100 ng/ml TNF, or serum-free X-Vivo 15 for 4 h, respectively. Afterwards, dendritic cell differentiation

was initiated by adding 20 ng/ml GM-CSF and 40 ng/ml IL-4 in 1.5 ml X-Vivo 15 supplemented with 20% autologous serum. GM-CSF and IL-4 were renewed on day 3 and 5 after isolation. On day 7 after isolation, dendritic cells were detached by adding 1 ml ice-cold 5 mM EDTA in PBS and incubation for 5 min on ice. Detached dendritic cells were collected and washed in serum-free X-Vivo 15. 2×10^4 dendritic cells per well were seeded into a 96-well f-bottom plate in 100 µl serum-free X-Vivo. On the same day as dendritic cell seeding, T cells were isolated from an allogeneic blood donor. After washing in serum-free X-Vivo 15, T cells were re-suspended in prewarmed (37°C) 0.1% BSA in PBS at a final concentration of 1×10^6 cells/ml and stained with 0.5 µM of the green fluorescent dye CFSE for 10 min at 37°C. Staining was stopped by adding an excessive volume of ice-cold serum-free X-Vivo 15 to the T cells, following incubation on ice for 5 min. CFSE-stained T cells were washed three times in serum-free X-Vivo 15 and finally re-suspended in X-Vivo 15 supplemented with 20% human AB-serum to a concentration of 1×10^6 cells/ml. 100 µl of the T cell suspension were added to the dendritic cells (DC to T cell ratio=1:5) and both cell types were co-incubated for 5 days at 37°C and 5% CO_2. Afterwards, T cells were collected and washed in PBS. T-cells were re-suspended in 100 µl ice-cold FACS staining buffer and transferred into 96-well v-bottom plates. After centrifugation (314 g, 5 min, 4°C), the supernatants were discarded, and 1 µl of anti-CD3-PE-Cy7, 2 µl of anti-CD4-PE, and 2 µl of anti-CD8-APC or isotype controls in 50 µl FACS staining buffer were added to the T cells. Antibody binding was allowed for 30 min on ice in the dark. Subsequently, T cells were washed twice in FACS staining buffer, and fluorescence of CFSE, PE-Cy-7, PE, and APC was analyzed with the flow cytometer. Since CFSE is distributed equally to the two daughter cells of a dividing T cell, loss of CSFE fluorescence intensity is a marker for cell proliferation. The percentage of proliferated $CD4^+$ and $CD8^+$ T cells was calculated as the amount of $CD3^+CFSE^{low}CD4^+$ or $CD3^+CFSE^{low}CD8^+$ cells on the basis of all $CD3^+CD4^+$ or $CD3^+CD8^+$ cells, respectively. The fold increase in T cell proliferation was calibrated on the 0 Gy sample.

6.2.6.7 Leukocyte infiltration into air pouches

The different subsets of myeloid cells infiltrating into the air pouches in response to HCC1937 cell-free culture supernatants were analyzed by flow cytometry. Therefore, air pouches on the back of 9-10 weeks old female Balb/c mice were generated and

stimulated as described in chapter 6.2.9. At indicated time points, mice were euthanized, and the pouches were washed three times with physiological saline solution (154 mM NaCl). The washing solutions were combined, and infiltrated cells were pelleted (314 g, 5 min). Cell pellets were washed in FACS staining buffer and re-suspended in 500 µl FACS staining buffer for cell counting (see chapter 6.2.2). Afterwards, 0.1 to 0.5 × 10^6 cells were stained either with 0.5 µl of anti-CD45-APC-Cy7, anti-CD11b-FITC, anti-CD11c-PerCP-Cy5.5, anti-F4/80-eFluor450, anti-Ly6C-PE-Cy7, anti-Ly6G-BUV395, anti-H-2-Alexa Fluor700, anti-PDCA1-APC, and anti-Siglec-H-PE or isotype controls in 50 µl FACS staining buffer for 20 min on ice in the dark. Stained cells were washed twice with FACS staining buffer, re-suspended in 100 µl FACS staining buffer, and subjected to flow cytometry. The gating strategy for the discrimination of different leukocyte subsets is shown in Figure 7.
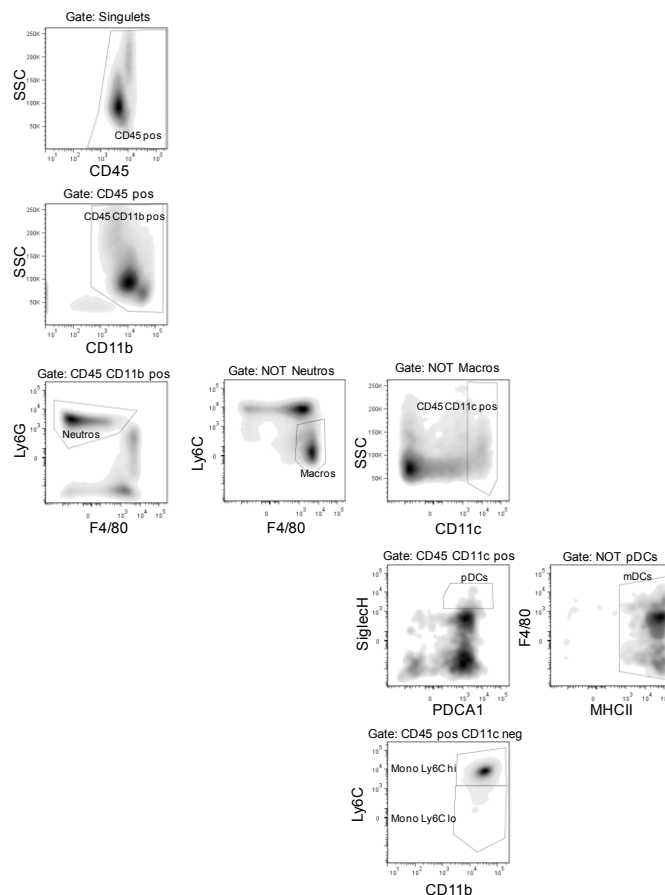
Figure 7 Gating strategy for the discrimination of infiltrating myeloid subpopulations.

Within all CD45$^+$ cells (after doublet discrimination), CD11b$^+$ cells were determined to identify leukocytes of the innate immune system. Among these, neutrophils (Ly6G$^+$F4/80$^-$) and macrophages (Ly6C$^-$F4/80$^+$) were identified. To distinguish between dendritic cells and monocytes, CD11c expression was used. Among dendritic cells (CD11c$^+$), plasmacytoid dendritic cells (Siglec-H$^+$PDCA1$^+$) and myeloid dendritic cells (F4/80$^-$H-2$^+$) were subclassified. Monocytes (CD11c$^-$) were divided into the two known murine subsets by their Ly6C expression: Inflammatory (Ly6C^{hi}) and resident (Ly6C^{low}).

Absolute cell numbers of each leukocyte subset were calculated on the basis of all CD45$^+$ cells. To obtain absolute CD45$^+$ cell numbers, measured CD45$^+$ cells of each sample were normalized on measured singlet events and multiplied by the total cell numbers obtained from the air pouch lavages. The absolute numbers of each leukocyte subset were calculated on the basis of the leukocyte subset percentage (ratio between measured leukocyte subset events and CD45$^+$ events of each sample) multiplied by absolute CD45$^+$ cell numbers.

6.2.7 Molecular biology

6.2.7.1 RNA extraction and quantification

Total RNA was extracted from cells by using the NucleoSpin® RNA kit II according to the supplier's protocol. Breast cancer cells were seeded into 6-well plates (0.5-2 × 10^6 cells per well) in medium supplemented with 10% FCS and irradiated with the indicated doses as described (see chapter 6.2.4). After incubation for the indicated times, medium was removed, cells were washed with ice-cold PBS and collected with a rubber spatula on ice. Cell suspensions were transferred into 2 ml tubes on ice, centrifuged (16,200 g, 5 min, 4°C) and dry cell pellets were stored at -80°C. For RNA isolation, the cell pellets were lysed in 350 µl RA1 buffer (from the NucleoSpin® RNA kit II) supplemented with 1% 2-Mercaptoethanol. Nucleic acids were precipitated with 70% ethanol and bound to a silica membrane. Subsequently, the membrane was desalted, and contaminating DNA was digested with rDNase for 15 min at room temperature. The samples were washed three times and eluted in RNase-free H$_2$O. The concentration and purity of the extracted RNA was measured on a NanoDrop 2000c UV-Vis spectrometer. The RNA concentration was calculated based on Lambert-Beer's law with the absorption of the RNA solution at 260 nm and the specific extinction coefficient for a pure RNA solution at a concentration of 40 ng/ml. The purity of the RNA solution is described by the ratio of the solution's absorption at 260 nm and 280 nm (A260/A280 ratio). An A260/A280 ratio between 1.7 and 2.0 is generally defined as pure for RNA solutions. The isolated RNA was stored at -80°C for further use.

For preparation of HUVEC RNA after incubation with the relevant stimuli, supernatants were removed, and cells were directly lysed in 350 µl RA1 buffer from

the NucleoSpin® RNA kit II supplemented with 1% 2-Mercaptoethanol. Subsequent RNA extraction was done as described for breast cancer cells.

6.2.7.2 Reverse transcription

To obtain cDNA for quantitative real-time PCR, 1 µg of RNA was reversely transcribed with 200 U Revert Aid H Minus M-MuLV reverse transcriptase in the presence of 50 µM random hexamers, 5 µM Oligo(dT)$_{18}$, 400 µM dNTPs, and 1 U/µl Ribolock RNase inhibitor. First, RNA was mixed with random hexamers, Oligo(dT)$_{18}$, and dNTPs and heated to 65°C for 15 min. After chilling on ice, reverse transcriptase and RNase inhibitor, both provided in reaction buffer, were added to the RNA. For reverse transcription, samples were incubated at 25°C for 10 min, following heating to 42°C for 60 min allowing reverse transcription, and heat inactivation at 72°C for 10 min. The synthesized cDNA was stored at -20°C until further use.

6.2.7.3 Quantitative real-time PCR

The expression levels of genes of interest (see Table 13) were analyzed by quantitative real-time PCR. 20-80 ng cDNA were mixed with 300 nM forward and reverse primers (sequences see Table 13), and 1× Maxima SYBR Green qPCR Master Mix. Real-time PCRs were performed with a standard cycling protocol (10 min 95°C, 45 × (15 s 95°C, 30 s 60°C)) on an LC480 qPCR cycler. Relative quantification was performed using the standard curve method and results were normalized to the means of 18S rRNA, β$_2$-microglobulin, and δ-ALAS. The fold increase was calculated on the basis of the respective medium sample.

6.2.8 Protein methods

6.2.8.1 SDS-PAGE

2-4.5 × 10^6 cells were seeded in cell culture dishes in medium supplemented with 10% FCS and irradiated on the next day as described in chapter 6.2.4. At the indicated time points, cells were collected with a rubber spatula on ice and transferred into 2 ml tubes. After washing with ice-cold PBS, dry cell pellets were stored at -80°C until lysis. 1 × 10^6 Cells were lysed in 100 µl western blot lysis buffer (see Table 5) for 20 min on ice with occasional vortexing. Lysates were cleared by centrifugation (16,200 g, 10 min, 4°C) and transferred to fresh tubes on ice.

To determine the protein content of the cell lysates, Bradford protein assays [120] were performed. For protein quantification, an 8-point BSA standard curve (0-300 µg/ml in PBS) was used. Cell lysates were diluted with H_2O to appropriate concentrations in the range of the standard curve. Bradford standards and cell lysates were mixed with 1× Bradford Reagent in a ratio of 1:50 (final volume 250 µl) in a 96-well f-bottom plate and incubated for 5 min at room temperature. The absorption was measured at 595 nm. Protein concentrations of cell lysates were intrapolated from the standard curve. 300 µg protein per sample was used for gel electrophoresis.

Denaturing, reducing gel electrophoresis for separation of proteins was carried out on linear gradient gels with an acrylamide content of 6-15%. Two separation gels with 6% and 15% acrylamide were prepared by mixing separation gel buffer (pH 8.8, see Table 5), and an appropriate amount of Rotiphorese® Gel 30 (30% acrylamide, 0.8% bis-acrylamide) in ddH$_2$O. Polymerization was started by addition of 0.1% APS, and catalyzed by 0.08% TEMED (see Table 5). Both separation gel mixtures were transferred into a gradient mixer connected with the gel apparatus. After casting, the gradient separation gel was covered with 2-propanol and polymerization was allowed for 1 h. After polymerization, 2-propanol was discarded, and the top of the separation gel was washed with H_2O. For the stacking gel, stacking gel buffer (pH 6.8, see Table 5), and an appropriate amount of Rotiphorese® Gel 30 (30% acrylamide, 0.8% bis-acrylamide) were mixed in ddH$_2$O. Polymerization was started by addition of 0.1% APS, catalyzed by 0.08% TEMED (see Table 5), and the stacking gel was cast onto the separation gel. A comb was placed into the stacking gel to create sample slots, and polymerization was allowed for 20 min. The gel was mounted into the gel electrophoresis chamber, and buffer reservoirs were filled with 1× SDS-PAGE running buffer (see Table 5). Samples were mixed with Laemmli buffer (final: 1× concentrated, see Table 5), boiled at 95°C for 5 min, spun down (16,200 g, 5 min) and loaded into the stacking gel slots with a Hamilton syringe. For the estimation of protein size, a pre-stained protein ladder (PageRuler™) was used. Electrophoresis was run with 800 Vh until the bromophenol blue front had reached the lower edge of the gel.

6.2.8.2 Western blotting and immunodetection

Following separation by gel electrophoresis, proteins were transferred onto Immobilon-FL PVDF membranes employing a tank-blot system from Bio-Rad. PVDF

membranes were equilibrated in 100% methanol, washed in H_2O and rinsed in 1× western blot transfer buffer without methanol (see Table 5). The western blot sandwich was assembled according to the supplier's protocol and protein transfer was allowed for 2 h at 4°C at 0.5 A in western blot transfer buffer supplemented with 20% methanol. After protein transfer, PVDF membranes were blocked with western blot blocking buffer (see Table 5) for 1 h at room temperature. The blocked membranes were washed twice in western blot washing buffer (see Table 5), and incubated with primary monoclonal mouse anti-p21^{WAF1} (1:1000) or anti-vinculin (1:1000) antibodies overnight at 4°C. Thereafter, membranes were washed three times and incubated with the corresponding secondary IRDye-conjugated antibody (1:20,000) for 1 h at room temperature. Finally, after extensive washing in western blot wash buffer, IRDye fluorescence was read with an LI-COR Odyssey® CLx infrared imaging system.

6.2.8.3 Immunofluorescence microscopy of important adhesion molecules on HUVECs

All immune fluorescence pictures were recorded on an AxioObserver Z1 inverted microscope at 63× magnification. The immune fluorescence staining procedure of the adhesion molecules ICAM-1, VCAM-1 and E-selectin on HUVECs was carried out without fixation on native cells. HUVECs were seeded onto sterile cover slips into 24-well plates (4×10^4 cells per well) in full endothelial growth medium and incubated at 37°C and 5% CO_2. After 48 h of adherence, HUVECs were incubated with 400 µl of conditioned cell-free culture supernatants diluted 1:2 in full endothelial growth medium, 50 ng/ml TNF, or full endothelial growth medium, respectively, for 4 h at 37°C and 5% CO_2. HUVECs were washed carefully with FACS staining buffer before they were stained with 6 µl of anti-ICAM-1-PE, or anti-VCAM-1-PE or anti-E-selectin-PE and Hoechst-33342 (1:500) in 150 µl FACS staining buffer for 30 min on ice in the dark. HUVECs were washed twice with FACS staining buffer and mounted with 5 µl Fluoromount. The cover slips were sealed upside down onto glass slides with nail polish before microscopy.

6.2.8.4 Quantification of ICAM-1 expression on HUVECs

Surface expression of ICAM-1 on HUVECs was carried out as described for the immunofluorescence microscopy of adhesion molecules. However, HUVECs were

seeded in 96-well f-bottom plates (9,000 HUVECs per well) in full endothelial growth medium and incubated up to 48 h at 37°C and 5% CO_2. Induction of ICAM-1 with 190 µl of 1:2 diluted cell-free culture supernatants and controls was carried out as described in chapter 6.2.8.3. HUVECs were washed carefully in FACS staining buffer and incubated with 2 µl of anti-ICAM-1-PE or isotype in 50 µl FACS staining buffer for 30 min at 4°C in the dark. HUVECs were washed twice with FACS staining buffer, and PE-fluorescence was measured on a Synergy Mx plate reader (wavelength=Ex. 480+/- 20 nm, Em. 578+/- 20 nm). Relative surface expression of ICAM-1 was calculated by subtraction of the fluorescence intensity of the matching isotype control, and the fold increase was calibrated on the 0 Gy sample.

6.2.8.5 Multiplex immunoassays

The concentrations of cytokines and chemokines released from HUVECs in response to tumor-derived signals were measured on a Bio-Plex 200 System. The panel of reactants is shown in Table 17. Assays were performed according to the manufacturer's protocol with commercial 1 × 96 well kits (see Table 6 and Table 17). The commercial kits included standards, the detection antibody, reagents and buffers needed for the Multiplex assays. For sample generation, HUVECs were seeded and treated with 1:2 diluted cell-free culture supernatants or controls as described for the qRT-PCR experiments (see chapter 6.2.7.1). After 4 h incubation, supernatants were harvested as described in chapter 6.2.4 and stored at -80°C until analysis. 50 µl of HUVEC supernatant were incubated with 2.5-5 µl chemokine-binding beads for 1 h at room temperature. Following three washing steps, 1.25-2.5 µl biotinylated detection antibody was added in 25 µl diluent buffer, and samples were incubated for 30 min at room temperature. Subsequently, the biotinylated detection antibody was bound by PE-labeled streptavidin (1:10 in assay buffer) and samples were measured in the Bio-Plex 200 system. 50 beads per region within the doublet discriminator gates (5,000-25,000) were recorded per sample. Chemokine concentrations were calculated on the basis of the standard curves formerly cleared from outliers.

Table 17. Measured chemokines in the Bio-Plex Pro Human Chemokine Assay

CCL3	CCL15	CCL17	CCL19	CCL20	CCL22	CCL23	CCL25
CX3CL1	CXCL1	CXCL2	CXCL6	CXCL9	CXCL16	Eotaxin-1	Eotaxin-2
Eotaxin-3	GM-CSF	HCC1/2	I-309	IL-1β	IL-2	IL-4	IL-6
IL-8	IL-10	IL-16	IFNγ	IP-10	I-TAC	MCP-1	MCP-2
MCP-3	MCP-4	MIF	MIP-2a	RANTES	SDF-1α	TNF	

6.2.8.6 ELISA

6.2.8.6.1 Detection of HSP70

HSP70 levels in the supernatants of dying HCC1937 cells were measured with the DuoSet® IC ELISA kit from R&D Systems according to the supplier's protocol. Reagents, buffers, and antibodies necessary for the ELISA were included in the DuoSet® IC kit. The substrate solution for the color reaction was a 9:1 mixture of Solution B and Solution A from the TMB Peroxidase EIA Substrate kit (see Table 6). Briefly, cell-free culture supernatants of irradiated HCC1937 cells were produced as described in chapter 6.2.4. Each incubation step of the ELISA was carried out at room temperature (except the capture antibody coating) and, after each incubation, the 96-well plate was washed three times with washing buffer. One day before analysis, a 96-well f-bottom solid white plate was coated with 100 µl capture antibody (2 µg/ml) per well at 4°C in the dark overnight. On the day of the ELISA, the coated 96-well plate was blocked for 2 h with 100µl blocking buffer. Samples were diluted 1:10 in serum-free RPMI-1640 medium and 100 µl were transferred into the blocked 96-well plate. After incubation for 2 h, the 96-well plate was incubated with 100 µl of biotinylated detection antibody (100 ng/ml) per well for another 2 h. For the color reaction, 100 µl streptavidin coupled HRP (1:200) per well were added into the 96-well plate for 20 min. The substrate solution was mixed as mentioned above, 100 µl were added, and substrate conversion was allowed for 20 min. The color reaction was terminated with 50 µl stopping solution before reaching saturation, and absorption was measured at 450 nm on the Synergy Mx reader. HSP70 concentrations were calculated by using an 8-point standard curve of purified human HSP70 (0-10 ng/ml).

6.2.8.6.2 Detection of HMGB1

For the quantification of HMGB1 released from irradiated HCC1937 cells, the HMGB1-ELISA kit from IBL International was used. The kit included a pre-coated 96-well microtiter plate and all reagents and buffers necessary for the HMGB1-ELISA. All steps were carried out according to the supplier's protocol. The incubation steps were carried out at room temperature. Cell-free culture supernatants of HCC1937 cells were produced as described in chapter 6.2.4. In the HMGB1-ELISA, 100 µl diluent buffer per well were added to a pre-coated 96-well microtiter plate and 10 µl

of standards, a positive control (pig HMGB1), and cell-free culture supernatants (1:5 diluted in serum-free RPMI-1640) were added after incubation for 24 h, the plate was washed five times with 1× washing buffer and 100 µl enzyme conjugate were added to each well. 2 h later, the plate was washed again five times and samples were exposed to the color solution for 25-30 min. The color reaction was terminated with stopping solution, and absorption was measured at 450 nm on the Synergy Mx. Concentrations of HMGB1 in cell-free culture supernatants were calculated using a 7-point standard curve (0-80 ng/ml).

6.2.8.6.3 Detection of S100A8/A9

The detection of S100A8/A9 in cell-free culture supernatants of irradiated HCC1937 cells was kindly performed by Prof. Dr. Thomas Vogl at the Institute of Immunology of the University of Muenster, Muenster, Germany, according to their inhouse ELISA protocol [121].

6.2.9 The air pouch mouse model

In order to determine the attraction of myeloid cells by supernatants of irradiated HCC1937 cells in vivo, the air pouch mouse model was used [122]. For pouch generation, the backs of 9-10 weeks old female BALB/c mice were depilated before 5 ml of sterile air were injected subcutaneously. After 3 days, 3 ml sterile air were reinjected. At day 7 after pouch generation, 1 ml of cell-free culture supernatants of HCC1937 cells 4 days after irradiation (see chapter 6.2.4) was injected into the air pouches. As negative and positive control, 1 ml of RPMI-1640 supplemented with 2.5% FCS, and 1 ml of 50 ng/ml mouse TNF in RPMI-1640 supplemented with 2.5% FCS were used, respectively. At the indicated time points, pouches were lavaged 3x with 2 ml saline, and the resulting cell suspensions were subjected to FACS analyses of leukocyte subsets (see chapter 6.2.6.7 In addition to the air pouch lavage, the skin of each air pouch was isolated for further confocal microscopy studies of leukocyte subsets (see chapter 6.2.10).

Throughout the experiments, mice received water and food ad libitum, and mice were kept in individual cages at standard conditions (humidity 55-65%, temperature 22-24°C) with a 12 h day/night cycle. All studies were performed in accordance to the guidelines of the Federation of European Laboratory Animal Science Associations (FELASA) and were approved by the *Regierung von Oberbayern*.

6.2.10 Confocal microscopy of air pouch skin

For confocal microscopy of leukocyte subsets, the air pouch skin samples were fixed in 3.5% paraformaldehyde (in 1× PBS) for 1 h. The fixed air pouch skin samples were handed to Dr. Gabriele Zuchtriegel from the Walter Brendel Centre of Experimental Medicine, Klinikum der Universität München, Munich, Germany, who kindly performed the staining and confocal microscopy on a Leica TCS SP5 Confocal microscope. The fixed skin samples were washed in 1× PBS and permeabilized in 0.1% Triton X-100 containing 2% BSA at 4°C overnight. On the next day, the permeabilized samples were stained with 1:100 diluted anti-CD31-Alexa Fluor647 (detection of vessels), anti-F4/80-Alexa Fluor488 (detection of monocytes/macrophages), and anti-Ly6G (detection of neutrophils) antibodies at 4°C for 72 h. The stained samples were washed three times in 1× PBS, and the secondary anti-Rat IgG-Alexa Fluor546 antibody was added (1:400) for visualization of Ly6G. After 3 h of incubation at room temperature, the samples were washed three times in 1× PBS, and embedded in PermaFluor mounting medium between microscope slides and cover slips. After drying at room temperature, confocal microscopy was performed.

6.2.11 Statistical analyses

Data are presented as means ± standard deviation, unless stated otherwise. Statistical significance was tested by two-tailed, unpaired Student's t-test or ANOVA; p-values <0.05 were considered as significant. For determination of linear correlation between distinct values, Pearson's correlation coefficient was calculated. Principal component analysis was carried out in OriginPro 9.1 as previously described [123].

7 Results

7.1 Different breast cancer cell lines vary in p53 status and doubling time

To cover the spectrum of breast cancer varieties, a panel of three breast cancer cell lines with different molecular subtypes, varying in hormone receptor and epidermal growth factor receptor expression as well as p53 status, was chosen (Figure 8A).

A

Breast cancer cell line	Mol. subtype	Tumor type	ER	PR	Her2/ neu	p53
BT474	Luminal	invas. duct. ca.	+	+	+	285 E>K
MCF7	Luminal	invas. duct. ca.	+	+	-	WT
HCC1937	Basal A	prim. duct. ca.	-	-	-	306 R>Stop
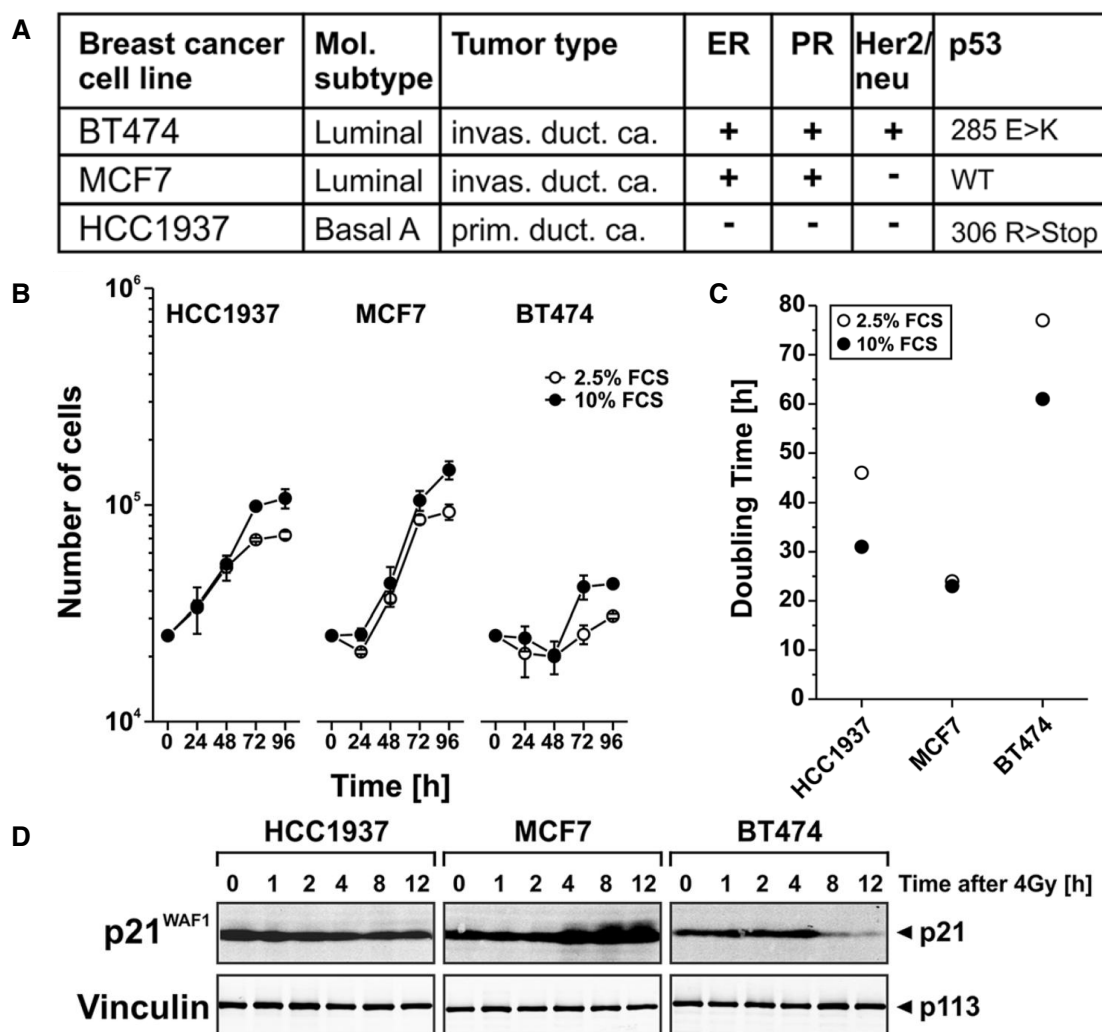
Figure 8 Breast cancer cell lines of different origin vary in doubling time and p53 functionality (adapted from [124]).

(A) List of breast cancer cell lines used in the present study. Molecular subtype, tumor type, and receptor expression pattern have been described [124]. The p53 mutational status was determined by cDNA sequencing. **(B)** Growth curves of breast cancer cell lines were investigated in the presence of 2.5% or 10% FCS, respectively. Means ± s.d. of triplicates are shown. **(C)** Doubling times of breast cancer cells calculated on the basis of the data shown in **(B)**. **(D)** p53 functionality was verified by induction of p21[WAF1] in whole cell lysates after irradiation with 4Gy at the indicated time points by 6-15% SDS-PAGE (300µg protein extract per lane) followed by immunoblot analysis. Vinculin served as a loading control.

BT-474 and MCF7 cells represent a common form of breast cancer in elderly women and with good prognosis (estrogen receptor positive, with or without Her2 overexpression and p53 mutated or wild-type, respectively), while HCC1937 cells represent an aggressive form of breast cancer, mostly found in young women with poor prognosis (i.e. tumor growth is independent of hormone receptors and Her2/neu overexpression (triple-negative phenotype), and mutated p53).

The mutation status of p53 in the three breast cancer cell lines was determined by cDNA sequencing. The functionality of p53 was verified by irradiation-induced upregulation of the p53 target p21^{WAF1} (Figure 8D). Starting 4 h after irradiation with 4 Gy, an increase in p21^{WAF1} protein levels was observed in the p53 wild-type cell line MCF7. This increase was stable for up to 12 h after irradiation. In BT-474 and HCC1937 cells, both mutated in p53, irradiation did not induce an increase in p21^{WAF1} as expected. The proliferation rates of the three cell lines showed clear differences with short (MCF7), intermediate (HCC1937) and long (BT-474) doubling times in the presence of 2.5% FCS (Figure 8B, C). Hence, the differences between breast cancer cells of distinct origin are mirrored not only by varying expression of hormone/growth receptors and p53 mutation status, but also by proliferation rate.

7.2 Breast cancer cell lines respond differently to distinct ionizing radiation regimens

Next, the cellular responses of the breast cancer cells to ionizing radiation were investigated. With regard to the clinical practice, single low dose (1 × 2 Gy), fractionated (4 × 2 Gy), and ablative (1 × 20 Gy) irradiation was performed. Non-irradiated cells served as a control. Induction of apoptosis, necrosis, and senescence was measured flow cytometrically for 1 to 4 days upon irradiation (Figure 9A). Primary and secondary (post-apoptotic) necrosis were distinguished by using the poly-caspase inhibitor zVAD-fmk, which impedes apoptosis and the subsequent transit into secondary necrosis (Figure 9B). The necroptosis inhibitor necrostatin-1 was employed to delineate the contribution of necroptosis (Figure 9C). There were clear differences in the cell death profiles of the three cell lines: Slow-proliferating BT-474 cells showed very low levels of apoptosis or primary or secondary necrosis after irradiation.
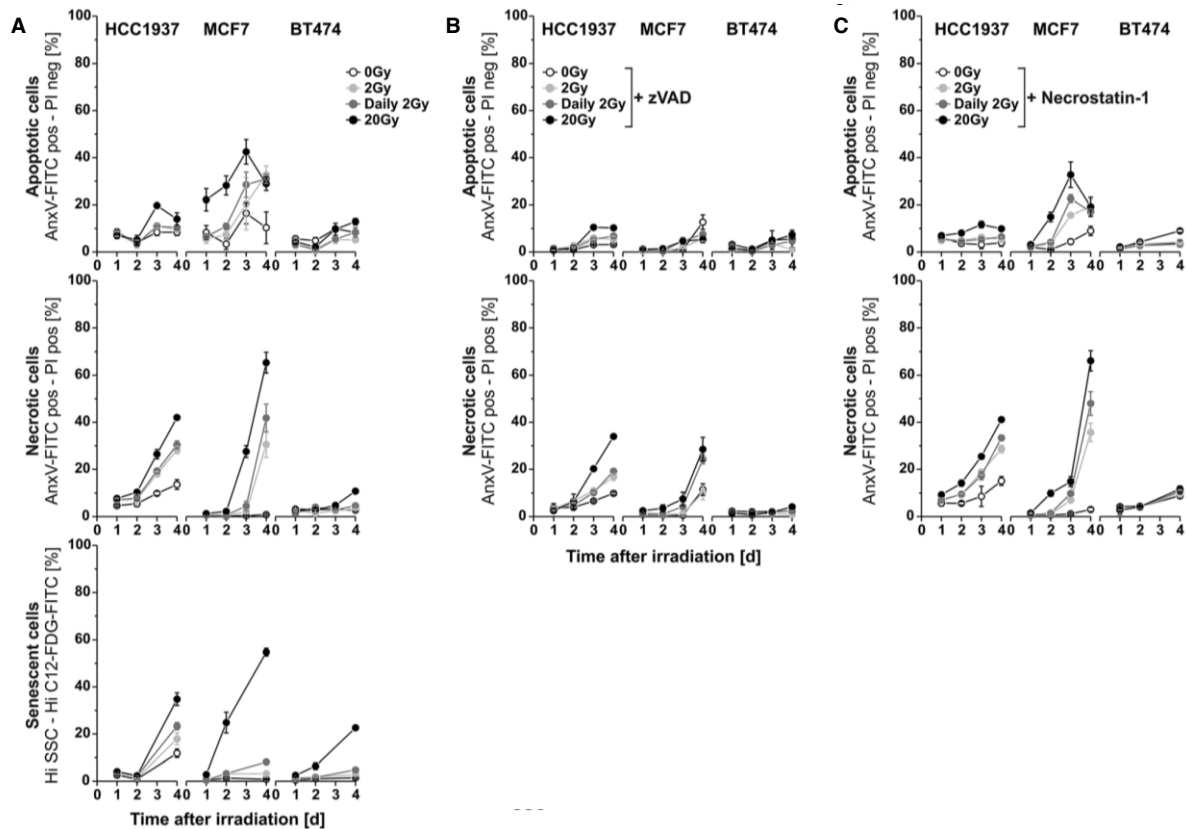
Figure 9 Induction of apoptosis, necrosis, and senescence by ionizing radiation in different breast cancer cell lines is dependent on the irradiation regimen (modified from [124])

(A) Induction of apoptosis, necrosis, and senescence in breast cancer cell lines was measured by flow cytometry over 4 days after irradiation. Cells were irradiated with 2 Gy, daily 2 Gy, and 20 Gy or left untreated as control. Apoptosis and necrosis were determined by Annexin V-FITC/PI staining. Annexin V-FITC positive, PI negative cells were considered as apoptotic, Annexin V-FITC/PI double positive cells as necrotic. Senescence induction was measured by SA-β-gal staining with the fluorogenic substrate C12-FDG. Cells with high SSC and high C12-FDG signal were considered senescent. Means ± s.d. of triplicates are shown. **(B)** Determination of secondary necrosis. Apoptosis and necrosis induction were measured as in **(A)** in the presence of 50 µM of the poly-caspase inhibitor zVAD-fmk. Means ± s.d. of triplicates are shown. **(C)** Determination of necroptosis. Apoptosis and necrosis induction were measured as in **(A)** in the presence of 50 µM of the necroptosis inhibitor necrostatin-1. Means ± s.d. of triplicates are shown.

A strong induction of primary necrosis was observed in HCC1937 cells after ablative irradiation, and fast-proliferating MCF7 cells revealed a strong increase in apoptosis, especially after ablative irradiation, and, consequently, high levels of secondary necrosis. However, MCF7 cells also underwent primary necrosis after ablative irradiation to a comparable extent as HCC1937 cells did. None of the cell lines showed relevant levels of necroptosis, but induction of senescence was clearly detectable in all three cell lines, particularly after ablative irradiation. In conclusion, the most prominent cell death effects were observed in fast-proliferating breast

cancer cells after ablative irradiation. In cells with wild-type p53, a combination of apoptosis, primary, and secondary (post-apoptotic) necrosis was the major consequence, whereas cells lacking functional p53 mainly underwent primary necrosis and senescence.

7.3 Dying breast cancer cells can attract monocytic cells

One of the first steps in the induction of an adaptive immune response is the recruitment of antigen-presenting cells (APCs) to sites of pathogen invasion or tissue damage, where pathogen- and/or danger-associated molecular patterns (PAMPs or DAMPs, respectively) are enriched. APCs are attracted by 'find-me' signals released from dying cells [125]. To examine the APC attracting potential of dying breast cancer cells, cells were irradiated with the aforementioned radiation regimens, and conditioned cell-free culture supernatants were subjected to transmigration assays with the monocytic cell line THP-1 (Figure 10A). Time-dependent transmigration of THP-1 cells was observed with supernatants of ablatively irradiated HCC1937 cells. The extent of THP-1 transmigration paralleled the levels of primary necrosis in HCC1937 cells (see Figure 9). Attraction of THP-1 cells by supernatants generated upon fractionated irradiation was significantly lower than in case of supernatants of ablatively irradiated cells. Importantly, culture supernatants of irradiated BT-474 or MCF7 cells only marginally attracted THP-1 cells, irrespective of the radiation regimen and incubation time applied. Since BT-474 cells did not show any measurable cell death induction upon radiation (see Figure 9), this result was expected. However, the extent of primary (and secondary) necrosis in MCF7 cells after ablative irradiation was comparable to that of HCC1937 cells (see Figure 9), but THP-1 cell attraction was not observed. Before addressing this issue, the biochemical composition of the attraction signals released from HCC1937 cells was further characterized. Numerous dying cell-derived 'find-me' signals have been described in the literature [9]. The molecular entities range from proteins (e.g. HSP70, HSP90, HMGB1) to small molecules, such as nucleotides (e.g. ATP, UTP) and monosodium urate crystals.
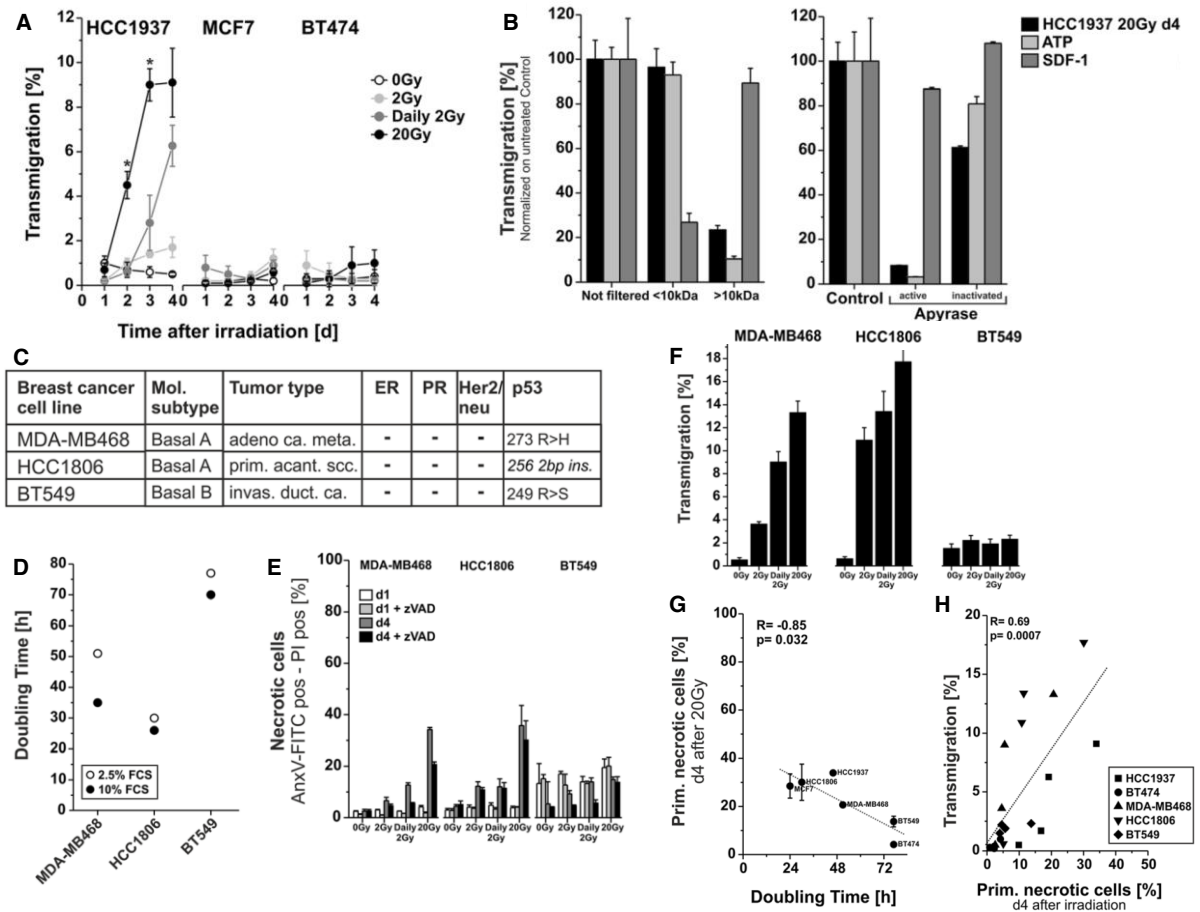
Figure 10 Primary necrotic, fast-proliferating and p53 mutated irradiated breast cancer cells attract monocytic cells by releasing nucleotides after irradiation (adapted from [124]).

(A) Trans-well migration of THP-1 cells to cell-free culture supernatants of irradiated HCC1937, MCF7, and BT-474 cells. Breast cancer cells were irradiated as in Figure 9, and supernatants were isolated on day 1-4 after irradiation. Means ± quadruplicates are shown. Asterisks indicate p<0.05 as determined by unpaired Student's *t*-test (20 Gy vs. daily 2 Gy). **(B)** Biomolecular characterization of monocytic attraction signals. Cell-free culture supernatants of HCC1937 cells irradiated with 20 Gy were collected on day 4 after irradiation, and subsequently subjected to ultracentrifugation with Vivaspin 2 columns (molecular weight cut-off 10 kDa) or apyrase treatment (33.3 milliunits active or heat-inactivated apyrase/ml, 30 min at 37°C). Culture medium supplemented with 200 nM ATP or 200 ng/ml SDF-1α served as controls. After treatment, supernatants were subjected to trans-well migration assays with THP-1 cells. The percentage of transmigrated cells was normalized on the corresponding untreated samples. Means ± s.d. of quadruplicates are shown. **(C)** Additional breast cancer cell lines used in the present study. The molecular subtype, the tumor type, and the receptor expression have been described [124]. The p53 mutational status was determined by cDNA sequencing. HCC1806 cells gave no PCR product, but the mutation in codon 256 was described in the literature [124]. **(D)** Growth curves of additional breast cancer cell lines were determined as in Figure 8. **(E)** Necrosis induction ± 50µM zVAD-fmk was measured at the indicated doses as in Figure 8. Means ± s.d. of triplicates are shown. **(F)** Trans-well migration of THP-1 cells to cell-free culture supernatants of irradiated MDA-MB468, HCC1806, and BT-549 cells. Cell-free culture supernatants of irradiated breast cancer cells were collected on day 4 after irradiation and subjected to trans-well migration assays with THP-1 cells as in **(A)**. Means ± s.d. of quadruplicates are shown. **(G)** Fast-proliferating breast cancer cells undergo primary necrosis after ablative irradiation as revealed by Pearson's correlation analysis between doubling time and percentage of primary necrosis on day 4 after ablative irradiation. **(H)** Fast-proliferating, p53 mutated breast cancer cells showing a strong induction of primary necrosis upon

ablative irradiation are the source of monocytic attraction signals. Pearson's correlation analysis was performed between percentage of transmigration and primary necrosis on day 4 after ablative irradiation.

For biochemical characterization of the responsible attraction signals in our experimental setting, ultracentrifugation against a membrane with 10 kDa cut-off and apyrase (nucleotide-diphosphatase) digestion were performed with HCC1937 supernatants collected 4 days after ablative irradiation. ATP (apyrase-sensitive, M_w=507 Da) and SDF-1α (apyrase-insensitive, M_w=11 kDa) served as controls. The results show that ablatively irradiated, necrotic HCC1937 cells release apyrase-sensitive compounds with an apparent molecular weight <10 kDa, which are responsible for THP-1 attraction (Figure 10B). Hence, nucleotides appear to be the relevant 'find-me' signals in this scenario.

To confirm the conclusions of the transmigration assays, three additional cell lines with comparable properties to HCC1937 cells, i.e. triple-negative and p53 mutant, were chosen (Figure 10C). HCC1806 and MDA-MB-468 cells revealed short doubling times similar to HCC1937 cells, whereas BT-549 had a slow-proliferation rate similar to that of BT-474 cells (Figure 10D). Fast-proliferating HCC1806 and MDA-MB-468 cells showed high levels of primary necrosis after ablative irradiation, while slow-proliferating BT-549 cells did not (Figure 10E). Correlation analyses between the extent of primary necrosis induction and doubling time revealed that the faster cells proliferated, the more primary necrosis was induced after ablative irradiation (Figure 10G). Transmigration assays with cell-free culture supernatants of BT-549, HCC1806, and MDA-MB-468 cells collected 4 days after irradiation confirmed the observation that only fast-proliferating cells (HCC1806 and MDA-MB-468) release THP-1 attraction signals, preferentially upon ablative irradiation (Figure 10F). Since (primary) necrotic cells are known to release 'find-me' signals, the positive correlation between THP-1 cell migration and the percentage of primary necrotic cells suggests that primary necrotic cells are the source of the attraction signals (Figure 10H).

In summary, fast- but not slow-proliferating, triple-negative, and p53 mutant breast cancer cells predominantly undergo primary necrosis, particularly after ablative irradiation. Primary necrosis is accompanied by the release of nucleotides which in turn attract monocytic cells.

7.4 Monocytic cell attraction is prevented by ectonucleotidases expressed on dying, p53 wild-type breast cancer cells

Although MCF7 cells are fast-proliferating, and high levels of primary necrosis are induced by ablative irradiation (see Figure 8, Figure 9), they do not release THP-1 cell attracting 'find-me' signals (Figure 10). Considering that nucleotides were identified as the responsible monocytic attraction signals, the expression of nucleotide-degrading enzymes (i.e. ectonucleotidases) on the surface of BT-474, HCC1937, and MCF7 cells was investigated (Figure 11).
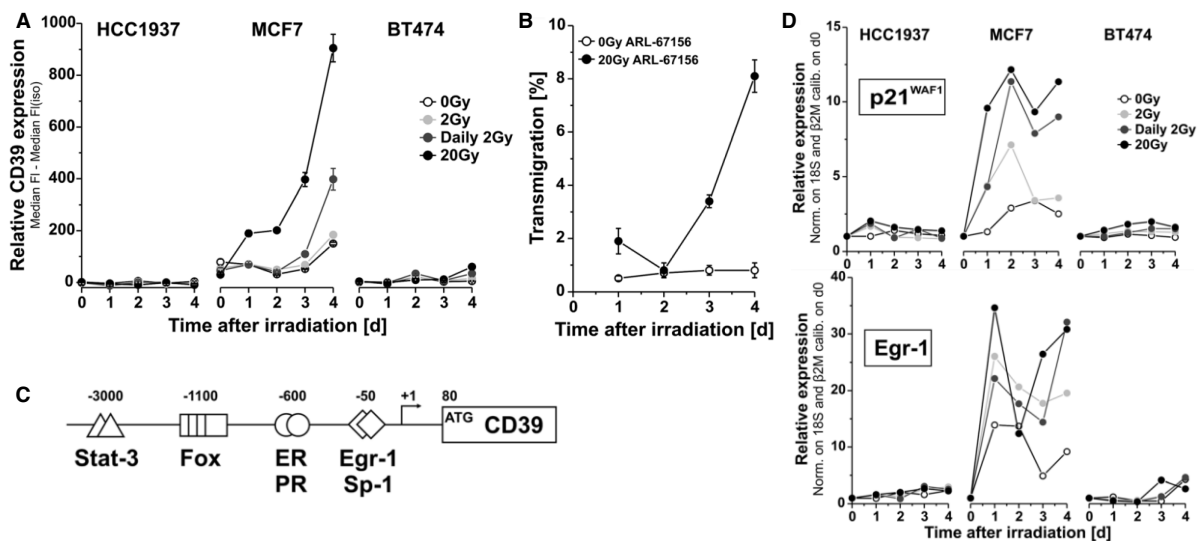
Figure 11 Nucleotide-guided transmigration is abrogated by upregulation of CD39 in MCF7 cells upon irradiation (adapted from [124]).

(A) Relative CD39 surface expression on breast cancer cell lines after irradiation with the indicated doses. Flow cytometric measurements were performed on day 4 after irradiation. Relative fluorescence was calculated as the medians of anti-CD39 staining subtracted by corresponding isotype controls. Means ± s.d. of triplicates are shown. **(B)** Trans-well migration of THP-1 cells to cell-free culture supernatants of irradiated MCF7 cells after pharmacological inhibition of CD39. Upon irradiation with the indicated doses, 100 µM of the CD39 inhibitor ARL-67156 were added to MCF7 cells and refreshed daily. MCF7 supernatants were collected up to 4 days after irradiation, and subjected to trans-well migration assays. Means ± s.d. of quadruplicates are shown. **(C)** In silico analysis of the CD39 promotor revealed putative binding sites for the female sexual hormone receptors (ER, PR), as well as Sp-1, Egr-1, Stat3, and members of the fork head transcription factor family (Fox). **(D)** Time-course analysis of p21^{WAF1} (*upper panel*) and Egr-1 (*lower panel*) mRNA expression in breast cancer cell lines upon irradiation. mRNA was isolated on day 0-4 after irradiation with the indicated doses and analyzed by qRT-PCR. Results were normalized on the means of 18S rRNA and β_2-microglobulin and calibrated on the d 0 controls. Means of duplicates are shown.

In contrast to HCC1937 and BT-474, the ectonucleotidase CD39 was already basally expressed on MCF7 cells, and its expression level increased strongly in a time- and dose-dependent manner upon irradiation (Figure 11A). Inhibiting CD39 with the small

molecule inhibitor ARL-67156 restored THP-1 cell migration towards cell-free supernatants of ablatively irradiated MCF7 cells suggesting that extracellular nucleotides released by necrotically dying MCF7 cells are degraded by CD39, thus preventing monocyte attraction (Figure 11B).

The mechanisms responsible for the differences of CD39 expression between MCF7, HCC1937 and BT-474 cells are poorly understood. Putative binding sites for transcription factors were identified in the promotor region of CD39 by in silico analysis using the AliBaba 2.1 platform (Figure 11C). Among those, estrogen and progesterone receptor binding sites were found. These hormone receptors are suitable candidates for the regulation of CD39 expression, since MCF7 cells are positive for both. Yet, BT-474 cells are also hormone receptor positive (see Figure 8), but do not express CD39. In contrast to BT-474 cells, MCF7 cells possess wild-type p53. It has been reported that the estrogen receptor and p53 can act coordinately as regulators of target gene expression [126] [127] [128], hence providing an explanation for the basal expression of CD39 on MCF7 cells. The irradiation-induced increase in CD39 expression on MCF7 cells might as well depend on functional p53 (and the estrogen receptor), because p53 is activated upon irradiation. This activation was confirmed by the upregulation of the p53 target p21^{WAF1} on mRNA and protein level (Figure 11D). Another transcription factor, whose binding site was found within the CD39 promotor is Egr-1. Egr-1 expression is known to be induced by ionizing radiation [129] as confirmed by our qRT-PCR analyses (Figure 11D), thus strengthening the role of Egr-1 as potential candidate which modulates ionizing radiation-induced upregulation of CD39.

Taken together, irradiation-induced expression of the ectonucleotidase CD39 in MCF7 cells is apparently responsible for the degradation of dying cell-derived, THP-1 attracting nucleotides.

7.5 In vitro attraction of monocytic cells by nucleotides released from primary necrotic breast cancer cells is not directed

Leukocyte attraction to sites of infection or inflammation is finely regulated by directional signals, i.e. attraction signal gradients. However, trans-well migration assays do not allow any conclusion concerning the directionality of migration (directed vs. not directed). This question was addressed in 2D chemotaxis assays, in which migration paths of individual cells can be delineated (Figure 12).
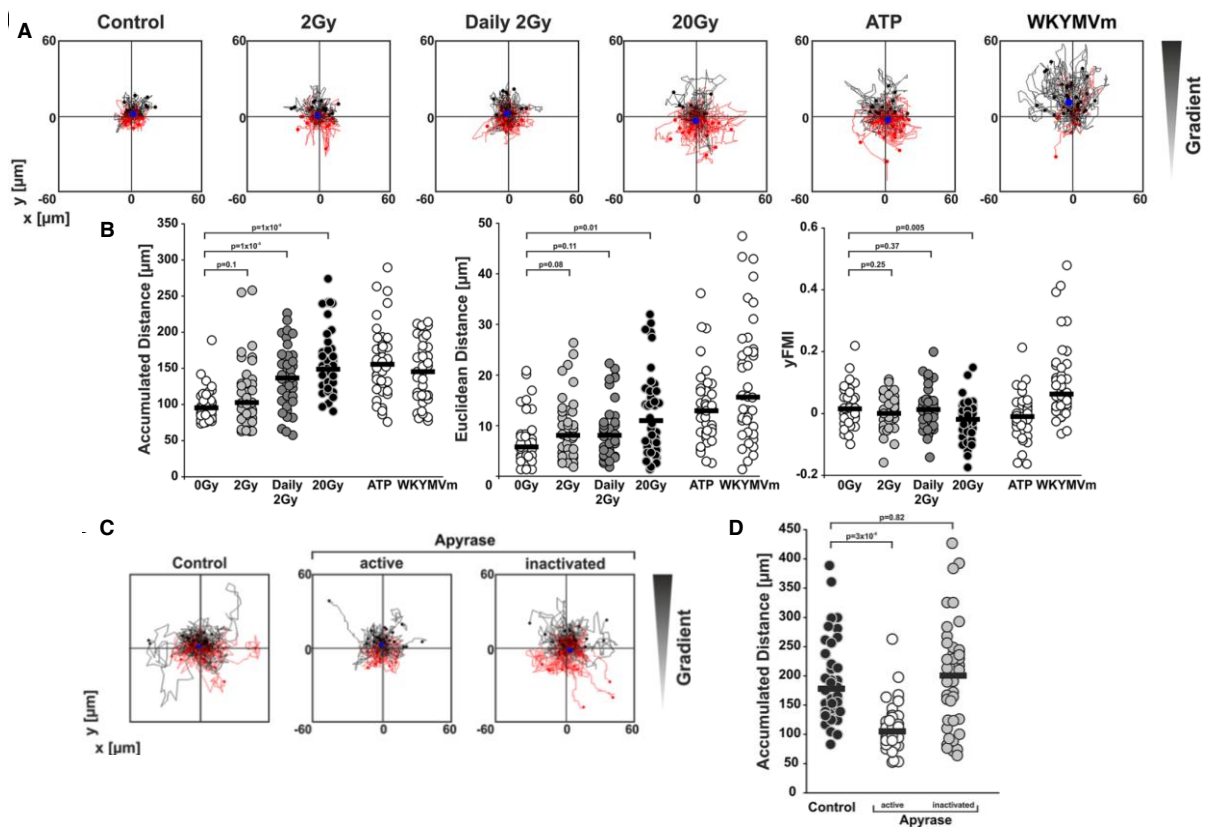
Figure 12 Nucleotides released from necrotic HCC1937 breast cancer cells induce undirected migration of monocytes in vitro (adapted from [124]).

(A) Chemotaxis/chemokinesis of primary human monocytes to cell-free culture supernatants of irradiated HCC1937 cells. HCC1937 cells were treated with the indicated doses. On day 4 after irradiation, cell-free culture supernatants were collected and subjected to 2D chemotaxis/chemokinesis assays with primary human monocytes. Live-cell tracking was performed in ibidi µ-slide chemotaxis 2D chambers for 2 h. ATP (1 µM) and the FPR-agonist WKYMVm (1 µg/ml) served as controls. Trajectory paths of 40 randomly picked cells are shown. Monocytes with net migration in the direction of the gradient are depicted in black, those with net migration in opposite direction are depicted in red. The center of mass is represented by the filled blue circle. **(B)** Parameters of monocyte migration behavior. Trajectory paths of 40 randomly picked cells as shown in **(A)** were analyzed for accumulated distance, Euclidean distance (linear distance between start- and endpoint of migration), and forward migration index in y-direction to the gradient (yFMI=endpoint in y-direction/accumulated distance). Time frame for analysis was 2 h. Bars indicate the median values of 40 cells analyzed. p-values were determined by unpaired Student's *t*-test against 0 Gy. **(C)** Chemokinesis-inducing attraction signals are apyrase-sensitive. Cell-free culture supernatants of HCC1937 cells, irradiated with 20 Gy, were harvested on day 4 after irradiation, and treated with apyrase (33.3 milliunits active or heat-inactivated apyrase/ml, 30 min at 37°C). Subsequently, 2D chemotaxis/chemokinesis assays with primary human monocytes were performed as in **(A)**. **(D)** The accumulated distance was analyzed as in **(B)**. Bars indicate the median values of 40 randomly cells analyzed. p-values were determined by unpaired Student's *t*-test against 0 Gy.

Here, the migratory behavior of primary human monocytes towards cell-free supernatants of irradiated HCC1937 cells was similar to that of the ATP control: Cells

migrated faster and over longer distances than in the not irradiated controls, but migration was not directed as compared to the chemotactic formyl-peptide receptor agonist WKYMVm (Figure 12A). Accumulated and euclidean distances were significantly increased with cell-free supernatants of irradiated HCC1937 cells in comparison to the not irradiated controls. However, the forward migration index (yFMI) as a measure of directionality was clearly positive only for WKYMVm. Again, the strongest effects were seen when cell-free supernatants of ablatively irradiated HCC1937 cells were used as stimulus (Figure 12B). Apyrase digestion virtually abrogated migration of primary human monocytes towards cell-free supernatants of ablatively irradiated HCC1937 cells (Figure 12C, D).

In conclusion, monocyte migration stimulated by necrotic cell-derived nucleotides upon irradiation is not chemotactic, but rather chemokinetic (i.e. non-directional). Alone, nucleotides obviously fail to orchestrate directional leukocyte migration – a finding which has also been reported by others [130] [55]. However, the obtained data were generated in vitro. In vivo, other mediators and cell populations might well contribute to directional leukocyte recruitment by dying cancer cells.

7.6 Cells of the innate immune system are recruited by dying breast cancer cells in vivo

To investigate the attraction potential of cell-free supernatants of irradiated HCC1937 cells in vivo, an air pouch model was used. Supernatants were injected into the air pouches of BALB/c mice, and infiltrating myeloid cell populations were examined over 3-24 h (Figure 13). Confocal microscopy analyses of the airpouch skin revealed a clear accumulation of Ly6G$^+$ neutrophils, probably infiltrated from the small vessels into the tissue, as early as 3 h after supernatant injection, which further increased during the next 3 h (Figure 13A). 12 h after injection, neutrophils gradually disappeared, and a substantial increase in F4/80$^+$ monocytes/macrophages was detected until 24 h after injection.

Importantly, clear differences between the injected supernatants were observed: Whereas supernatants of non-irradiated HCC1937 cells induced infiltration of neutrophils and monocytes/macrophages only marginally and to a comparable extent as unconditioned control medium did, supernatants of irradiated HCC1937 cells led to a strong infiltration of myeloid cell subsets, particularly in case of the ablative and the fractionated irradiation regimens.
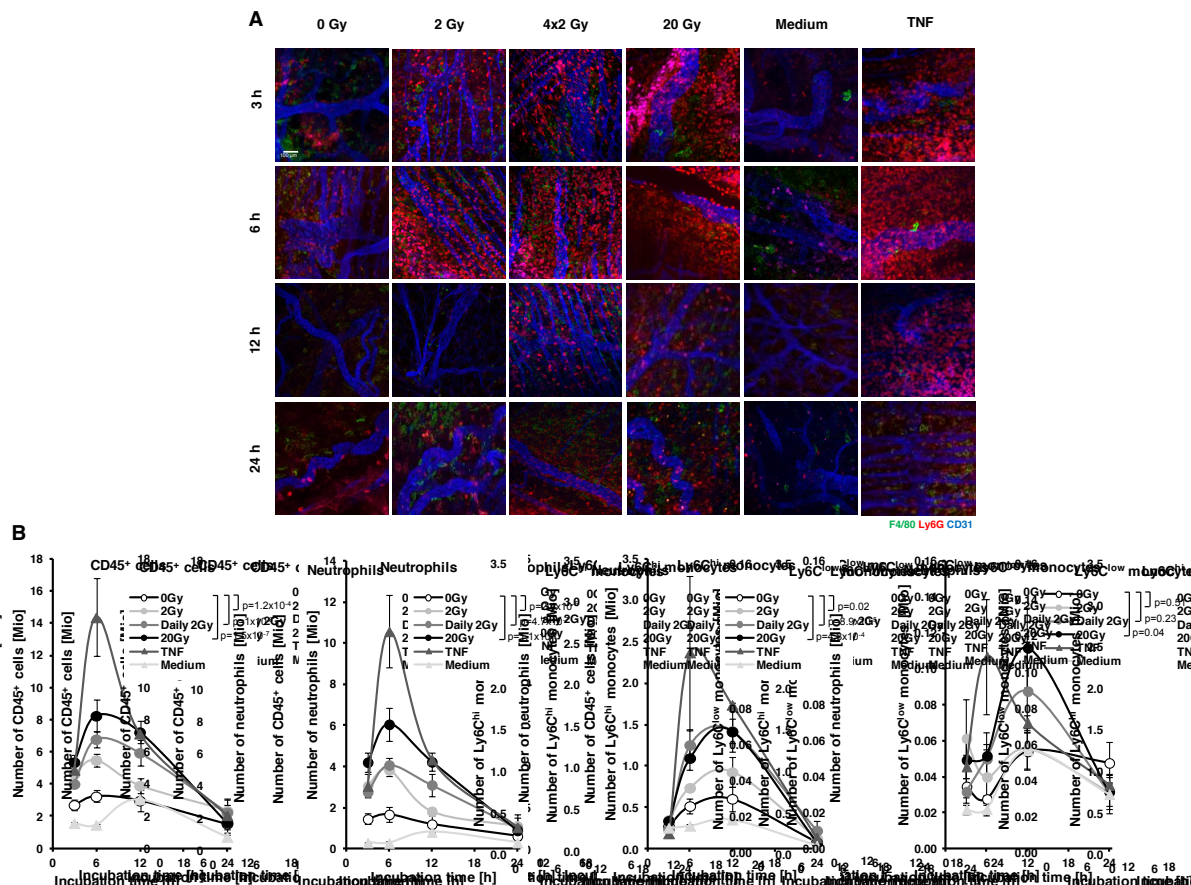
Figure 13 Neutrophils and monocyte subsets are actively recruited by supernatants of irradiated breast cancer cells in vivo.

In the air pouch mouse model, 1 ml of supernatants of irradiated HCC1937 cells (collected 4 days after irradiation with the indicated doses) was injected into the pouches of Balb/c mice (n=6 per radiation treatment schedule). Fresh culture medium (n=2) and TNF (50 ng/ml, n=2) served as controls. **(A)** Representative confocal microscopy pictures of air pouch skin samples after injection of the indicated supernatants. Air pouch skin samples were isolated 3 h, 6 h, 12 h, and 24 h after injection. Upon fixation and permeabilization, air pouch skin samples were stained with primary anti-F4/80-Alexa Fluor488 for the visualization of macrophages (green), anti-CD31-Alexa Fluor647 for endothelial cell surface staining (blue), and anti-Ly6G combined with secondary anti-rat IgG-Alexa Fluor546 for the visualization of neutrophils (red). **(B)** Flow cytometric analyses of leukocyte infiltration into air pouches. The pouch lavages were collected at the indicated time points after injection and infiltrating leukocyte subsets were stained against various surface markers for flow cytometric analysis. For greater detail and gating strategy, see Figure 7. *Panels from left to right:* Time-dependent infiltration of CD45$^+$ leukocytes, neutrophils, Ly6C^{hi} monocytes, and Ly6C^{low} monocytes into air pouches are shown in total numbers. Means ± s.e.m are depicted. Comparison of curves from irradiated samples to 0 Gy was performed by two-way ANOVA. Data of additional leukocyte subsets are not shown.

Quantitative flow cytometry analyses of the pouch lavages further strengthened the observations from confocal microscopy (Figure 13B). The numbers of CD45$^+$ cells that were recruited into the air pouches clearly increased over time, with a maximum around 6 h after injection. Later on, CD45$^+$ cell numbers decreased again reaching baseline levels 24 h after injection. Apart from the positive control TNF, the strongest

effects were observed with supernatants of ablatively irradiated HCC1937 cells. CD45$^+$ cell recruitment was clearly attenuated with supernatants of fractionatedly (4x2 Gy) and single low dose (2 Gy) irradiated cells, and it was basically not detectable with supernatants of non-irradiated controls. Subclassification of CD45$^+$ cells into neutrophils and monocytic subsets (Ly6C^{low} and Ly6C^{hi}) revealed that neutrophils were the dominating cell fraction, and that the kinetic pattern was similar to that of all CD45$^+$ cells. In contrast, Ly6C^{hi} and Ly6C^{low} monocytes, which were recruited in smaller but well detectable absolute numbers, displayed a delayed infiltration pattern reaching a maximum 12 h after supernatant injection. Only in case of Ly6C^{low} but not for Ly6C^{hi} monocytes recruitment by supernatants of ablatively irradiated exceeded recruitment stimulated by supernatants of fractionatedly irradiated cells.

Taken together, neutrophils and monocytes are potently recruited by supernatants of irradiated breast cancer cells into air pouches in vivo, and the highest numbers of infiltrating myeloid cells are observed with supernatants of ablatively irradiated samples. The question that arises at this point is how directionless chemokinesis as observed in vitro can be converted into directional recruitment in vivo.

7.7 Endothelial cells are activated by proteins released from dying breast cancer cells

A *conditio sine qua non* in leukocyte recruitment is the activation of endothelial cells. This includes upregulation of adhesion molecules and the release and/or deposition of distinct cytokines and chemokines on the luminal surface of the endothelium [81]. To analyze this aspect in the context of breast cancer radiotherapy, primary human umbilical vein endothelial cells (HUVECs) were treated with cell-free supernatants of irradiated HCC1937 cells, as well as TNF as positive and unconditioned medium as negative control. Surface expression of the adhesion molecules E-selectin, ICAM-1 and VCAM-1 was visualized by immunofluorescence (Figure 14A).

Clear differences between the radiation regimens were observed: HUVECs treated with supernatants of 2 Gy and daily 2 Gy irradiated HCC1937 cells showed only limited upregulation of E-selectin, ICAM-1, and VCAM-1 on their surface. In contrast, HUVECs exposed to supernatants of ablatively irradiated HCC1937 cells strongly upregulated E-selectin, ICAM-1, and VCAM-1 expression on their surface. Signal quantification for ICAM-1 clearly showed that supernatants of 2 Gy and daily 2 Gy

irradiated HCC1937 cells had only moderate, whereas supernatants of ablatively irradiated HCC1937 cells had strongest effects on adhesion molecule expression on HUVECs (Figure 14B).
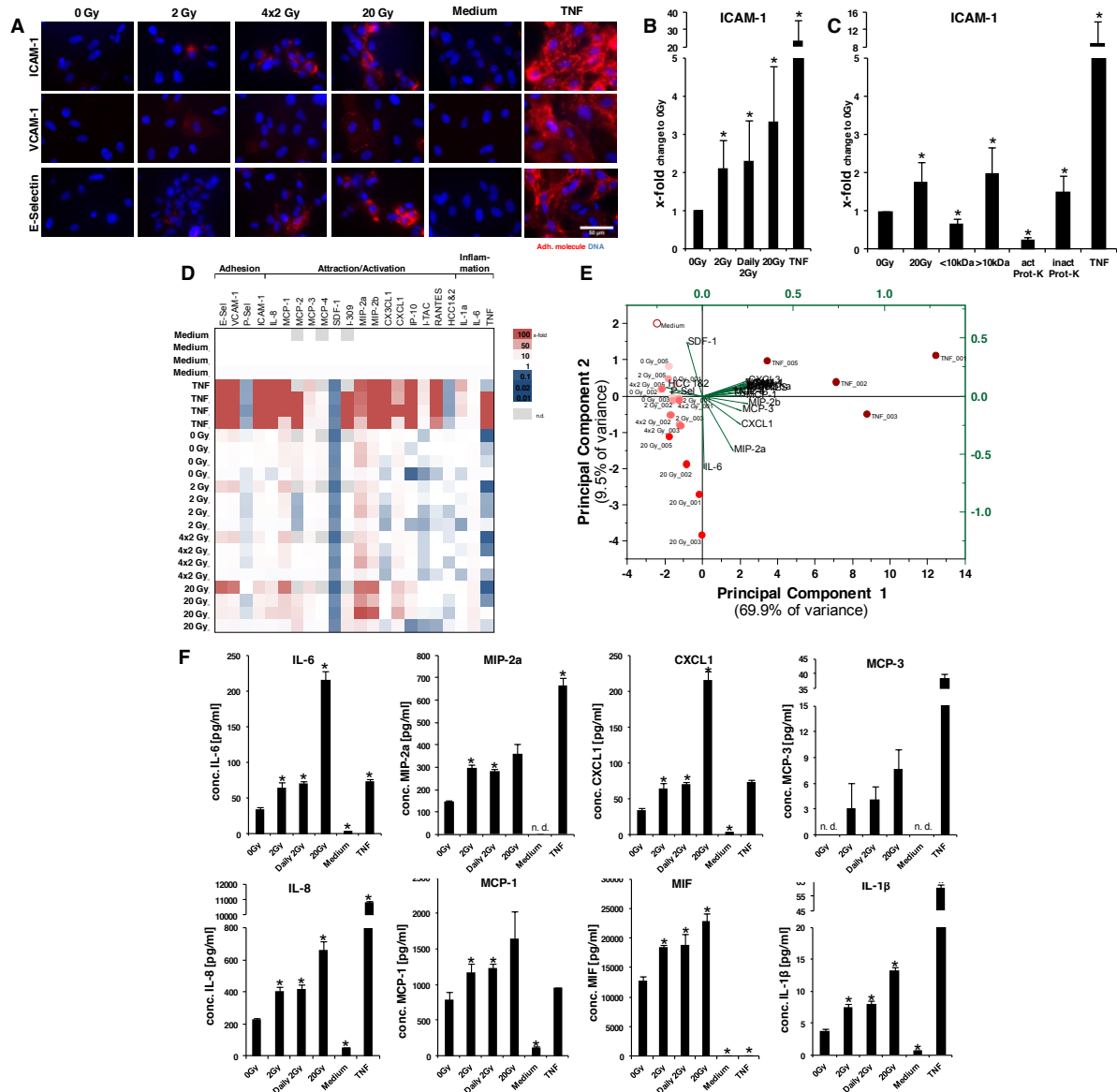

Figure 14 Endothelial cells are activated by dying breast cancer cell-derived protein DAMPs.

HUVECs were exposed for 4 h to cell-free culture supernatants of irradiated HCC1937 cells collected on day 4 after irradiation. Supernatants were diluted 1:2 in endothelial growth medium prior to HUVEC exposure. Endothelial growth medium alone and TNF (50 ng/ml) served as controls. **(A)** Representative immune fluorescence pictures of HUVECs after incubation with indicated samples. For immune fluorescence microscopy, HUVECs were natively stained with anti-ICAM-1-PE (*upper row*; red), anti-VCAM-1-PE (*middle row*; red), or anti-E-selectin-PE (*lower row*; red), respectively. Nuclei were visualized by Hoechst-33342 staining (blue). **(B)** Quantification of ICAM-1 expression on HUVECs after exposure to supernatants or respective controls. The fold increase in ICAM-1 surface expression was calculated as the means of fluorescence intensities of anti-ICAM-1 staining subtracted by the corresponding isotype controls and normalized to the results of the 0 Gy samples. Means ± s.d.

of six biological replicates are shown. Asterisks indicate p<0.05 as determined by unpaired Student's *t*-test against 0 Gy. **(C)** HUVEC-activating factors in supernatants of irradiated HCC1937 cells are larger than 10 kDa and Proteinase K-sensitive. On day 4 after irradiation, cell-free culture supernatants of HCC1937 cells irradiated with 20 Gy were subjected to ultracentrifugation with Vivaspin 2 columns (molecular weight cut-off 10 kDa) or Proteinase K treatment (20 µg/ml active or heat-inactivated Proteinase K, 30 min at 37°C), and subsequently exposed to HUVECs. TNF (50ng/ml) served as positive control. ICAM-1 surface expression was measured as in **(B)**. Means ± s.d. of five to six biological replicates are shown. Asterisks indicate p<0.05 as determined by unpaired Student's *t*-test against 0 Gy. **(D)** mRNA expression analyses of adhesion molecules and cytokines in HUVECs after stimulation by cell-free culture supernatants of irradiated HCC1937 cells and respective controls. mRNA was isolated 4 h after exposure to indicated samples, and analyzed by qRT-PCR. Results were normalized on the means of 18S rRNA, β_2-microglobulin, and δ-ALAS, and calibrated on the respective medium samples. Four biological replicates per treatment schedule were analyzed. **(E)** Dimensionality reduction of mRNA expression data was performed by principal component analysis (PCA). The eigenvectors of cytokine mRNAs are depicted in the subspace of the first two PCs (black coordinate system). The loadings are depicted in the green coordinate system. **(F)** Quantification of cytokines released from HUVECs after exposure to the indicated samples. HUVEC supernatants were collected 4 h after stimulation and subjected to multiplex protein measurements. Concentrations of depicted proteins were calculated on the basis of standard curves. Medians ± s.d. of triplicates are shown. Asterisks indicate p<0.05 as determined by unpaired Student's *t*-test against 0 Gy. Data of additional cytokines are not shown.

Notably, biochemical characterization of the responsible molecular entities within the culture supernatants by size exclusion filtration and protease digestion identified proteins >10 kDa to be responsible for the upregulation of ICAM-1 on HUVECs (Figure 14C). Increase in ICAM-1, VCAM-1, and E-selectin was not only detected on the surface expression level but also on the transcript level as measured by qRT-PCR. Again, HUVECs treated with supernatants of ablatively irradiated HCC1937 cells showed the strongest effects (Figure 14D).

In addition to adhesion molecule expression, cytokines and chemokines can be produced and released by activated endothelial cells in order to recruit distinct leukocyte subpopulations. These cytokine/chemokine gradients guide leukocytes to sites of inflammation or damage, respectively. To address this issue, mRNA levels of cytokines and chemokines known to be involved in the attraction and activation of leukocytes and general inflammation were measured in HUVECs after incubation with conditioned supernatants of HCC1937 cells, TNF, or unconditioned medium as controls, respectively (Figure 14D). qRT-PCR analyses revealed a heterogenic picture with different cytokines/chemokines being up- or downregulated depending on the treatment (e.g. MCP-2, CXCL1), and others being only marginally influenced (e.g. MCP-4, RANTES). Apart from the positive control TNF, supernatants of ablatively irradiated HCC1937 cells induced the strongest effects within the group of

upregulated cytokines/chemokines, while these increases in case of supernatants of fractionatedly or 2 Gy irradiated HCC1937 cells were clearly attenuated. This pattern was seen for IL-8, MCP-1, MCP-2, MCP-3, CXCL1, IP-10, MIP-2a, MIP-2b, and IL-6.

In order to better identify possible patterns of cytokine/chemokine expression for each treatment, relative expression levels were subjected to principal component analysis (Figure 14E). Notably, three clusters were obtained: (i) the TNF samples, (ii) the 20 Gy samples, and (iii) the remaining samples, including 0 Gy, 2 Gy, daily 2 Gy, and unconditioned medium. On the mRNA level, the response of HUVECs to TNF stimulation was characterized by a pleiotropic panel of produced cytokines/chemokines. In contrast, exposure to 20 Gy supernatants stimulated a response in HUVECs which was mainly defined by (in descending order) IL-6, MIP-2a, CXCL1, MCP-3, and MIP-2b. IL-6 is one of the master regulators of inflammation [131]. It affects not only cells of the innate and adaptive immune system, but also activates the acute phase response, and stimulates systemic effects such as fever. MIP-2a and CXCL1 are both well known chemoattractants for neutrophils [52].

Next, it was examined whether the increase in IL-6, MIP-2a, CXCL1, MCP-3, and MIP-2b expression on the mRNA level was also translated to the protein level. Indeed, multiplex ELISA measurements in HUVEC supernatants after incubation with conditioned media of irradiated HCC1937 cells revealed elevated levels of IL-6, MIP-2a, CXCL1, and MCP-3 in comparison to the non-irradiated control (Figure 14F). Unfortunately, detection reagents for MIP-2b were commercially not available for this experimental setup. However, the measured chemokine levels revealed the same pattern as had already been observed on mRNA level: Strongest effects with supernatants of 20 Gy irradiated HCC1937 cells, equally low effects with supernatants of single 2 Gy and fractionatedly irradiated HCC1937 cells. This pattern was consistently noticed also with other chemokines found in the HUVEC supernatants: IL-8, MCP-1 (both were also increased on mRNA level), and MIF. IL-8, MCP-1, and MIF have been shown to be essential not only for neutrophil but also for monocyte recruitment [97]. Moreover, IL-1β and diverse other cytokines/chemokines (data not shown), all following the described pattern, were found in the HUVEC supernatants after exposure to conditioned media of irradiated HCC1937 cells.

In summary, these data support the notion that proteins which are released from irradiated HCC1937 cells activate endothelial cells to express adhesion molecules on

their surface and to produce and secrete cytokines and chemokines – both essential processes for the directional recruitment of neutrophils and monocytic cells. Adhesion molecule expression and cytokine generation by HUVECs were strongest after incubation with supernatants of ablatively irradiated HCC1937 cells, while supernatants of 2 Gy and daily 2 Gy irradiated cells showed clearly more subtle effects. Intriguingly, the cytokine/chemokine response of HUVECs to supernatants of ablatively irradiated HCC1937 cells was unique and different from that induced by TNF suggesting that high single dose irradiation of breast cancer cells may induce distinct immunological mechanisms different from prototypical, TNF-driven inflammation.

7.8 Monocytic cell differentiation and dendritic cell maturation are influenced by protein DAMPs released from dying breast cancer cells

In the context of anthracycline-based chemotherapy it was shown that, apart from leukocyte recruitment, dying cancer cells can stimulate the differentiation of intra-tumoral monocytes into antigen-presenting cells and subsequently initiate adaptive anti-tumor immune responses [132] [133]. Along this line, the influence of tumor cell-derived material released from primary necrotic cells after irradiation on monocyte differentiation and dendritic cell maturation was evaluated. Important markers of the immunological synapse were monitored on monocytes and dendritic cells upon exposure to conditioned media of irradiated HCC1937 cells. These markers included the co-stimulatory ligands CD80 and CD86, the co-stimulatory receptor CD40, the dendritic cell maturation marker CD83, and the MHC class II receptor HLA-DR.

In the differentiation approach, isolated monocytes were incubated with cell-free supernatants of irradiated HCC1937 cells and the respective controls (LPS and serum-free X-Vivo 15 medium) followed by treatment with GM-CSF and IL-4 for 5 days to stimulate dendritic cell differentiation. FACS analyses revealed that the expression of CD86, CD40, CD83, and MHC class II was elevated on dendritic cells after treatment with cell-free supernatants of irradiated HCC1937 cells in comparison to supernatants of untreated control cells (Figure 15A). The most prominent effect in this regard was seen for CD80 expression. Supernatants of ablatively irradiated HCC1937 cells led to the strongest upregulation of CD80, while cell-free supernatants of 2 Gy and daily 2 Gy irradiated HCC1937 cells showed clearly less

effects. The signals released from irradiated HCC1937 cells that were responsible for CD80 upregulation were sensitive to proteinase K treatment and predominantly exhibited an apparent molecular weight of >10 kDa as disclosed by biochemical characterization (Figure 15B).
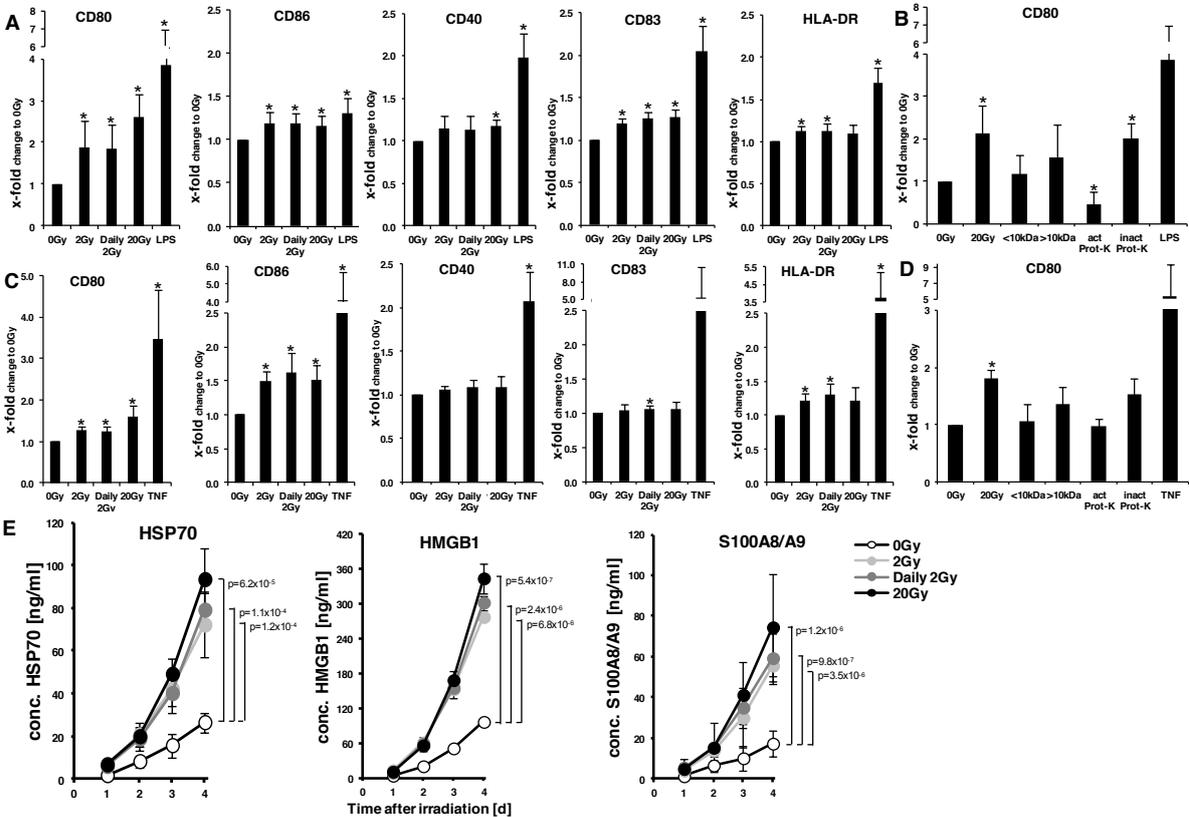

Figure 15 Expression of prominent surface markers on monocyte-derived dendritic cells is modulated by dying tumor cell-derived protein DAMPs.

(A) Flow cytometric analysis of the surface markers CD80, CD86, CD40, CD83, and HLA-DR on monocyte-derived dendritic cells. Primary human monocytes were stimulated for 4 h with supernatants of irradiated HCC1937 cells, collected on day 4 after irradiation. LPS (200 ng/ml) was used as a positive control. Following stimulation, monocytes were differentiated to dendritic cells by GM-CSF (20 ng/ml) and IL-4 (40 ng/ml) treatment over 5 days, and subsequently subjected to flow cytometry. The fold increase in surface marker expression was calculated as the means of fluorescence intensities of anti-surface marker staining subtracted by the corresponding isotype controls and normalized on the results of the 0 Gy samples. Means ± s.d. of five biological replicates are shown. Asterisks indicate p<0.05 as determined by unpaired Student's *t*-test against 0 Gy. **(B)** CD80 upregulation is mediated by Proteinase K-sensitive proteins released from irradiated HCC1937 cells. Cell-free culture supernatants of HCC1937 cells irradiated with 20 Gy were collected on day 4 after irradiation and subjected to ultracentrifugation with Vivaspin 2 columns (molecular weight cut-off 10 kDa) or Proteinase K treatment (20 µg/ml active or heat-inactivated Proteinase K, 30 min at 37°C). Afterwards, primary human monocytes were stimulated with the treated samples, and CD80 surface expression was measured as in **(A)**. LPS (200 ng/ml) served as a positive control. Means ± s.d. of eight to ten biological replicates are shown. Asterisks indicate p<0.05 as determined by unpaired Student's *t*-test against 0 Gy. **(C)** Flow cytometric analysis of the marker panel from **(A)** on differentiated dendritic cells. Primary human monocytes were differentiated to dendritic cells with GM-CSF (20 ng/ml) and IL-4 (40 ng/ml) for 5 days. On day 5, dendritic cells were stimulated with cell-free supernatants of

80

irradiated HCC1937 cells as in **(A)**. TNF (100 ng/ml) served as a positive control. 2 days after stimulation, surface marker expression was analyzed by flow cytometry. The fold increase of surface markers was calculated as in **(A)**. Means ± s.d of five biological replicates are shown. Asterisks indicate p<0.05 as determined by unpaired Student's *t*-test against 0 Gy. **(D)** For biochemical characterization of HCC1937-derived factors responsible for CD80 upregulation, supernatants of HCC1937 cells, irradiated with 20 Gy, were treated as in **(B)**. TNF (100 ng/ml) served as positive control. Dendritic cells were differentiated for 5 days, and subsequently exposed to the treated samples for 4 h. 2 days after exposure, surface expression of CD80 was measured by flow cytometry and fold change was calculated as in **(A)**. Means ± s.d. of four biological replicates are shown. Asterisk indicates p<0.05 as determined by unpaired Student's *t*-test against 0 Gy. **(E)** Release of HSP70, HMGB1, and S100A8/A9 from irradiated HCC1937 cells. ELISAs were performed with supernatants of irradiated HCC1937 cells collected on day 1-4 after irradiation. Concentrations were calculated on the basis of standard curves. HSP70: Means ± s.d. of three biological replicates are shown. HMGB1: Means ± s.d. of triplicates are depicted. S100A8/A9: Means ± s.d. of five biological replicates are shown. Comparison of curves from irradiated samples to 0 Gy was performed by two-way ANOVA.

In the maturation approach, monocytes were differentiated to dendritic cells with GM-CSF and IL-4 for 5 days and subsequently were treated with supernatants of irradiated HCC1937 cells and the respective controls (TNF or serum-free X-Vivo 15 medium) (Figure 15C). The expression of the dendritic cell markers showed the same pattern as in the differentiation approach, only to lower extents, and the strongest effects were observed for upregulation of CD80 expression. Supernatants of ablatively irradiated HCC1937 cells clearly increased CD80 expression, whereas only moderate effects were seen for supernatants of 2 Gy and daily 2 Gy irradiated HCC1937 cells. Again, CD80 upregulation was predominantly mediated by proteins >10 kDa (Figure 15D). Overall, the influence of supernatants of irradiated HCC1937 on monocyte differentiation was more pronounced than that on dendritic cell maturation.

So far, these results show that supernatants of ablatively irradiated HCC1937 cells stimulate and support endothelial cell activation (Figure 14), monocyte differentiation, and dendritic cell maturation (Figure 15). The responsible molecular entities in this regard are of high molecular weight (i.e. larger than 10 kDa) and sensitive to proteinase digestion. Consequently, we next measured the levels of prototypical, proteinaceous DAMPs known to cause the observed effects in supernatants of irradiated HCC1937 cells (Figure 15E). HSP70, HMGB1, and the S100A8/A9 dimer were taken into closer consideration, since these proteinaceous DAMPs have been reported to be released from necrotic cells, are larger than 10 kDa (HSP70: M_w=70 kDa, HMGB1: M_w=25 kDa, S100A8/A9 dimer: M_w=36.5 kDa), and possess

modulatory functions in neutrophil and monocyte attraction, endothelial cell activation, and dendritic cell maturation [50]. Evident radiation- and time-dependent increases in HSP70, HMGB1, and S100A8/A9 dimer levels in the supernatants of irradiated HCC1937 cells were detected, clearly reflecting the profiles of endothelial cell activation, monocyte differentiation, and dendritic cell maturation. More precisely, lowest effects were observed with 0 Gy samples, increased and similar effects were found for 2 Gy and daily 2 Gy, and strongest effects were noticed with ablatively irradiated samples (Figure 14, Figure 15).

Taken together, not only endothelial cell activation but also dendritic cell differentiation and maturation are supported by proteins (larger than 10 kDa) released from dying breast cancer cells, especially after ablative irradiation. Proteinaceous DAMPs, including HSP70, HMGB1, and S100A8/A9 dimer are potential candidates, which may mediate the observed immunological effects.

7.9 Dendritic cell effector functions are crucially influenced by dying breast cancer cells

After monocyte recruitment and dendritic cell differentiation, the induction of an adaptive immunity requires the (cross-) presentation of antigens by dendritic cells to T cells. Phagocytosis of antigen material and/or cell debris by dendritic cells is a prerequisite in this context.
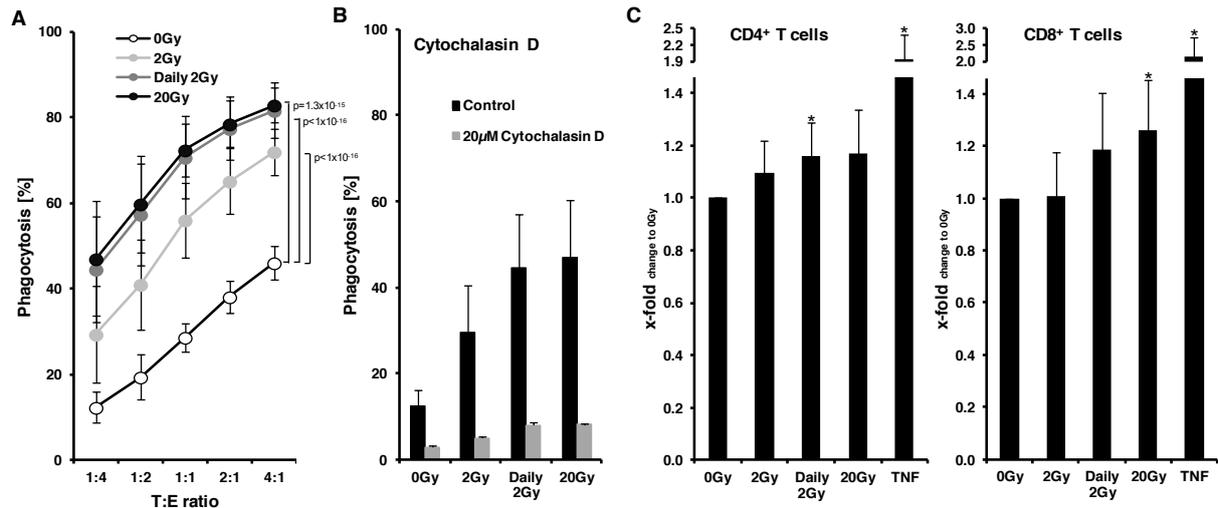
Figure 16 Pivotal effector functions of dendritic cells are enhanced after contact with irradiated breast cancer cells.

(A) Irradiated HCC1937 cells were subjected to phagocytosis assays using dendritic cells as phagocytes. Primary human monocytes were labelled with PKH67 (green), and differentiated to dendritic cells with GM-CSF (20 ng/ml) and IL-4 (40 ng/ml) for 5 days. Afterwards, dendritic cells (effector cells; E) were added to irradiated, PKH26-labeled (red) HCC1937 cells (target cells; T) on day 4 after irradiation at the depicted T:E ratios. Phagocytosis of irradiated HCC1937 cells by dendritic cells was allowed for 2 h. Subsequently, dendritic cells were analyzed by flow cytometry. Phagocytosis rates were calculated as the percentage of PKH67/PKH26 double-positive dendritic cells of all PKH67-positive cells deployed. Means ± s.d. of five biological replicates are shown. Comparison of curves from irradiated samples to 0 Gy was performed by two-way ANOVA. **(B)** Active phagocytosis of irradiated HCC1937 cells by dendritic cells was confirmed by addition of the actin polymerization inhibitor cytochalasin D. Dendritic cells were incubated with 20 µM cytochalasin D for 1 h prior to the phagocytosis assay. Afterwards, the phagocytosis assay was performed as in **(A)** with a T:E ratio of 1:4. Means ± s.d. of five biological replicates are shown. **(C)** Proliferation of T cells stimulated by allogeneic dendritic cells differentiated in the presence of tumor-derived material. Primary human monocytes were incubated for 4 h with supernatants of irradiated HCC1937 cells collected on day 4 after irradiation. TNF (50 ng/ml) served as a positive control. Subsequently, monocytes were differentiated to dendritic cells in the presence of GM-CSF (20 ng/ml) and IL-4 (40 ng/ml). After 7 days, T cells from an allogeneic donor were isolated and labeled with CSFE. Dendritic cells and labeled T cells were cocultured at a ratio of 1:5 for 5 days. Afterwards, T cell proliferation was analyzed by flow cytometry. To distinguish between different subsets, T cells were stained against CD3, CD4, and CD8. The proliferation rate of CD4$^+$ and CD8$^+$ T cells was calculated as the percentage of CD3$^+$CFSE^{low}CD4$^+$ (*left panel*) or CD3$^+$CFSE^{low}CD8$^+$ (*right panel*) on the basis of all CD3$^+$CD4$^+$ or CD3$^+$CD8$^+$ cells, respectively, and normalized on the corresponding 0 Gy sample. Means ± s.d. of six biological replicates are shown. Asterisks indicate $p < 0.05$ as determined by unpaired Student's *t*-test against 0 Gy.

The capacity of dendritic cells to phagocytose irradiated breast cancer cells in vitro was assessed by flow cytometry. Green PKH67-labeled dendritic cells (effector cells) were added to irradiated, orange PKH26-labeled HCC1937 cells (target cells) in increasing target to effector ratios (T:E), and internalization of dying cell material was quantified by flow cytometry. With increasing T:E ratios, the percentage of

phagocytosing dendritic cells increased. Importantly, uptake of irradiated HCC1937 by dendritic cells was significantly higher as compared to non-irradiated control HCC1937 cells (Figure 16A). T cell-stimulation by dendritic cells is a key step in the induction of T cell-dependent adaptive immunity. Dendritic cells present and cross-present antigens on MHC class II and I molecules to the T cell receptor. Yet, the interaction between the MHC complex and the T cell receptor is necessary but not sufficient to stimulate T cells. Co-stimulatory ligands, including CD80 and CD86 on the dendritic cell are needed to bind to their corresponding receptors on the T cell (in this case CD28) in order to fully activate the T cell. As seen before, dendritic cells, which had been differentiated from monocytes in the presence of supernatants of irradiated HCC1937 cells, expressed higher levels of co-stimulatory ligands, especially CD80 (Figure 15). To investigate the T cell-stimulating potential of these dendritic cells, an allogeneic mixed leukocyte reaction (MLR) was set up. The proliferation of CFSE-labeled CD4$^+$ and CD8$^+$ T cells was monitored as a marker for T cell activation (Figure 16C). Dendritic cells stimulated with TNF or X-Vivo 15 medium served as positive or negative controls, respectively. There was a moderate but significant increase in CD8$^+$ T cell proliferation when dendritic cells were differentiated in the presence of supernatants of ablatively irradiated HCC1937 cells in comparison to the non-irradiated controls. CD4$^+$ T cell proliferation was also slightly increased, but this was independent of the irradiation regimen employed and did not reach statistical significance.

In summary, dendritic cells efficiently phagocytose irradiated HCC1937 cells. Moreover, dendritic cells differentiated from monocytes in the presence of irradiated breast cancer supernatants induce improved CD8$^+$ T cell proliferation. Thus, central steps in the induction of adaptive immunity, i.e. the recruitment of monocytic cells by activated endothelial cells, the differentiation and maturation of monocytes into dendritic cells, the phagocytosis of dying tumor cells, and the stimulation of T cell proliferation by these dendritic cells all were examined in the context of breast cancer irradiation, and the strongest effects were noticed for cancer cells subjected to ablative irradiation with a high single dose.

8 Discussion

In the present study, the immune-stimulatory effects of ionizing irradiation were examined in models of breast cancer. Comparing single low dose (2 Gy), classically fractionated (4x2 Gy), and ablative irradiation regimens (20 Gy), we analyzed the quality and the extent of cell death induction in different breast cancer cell lines, the subsequent release of DAMPs, as well as their impact on endothelial cell activation, myeloid cell recruitment in vitro and in vivo, APC differentiation and maturation. Finally, we assessed phagocytosis of irradiated breast cancer cells by dendritic cells, and measured their capacity to stimulate adaptive T cell responses. Our results show that irradiation – particularly in the ablative setting – is a potent inducer of immunogenic cell death in cancer cells and stimulates the release of different DAMPs that have strong effects on other cells in the tumor microenvironment. As such, released nucleotides from dying breast cancer cells favor increased monocyte migration and chemokinesis. Proteinaceous DAMPs, including S100A8/A9, HMGB1, HSP70, and others, mediate endothelial cell activation as characterized by upregulated expression of adhesion molecules, and increased production and secretion of cytokines and chemokines. They also stimulate differentiation and maturation of APCs. Upon phagocytosis of breast cancer cells, which is clearly improved by irradiation, these APCs can potently trigger adaptive CD8^{+} T cell responses.

8.1 Ablative irradiation as an inducer of immunogenic forms of cell death

Apoptosis, necrosis, and senescence are well-known cell death modalities induced by ionizing radiation [9]. However, they greatly differ in their immunogenic potential thus affecting the immunological consequences of irradiation. In this study, the mentioned cell death modalities were measured in different breast cancer cell lines after irradiation.

MCF7 cells time-dependently underwent apoptosis especially after ablative irradiation, whereas only low rates of apoptosis were observed in HCC1937 and BT-474 cells (Figure 8). Apoptosis is known as an immunogenically silent form of cell death: Professional phagocytes engulf apoptotic cells and produce anti-inflammatory cytokines, such as TGF-β and IL-10 [134] [75]. In the context of tumor biology, recent studies showed that apoptotic tumor cells support tumor repopulation by release of

PGE$_2$ in a caspase-3-dependent manner, and radiation-induced apoptosis was reported to promote tumor growth, accumulation of tumor-promoting macrophages, as well as angiogenesis [135] [136] [137]. Thus, apoptosis induction in tumor cells may not only favor tumor repopulation but also appears to contribute to shaping an immune-suppressive microenvironment [138]. Indeed, shifting apoptosis to more immunogenic forms of cell death by interfering with either apoptotic cell death pathways or the engulfment of apoptotically dying cells, respectively, may be an interesting approach for the induction of anti-tumor immune mechanisms [139] [140] [141].

In contrast to apoptosis, necrosis is a highly immunogenic form of cell death. Loss of plasma membrane integrity is a critical event in this context, because passively released DAMPs such as nucleotides (ATP, UTP), HMGB1, HSPs, S100A8/A9, and monosodium urate are main triggers for pro-inflammatory immune mechanisms stimulated by necrotic cells [9].

In our experimental setting, primary necrosis was preferentially observed upon ablative irradiation in the fast-proliferating breast cancer cell lines HCC1937 and MCF7 (Figure 9). In case of fractionated and single 2 Gy radiation, the levels of necrosis were clearly lower. This suggests a shift from weakly to highly immunogenic cell death, which can be induced by ablative irradiation. Notably, this pattern seen for the induction of necrotic cell death – i.e. strong effects after ablative irradiation and less pronounced effects after fractionated or single 2 Gy radiation – recurred in nearly all steps of the anti-tumor immune cascade investigated in this study (see Figure 3).

For the attraction of monocytic cells, necrotic cells appeared to be the main source of nucleotides, especially after ablative irradiation (Figure 10). This observation is in line with findings of others, who showed that intra-tumoral recruitment of monocytes was highly dependent on ATP released by dying cancer cells upon anthracycline treatment [142]. Nucleotides bind to purinergic receptors such as P2RY$_2$, thereby acting as 'find-me' signals for monocytes and macrophages [54]. The important role of nucleotides in this scenario is indicated by the abrogation of monocyte attraction through the expression of the ectonucleotidase CD39. As seen in the present study, MCF7 cells upregulated CD39 in response to irradiation, thus completely inhibiting nucleotide-mediated monocyte migration (Figure 11). CD39 expression as an immune escape mechanism has been described for several other types of cancer, including melanoma, and pancreatic cancer, as well as for cancer exosomes [143] [144]

[145] [146] [147]. Moreover, degradation of ATP to adenosine by CD39, in concert with CD73, is a key mechanism by which regulatory T cells and MDSCs inhibit effector T cells to eliminate cancer cells [148] [149] [150].

Despite potently stimulating monocytic cell migration in trans-well assays, supernatants of irradiated HCC1937 cells failed to induce directed chemotaxis of primary human monocytes in 2D chemotaxis assays. Instead, monocytes displayed undirected chemokinesis, which could be abrogated by apyrase treatment, and thus was mainly driven by nucleotides (Figure 12). Therefore, nucleotides per se appear unable to induce chemotaxis in vitro, a finding which also has been reported by others [130] [55]. This discrepancy between the in vivo observation of Ma et al. and our in vitro results might be resolved by recently published data from McDonald et al. They could show that, in the case of sterile inflammation, ATP activates $P2RX_7$ on tissue macrophages, leading to the release of IL-1β, which in turn activates endothelial cells thereby supporting neutrophil extravasation [52]. Hence, nucleotides alone may act as amplifiers through indirect activation of endothelial cells but not as direct stimulators of leukocyte recruitment.

In addition to nucleotides, high levels of the prototypical DAMPs HSP70, HMGB1 and S100A8/A9 were detected in the supernatants of irradiated HCC1937 cells particularly after ablative irradiation (Figure 15). The role of these DAMPs as pro-inflammatory mediators will be discussed in greater detail in chapter 8.5. However, it should be highlighted at this point that release of these DAMPs greatly contributes to the immunogenic potential of irradiation-induced cell death, especially in terms of endothelial cell activation and APC differentiation. Therefore, the quality of cell death induced by ablative irradiation, i.e. high levels of primary necrosis combined with the release of highly immunogenic DAMPs, indicates that ablative irradiation potently stimulates immunogenic forms of cell death.

Besides necrosis, necroptosis was described as another form of immunogenic cell death [151]. In the present study, only a marginal contribution of necroptosis upon irradiation could be detected by using the necroptosis inhibitor necrostatin-1 (Figure 8). The role of autophagy in cancer suppression/promotion is still discussed controversially and was not addressed in this study [152]. However, especially autophagy-induced release of nucleotides was shown to contribute to immunogenic effects of radiation and might thus be of interest for future studies [153].

Lastly, the induction of senescence upon irradiation was analyzed. Senescence is characterized by irreversible cell cycle arrest while senescent cells in principle maintain metabolic activity [77]. The immunogenic potential of senescent cells is described ambiguously in the literature. Senescent cells are known to secrete various cytokines, chemokines, and growth factors summarized as the senescence-associated secretory phenotype (SASP). The SASP exerts both immune-stimulating as well as immune-suppressive functions. For instance, secretion of various chemokines from senescent cancer cells was reported to mediate NK cell-dependent elimination of liver carcinoma cells [154]. However, continuous release of cytokines from senescent cells appears to switch the nature of tumor-infiltrating leukocyte subpopulations from an anti- to a pro-tumorigenic one [78]. Further studies should characterize the SASP of irradiation-induced senescent breast cancer cells in order to dissect their contribution to anti-tumor immune mechanism in greater depth.

8.2 Endothelial cells as potential organizers of myeloid cell recruitment to dying cancer cells upon ablative radiotherapy

Endothelial cells are of crucial importance for leukocyte recruitment during inflammation [81]. In principal, endothelial cells exhibit two essential functions: First, they release cytokines and chemokines for leukocyte attraction, and second, they express adhesion molecules on their surface for leukocyte extravasation. Both functions were analyzed in this study in order to assess whether endothelial cells are able to convert the observed chemokinetic migration of monocytic cells to supernatants of irradiated HCC1937 cells in vitro (Figure 12) into directed migration in vivo.

Incubation of HUVECs with cell-free supernatants of ablatively irradiated HCC1937 cells resulted in a strong upregulation of the adhesion molecules ICAM-1, VCAM-1, and E-selectin necessary for leukocyte-endothelial cell adhesion. This upregulation was less pronounced with supernatants of single 2 Gy or fractionatedly irradiated HCC1937 cells. ICAM-1 surface expression on HUVECs was dependent on proteins released from irradiated HCC1937 cells suggesting that proteinaceous DAMPs, such as HMGB-1, HSP70, S100A8/A9, and others, are involved (Figure 15). Indeed, HUVECs express several pattern recognition receptors for DAMPs, such as TLR4 and RAGE, which may render them susceptible to HMGB1, HSP70, and S100A8/A9 [155] [69] [156]. E-selectin is known to mediate capture and especially rolling of leukocytes

by interacting with PSGL1 and CD44, while ICAM-1 and VCAM-1 mediate leukocyte arrest and crawling on the endothelial cells by interacting with integrins [81]. P-selectin, which exerts similar functions as E-selectin during capture and rolling of leukocytes, could not be detected on HUVECs (data not shown). Since P-selectin expression in HUVECs is highly dependent on the culture conditions, this might explain its absence in our setting. The functional validation of adhesion molecule upregulation on HUVECs after exposure to cell-free supernatants of irradiated HCC1937 cells is currently under investigation with primary human neutrophils and monocytes in flow chamber assays in cooperation with Prof. Markus Sperandio from the Walter Brendel Centre of Experimental Medicine, Klinikum der Universität München, Munich, Germany.

In addition to adhesion molecule surface expression, supernatants of irradiated HCC1937 cells induced the production of various cytokines and chemokines in HUVECs (Figure 14). Upon incubation with supernatants of ablatively irradiated HCC1937 cells, HUVECs upregulated a unique cytokine mRNA profile. IL-6, MIP-2a, CXCL1, MCP-3, and MIP-2b were observed as the strongest determinants in this context. This cytokine profile was clearly different from the ones stimulated by supernatants of the other irradiation regimens and that of the positive control TNF, suggesting that HUVECs are strongly activated by supernatants of ablatively irradiated HCC1937 cells, but obviously distinct from TNF-dependent activation (as for instance during pathogen-associated inflammation). Of note, the mentioned cytokines IL-6, MIP-2a, CXCL1, MCP-3, and MIP-2b were also found at high concentrations in HUVEC supernatants after incubation with supernatants of ablatively irradiated HCC1937 cells. Additionally, IL-8, MIF, MCP-1, and IL-1β were secreted although the effects on mRNA levels were rather modest. The importance of these cytokines/chemokines for immune responses has been demonstrated in numerous studies, especially in the context of sterile inflammation and anti-tumor immunity. IL-6 has local and systemic functions during inflammation: Production and release of acute-phase proteins from the liver and the induction of fever rely strongly on IL-6. Locally, IL-6 promotes differentiation of naïve CD4$^+$ and CD8$^+$ T cells into T helper cells and cytotoxic T cells, respectively, and simultaneously suppresses regulatory T cells [157] [158]. Both MCP-1 and MCP-3 were shown to be important for intra-tumoral recruitment of leukocytes. In anthracycline-treated mouse

fibrosarcomas, MCP-1 was shown to be essential for the intra-tumoral recruitment of highly competent APCs [133], and MCP-3 delivery in murine mastocytoma facilitated dendritic cell-dependent tumor rejection by lymphocytes [159]. IL-1β, which has been reported to be produced by resident macrophages upon exposure to nucleotides released during sterile inflammation [160], can promote the upregulation of ICAM-1 on and the release of CXCL1 and MIP2a from endothelial cells, resulting in neutrophil recruitment to sites of sterile inflammation [52]. Hence, a pro-inflammatory milieu is generated by HUVECs after incubation with supernatants of irradiated cells via release of systemically and locally effective cytokines and chemokines. This effect was most apparent with ablatively irradiated HCC1937 cells. Recently, Stark and colleagues demonstrated that pericytes release a panel of cytokines and chemokines which attract neutrophils and monocytes in the context of sterile inflammation. Notably, this panel consisted of IL-6, CXCL1, IL-8, MIF, MCP-1 and IL-1β [97], showing a striking degree of overlap to the panel observed in the present study. Our results from the air pouch model further underline the parallels between myeloid cell recruitment in the context of cancer radiotherapy and sterile inflammation: Predominantly neutrophils as well as monocytes were time-dependently recruited into the pouches after injection of supernatants of irradiated HCC1937 cells. Notably, the sequence of leukocyte infiltration, i.e. initially neutrophils, followed by monocytes in a second wave, reflected the neutrophil-monocyte axis postulated for inflammation [161]. Interestingly, besides neutrophils, the number of Ly6C^{low} monocytes was significantly higher in pouches containing supernatants of ablatively irradiated HCC1937 cells as compared to those injected with supernatants of single 2 Gy or fractionatedly irradiated HCC1937 cells. In contrast, no significant differences between supernatants of ablatively and fractionatedly irradiated HCC1937 cells were seen for the numbers of infiltrating Ly6C^{hi} monocytes. These inflammatory monocytes are rapidly recruited from the blood to sites of inflammation were they differentiate into inflammatory dendritic cells [162]. During differentiation, Ly6C surface expression decreases, thereby giving rise to Ly6C^{low} monocytic cells. Tissue-resident monocytes and monocyte-derived cells, such as Langerhans cells, also are Ly6C^{low} [163,164]. Thus, supernatants of fractionatedly and ablatively irradiated HCC1937 cells might induce inflammatory monocyte recruitment to a similar extent, but either maturation and/or loss of Ly6C expression are accelerated in case of supernatants of ablatively

irradiated HCC1937 cells, or infiltration of tissue-resident monocytes/monocytic cells is elevated, respectively. In some studies, the infiltrating T cell-stimulating APC-subpopulation in the context of tumor therapy was described as Ly6C^{hi} [132] [133]. Therefore, it will be of relevant interest for future studies to analyze the phenotypes of monocyte-derived cells emerging from infiltrating monocytic subsets in further detail.

8.3 Dying cancer cell material stimulates the differentiation of dendritic cells to potent APCs

Dendritic cells are the most important APCs interacting with naïve T cells. The origin of (cross-) presented antigens, the expression of co-stimulatory receptors and the cytokine profile of mature dendritic cells determine whether naïve T cells become effector or tolerogenic T cells. Therefore, the phenotype of dendritic cells is crucial for the induction of adaptive immunity. Two scenarios of dendritic cell differentiation/maturation were investigated in this study: (i) dendritic cells that were differentiated from monocytes in the presence of cell culture supernatants of irradiated HCC1937 tumor cells, and (ii) dendritic cells that were exposed to culture supernatants of irradiated HCC1937 tumor cells after differentiation. These approaches were chosen to determine the effects of dying cancer cell-derived factors (i) on peripheral blood monocytes, which are newly recruited to the site of irradiation-induced tumor cell death, thereby undergoing differentiation to dendritic cells in the environment of the irradiated tumor ('new' dendritic cells), and (ii) on tissue-resident dendritic cells reacting to tumor cell death ('resident' dendritic cells).

Commonly, intra-tumoral dendritic cells are often described to have an immune-suppressive phenotype [165]. They are poorly differentiated, express only low levels of co-stimulatory molecules, and release anti-inflammatory cytokines, such as IL-10 and IL-13, leading to anergy of CTLs, immune tolerance, promotion of tumor growth, and metastasis [166] [167]. Recently, Broz et al. detected an intra-tumoral subpopulation of dendritic cells, which turned out to be highly potent APCs. However, this dendritic cell phenotype was rarely found in established mouse mammary carcinomas in comparison to MDSCs – a finding, which relativizes the immunogenic potential of these dendritic cells [168] [169]. Yet, the immune-suppressive effect of intra-tumoral MDSCs may be overcome by freshly recruited myeloid-derived dendritic cells. For anthracycline therapy it was shown that monocytes of CD11c$^+$CD11b$^+$Ly6C^{hi} phenotype can differentiate into potent CD86$^+$ dendritic cells after intra-tumoral

recruitment and induce potent anti-tumor immunity [132]. In accordance, emergence of an immune-stimulatory APC-phenotype in the presence of dying cancer cell-derived factors is suggested in the present study by the strong upregulation of CD80 on 'new' dendritic cells – particularly with supernatants of ablatively irradiated HCC1937 cells. Supernatants of single 2 Gy and fractionatedly irradiated HCC1937 cells also induced CD80 upregulation, but to a much lesser extent. Regarding the responsible molecular entities within the culture supernatants, the same pattern was seen as in the HUVEC activation experiments: Both the endothelial cells' response and the induction of co-stimulatory CD80 on dendritic cells were dependent on proteins of >10 kDa released from irradiated HCC1937 cells, suggesting the involvement of similar signals, presumably proteinaceous DAMPs, such as HMGB1, HSP70, and S100A8/A9 (Figure 15). In terms of the different irradiation regimens, the expression pattern of CD80 on 'resident' and 'new' dendritic cells was similar – i.e. supernatants of 2 Gy and fractionated irradiated cells stimulated CD80 upregulation less potently than those of ablatively irradiated cells did. However, the magnitude of induction was higher on 'new' dendritic cells. Since CD86 functions as a co-stimulator for T cells analogously to CD80, it might me dispensable. CD40 is a co-stimulatory receptor for dendritic cells, which is bound by CD40L on T cells, thereby activating the dendritic cells. It is known to be involved in upregulation of CD80 and CD86 [170]. Although supernatants of irradiated HCC1937 cells increased CD40 expression on dendritic cells only moderately, CD80 was robustly upregulated, indicating either a strong amplification cascade or a minor role for CD40 in this setting, respectively. Antigens presented on MHC class II molecules, such as HLA-DR, are recognized by CD4$^+$ T cells. Expression of HLA-DR on 'new' and 'resident' dendritic cells was only slightly altered upon exposure to supernatants of irradiated HCC1937 cells. However, in both cell populations basal HLA-DR expression levels were very high (data not shown) suggesting that these levels can only be further increased by very strong signals, as the positive control TNF. In addition to the analyzed surface receptors and co-stimulatory molecules, CCR7, the lymph node homing receptor for dendritic cells, is an important player in dendritic cell maturation, and has not been addressed in the present study [104]. Since (cross-) presentation of antigens by dendritic cells to T cells takes place in the lymph node, CCR7 expression should be investigated in further studies.

Another interesting issue, which should be addressed in the future, is the cytokine panel released from 'new' or 'resident' dendritic cells, respectively. T cell (cross-) priming by dendritic cells is dependent on three events, as mentioned earlier: (i) antigen (cross-) presentation on MHC molecules, (ii) co-stimulation by binding of CD80/CD86 to CD28, and (iii) release of distinct T cell-activating cytokines, such as IL-2, by dendritic cells. The capacity of different dendritic cell populations to release such cytokines and, especially, type I IFNs in the context of tumor radiotherapy should therefore be investigated in the future.

8.4 Dendritic cells connect innate and adaptive immune mechanisms in the context of anti-tumor immunity

Dendritic cells represent a crucial link between the innate and adaptive immune system, which is mirrored in their ability to phagocytose cell debris and (cross-) present the processed material to T cells. Their 'innate function', i.e. the engulfment of cell debris for antigen (cross-) presentation, was measured in phagocytosis assays. Irradiated HCC1937 cells were efficiently engulfed by dendritic cells. Notably, dendritic cells phagocytosed ablatively and fractionatedly irradiated HCC1937 cells to comparable extents, suggesting that from an efferocytic point of view, these prey cell populations look identical. Only cells subjected to the single low dose setting and viable control cells were clearly less engulfed.

HCC1937 cells primarily underwent primary necrosis after irradiation, but apoptosis and senescence were also induced, especially after ablative irradiation (see Figure 9). Since the (post-) phagocytic response is influenced by the cell death properties, it is important to discuss the observed cell death modalities in HCC1937 cells in the context of phagocytosis.

Exposure of phosphatidylserine (PS) is the main trigger for phagocytosis of apoptotic cells [171]. During apoptosis, PS translocates from the inner to the outer plasma membrane leaflet [172] [173]. PS binds either directly to specific receptors such as BAI-1 [174] and TIM-1,-4 [175] or indirectly via bridging proteins including MFG-E8 and Del-1, to $\alpha_v\beta_{3/5}$ integrins [176], leading to re-arrangements in the phagocyte's actin skeleton and finally to cell engulfment. However, as described before, HCC1937 cells predominantly underwent primary necrosis after irradiation. The engulfment of necrotic cells is less well understood, but rupture of the plasma membrane during (primary and secondary) necrosis also results in PS exposure. Therefore, PS-

dependent phagocytosis may also account for necrotic cell engulfment, however to a lesser extent [177]. To be more precise, oxidized PS in conjunction with non-oxidized PS has been described as a strong signal for phagocytosis of dying cells [178]. Since ionizing radiation induces the formation of reactive oxygen species, this might explain the difference between the uptake of fractionatedly and single 2 Gy irradiated HCC1937 cells: Cell death induction was found to be in the same range for both radiation regimens but daily doses of 2 Gy might lead to more oxidation of PS, and thus facilitate tumor cell engulfment.

The post-phagocytic response differs fundamentally between apoptotic and necrotic cells: As mentioned before, upon uptake of apoptotic cells, macrophages release immune-suppressive cytokines and dendritic cells induce immune-tolerance in T cells [179], while internalization of necrotic cells induces pro-inflammatory reactions of macrophages and dendritic cells, such as pro-inflammatory cytokine release and T cell priming. Therefore, the post-phagocytic response of dendritic cells after engulfment of irradiated HCC1937 cells might be of interest for further studies.

The clearance of senescent cells is only poorly understood. In murine liver carcinomas, p53-dependent senescent tumor cells were cleared by cells of the innate immune system [180]. However, the exact mechanisms, the involved signals, and receptors still remain elusive [9].

Finally, it should be noted that the phagocytosis assay was performed as a co-culture experiment, i.e. dendritic cells and irradiated HCC1937 cells were in direct contact. Therefore, effects induced by irradiated HCC1937 might be over-estimated in this assay in comparison to assays where dendritic cells/monocytes were stimulated with supernatants of irradiated HCC1937 cells. Moreover, it is noteworthy that dendritic cells and HCC1937 cells were obtained from different donors (allogeneic system), which most likely enhances the phagocytic activity of dendritic cells in comparison to an autologous situation where both dendritic cells and tumor cells are derived from the same individual.

Following ingestion of cell debris, dendritic cells process the engulfed material and (cross-) present antigens derived thereof on MHC molecules to T cells, thus stimulating adaptive immune responses. Investigating this 'adaptive function' of dendritic cells, the ability of dendritic cells to stimulate T cell proliferation was monitored in this study by allogeneic mixed leukocyte reactions (Figure 16). Dendritic

cells, which were differentiated in the presence of supernatants of ablatively or fractionatedly irradiated HCC1937 cells, induced CD8^{+} T cell proliferation significantly stronger than the controls which were differentiated upon exposure to supernatants of not irradiated cells. In contrast, CD4^{+} T cell proliferation was only slightly but not significantly increased. This suggests that dendritic cells differentiated from monocytes in the presence of supernatants of irradiated HCC1937 cells show a 'cross-presenting' rather than a 'presenting' phenotype (i.e. stimulation of CD8^{+} T cells rather than CD4^{+} T cells). Our results from the differentiation experiments, where the expression of CD4-binding HLA-DR was found to be independent of the irradiation regimen employed for the HCC1937 cell supernatants, further support this conclusion. In contrast, the co-stimulatory receptor CD80 was strongly upregulated upon exposure to supernatants of ablatively irradiated HCC1937 cells. Therefore, the surface receptor expression status of 'new' dendritic cells which have been differentiated in the presence of factors released from ablatively irradiated HCC1937 cells and their functional performance suggest a more CD8^{+} T cell stimulatory phenotype.

Previously, it has been shown that both local and systemic anti-tumor immunity induced by radiotherapy strongly rely on cytotoxic CD8^{+} T cells [13], while CD4^{+} T cells seem to be dispensable [22]. Cytotoxic CD8^{+} T cells directly kill infected or malignant cells, which present foreign or abnormal antigens on MHC class I molecules. CD4^{+} T cells consist of different subpopulations such as T helper cells or immunosuppressive regulatory T cell subsets, and are unable to kill cells directly. The CD4^{+} T cell subpopulations differ in their cytokine repertoire, resulting in either immune-suppressive or immune-promoting functions. CD4^{+} regulatory T cells inhibit cytotoxic CD8^{+} T cells and are often found in the immunosuppressive microenvironment in different cancer types (e.g. breast cancer, non-small cell lung cancer, and pancreatic adenocarcinoma [181] [182] [183]). It could be shown that the anti-tumor immune response is enhanced when CD4^{+} T cells were eliminated [23]. Therefore, enhancing CD8^{+} T cell proliferation and, concurrently, preventing CD4^{+} T cell proliferation may be favorable for a profound anti-tumor response. However, upon virus infections, it is well-known that CD4^{+} T cells are indispensable to maintain cytotoxic CD8^{+} T cell function [184]. Furthermore, effector memory CD4^{+} T cells were found in the blood of metastatic melanoma or renal cell carcinoma patients who showed abscopal, systemic immune

effects after stereotactic body radiotherapy plus IL-2 treatment [185]. Thus, for direct anti-tumor effects CD4$^+$ T cells might be dispensable but for long-lasting CD8$^+$ T cell-dependent tumor control, CD4$^+$ T cells appear to be required [14]. In the present study, tumor cell killing properties such as FasL upregulation, granzyme B and IFNγ production of activated CD8$^+$ T cells were not investigated. This issue should be addressed in further studies to confirm the anti-tumor effectiveness of CD8$^+$ T cells. Additionally, the relevance of different CD4$^+$ T cell subsets needs to be clarified in greater detail.

8.5 DAMPs as potential mediators of tumor immunogenicity stimulated by ablative irradiation

DAMP release is a key feature of immunogenic cell death [186]. As mentioned before, irradiation induced the liberation of nucleotides from necrotic breast cancer cells. Moreover, proteins derived from irradiated HCC1937 cells stimulated endothelial cell activation and dendritic cell differentiation in the described, recurring pattern: Strongest effects with supernatants of ablatively irradiated HCC1937 cells and lower, but similar effects for fractionatedly and single 2 Gy irradiated HCC1937 cells. In the present study, the proteinaceous DAMPs HSP70, HMGB1, and S100A8/A9, which are known to passively leak out during necrosis [50], were detected at high concentrations in the supernatants of irradiated HCC1937 cells. Notably, all of them were found to be released in a time-dependent manner reflecting the observed pattern of HUVEC activation and dendritic cell differentiation. S100A8/A9 release reflected this pattern best: The highest concentrations were observed in supernatants of ablatively irradiated HCC1937 cells, slightly less for 4x2 Gy and 1x2 Gy, and the lowest concentration was found in the not irradiated controls. Notably, the S100A8/A9 heterodimer, besides other S100 proteins, was found to be overexpressed in breast cancer [187]. Recent data support the ability of S100A8/A9 to activate endothelial cells as well as monocytes [188] [69]. S100A8/A9 was reported to induce an inflammatory phenotype in human microvascular endothelial cells, leading to the upregulation of pro-inflammatory chemokines such as IL-8 and CXCL1, and adhesion molecules such as ICAM-1 and VCAM-1 [188]. It was found that S100A8/A9 activates monocytes by binding to TLR4, thereby enhancing the expression of pro-inflammatory TNF [69]. Interestingly, HMGB1 is also known to exert its immune-supporting effects by binding to TLR4, and the same is true for HSP70 [62] [156].

Furthermore, slow rolling and adhesion of neutrophils seem to be controlled by S100A8/A9, resulting in increased neutrophil recruitment [189]. Therefore, S100A8/A9 may act as a strong immune-promoting DAMP. Nevertheless, immune-suppressive functions of S100A8/A9 are also found in the literature. MDSCs may be attracted by S100A8/A9 in a paracrine and autocrine fashion [190]. Furthermore, breast cancer metastasis into the lung was shown to be promoted by S100A8/A9 [191].

However, in the present study, the suggested contribution of S100A8/A9 to the observed effects on endothelial cell activation (see chapter 7.7) and dendritic cell differentiation (see chapter 7.8) seems to be of immune-supporting character. Presumably, HMGB1 and HSP70 may also be of importance for inducing the described effects, since both are well-established pro-inflammatory DAMPs [57] [60], which can be found at high levels in tumor cell supernatants after irradiation. Depleting these DAMPs or inhibiting their functions might help to dissect their individual contribution to the observed immune-stimulatory effects in the future. In summary, ablative irradiation is a strong inductor of DAMP release, strengthening the role of irradiation-induced necrosis as a form of immunogenic cell death.

9 Conclusions

The aim of the present study was to elucidate the differences between fractionated and ablative irradiation with regard to their immune-stimulatory effects in models of breast cancer. It could be shown that ablative irradiation induces an immunogenic, necrotic form of cell death especially in fast-proliferating, triple-negative breast cancer cells, thereby instigating different immune-stimulatory mechanisms: DAMPs released from necrotic breast cancer cells activated endothelial cells in vitro which resulted in the recruitment of myeloid cells in vivo. Dendritic cells did not only phagocytose dying tumor cells but also revealed enforced maturation upon exposure to necrotic cancer cell-derived material followed by improved stimulation of CD8$^+$ T cells. Thus, several key features of systemic anti-tumor immunity apparently can be induced by ionizing irradiation, and the magnitude of these effects was consistently greater in case of the ablative irradiation regimen with 1 x 20 Gy as compared to classical fractionation with daily 2 Gy. The validation of these immune-stimulatory mechanisms in an orthotopic, syngeneic mouse breast cancer model will be essential in order to gain deeper insights into their translational relevance. This is of crucial importance for a central question that arises from the present work: How can these systemic immune-stimulatory observations be transferred into therapeutic concepts? Some ideas should be taken into consideration: IORT with ablative irradiation doses is commonly applied to elderly patients with reduced mobility and/or impaired health status, to spare them the long treatment time of fractionated radiotherapy. In this patient subset, the most prevalent breast cancer phenotype is the hormone-receptor positive, slow-proliferating one with good prognosis. However, the present study demonstrates that particularly the aggressive, fast-proliferating triple-negative breast cancer subtype, which is mainly observed in younger women, is capable of inducing anti-tumor immune mechanisms upon ablative irradiation. Accordingly, IORT might represent a promising additional treatment option for younger patients with triple-negative breast cancer. Furthermore, most breast cancer patients receive radiotherapy in adjuvant settings, i.e. after tumor resection, and therefore the amount of tumor cell-derived, immune-stimulatory signals that can be generated during radiotherapy might be insufficient to induce systemic immunity. In consequence, neoadjuvant irradiation settings, i.e. irradiation before tumor resection, appear worth to be discussed in order to support the induction of anti-tumor immunity with relevant

amounts of tumor antigen. Finally, the role of the tumor-draining lymph nodes in breast cancer therapy needs to be reevaluated. Undoubtedly, they are crucially involved in metastasis formation, and their surgical removal can contribute to long-term tumor control. Nevertheless, (cross-) priming of T cells by dendritic cells – a key process in the induction of adaptive immunity – occurs in the draining lymph nodes. Hence, it is worth contemplating to adapt the treatment sequence, and – if possible – to allow T cell (cross-) priming prior to lymph node dissection.

In summary, the present study confirms that diverse immune mechanisms can be stimulated by radiotherapy, and future research might help to translate these findings into optimized clinical concepts for breast cancer treatment.

10 References

http://www.krebsdaten.de/Krebs/DE/Content/Krebsarten/Brustkrebs/brustkrebs_node .html as of 2016-07-08, 11:00 am

1.   Mole, R.H. Whole body irradiation; radiobiology or medicine? *Br J Radiol* **26**, 234-241 (1953).

2.   Nobler, M.P. The abscopal effect in malignant lymphoma and its relationship to lymphocyte circulation. *Radiology* **93**, 410-412 (1969).

3.   Postow, M.A. *et al.* Immunologic correlates of the abscopal effect in a patient with melanoma. *N Engl J Med* **366**, 925-931 (2012).

4.   Hiniker, S.M. *et al.* A systemic complete response of metastatic melanoma to local radiation and immunotherapy. *Transl Oncol* **5**, 404-407 (2012).

5.   Golden, E.B., Demaria, S., Schiff, P.B., Chachoua, A. & Formenti, S.C. An abscopal response to radiation and ipilimumab in a patient with metastatic non-small cell lung cancer. *Cancer Immunol Res* **1**, 365-372 (2013).

6.   Demaria, S. *et al.* Ionizing radiation inhibition of distant untreated tumors (abscopal effect) is immune mediated. *Int J Radiat Oncol Biol Phys* **58**, 862-870 (2004).

7.   Dunn, G.P., Koebel, C.M. & Schreiber, R.D. Interferons, immunity and cancer immunoediting. *Nat Rev Immunol* **6**, 836-848 (2006).

8.   Formenti, S.C. & Demaria, S. Radiation therapy to convert the tumor into an in situ vaccine. *Int J Radiat Oncol Biol Phys* **84**, 879-880 (2012).

9.   Lauber, K., Ernst, A., Orth, M., Herrmann, M. & Belka, C. Dying cell clearance and its impact on the outcome of tumor radiotherapy. *Front Oncol* **2**, 116 (2012).

10.   Lugade, A.A. *et al.* Local radiation therapy of B16 melanoma tumors increases the generation of tumor antigen-specific effector cells that traffic to the tumor. *J Immunol* **174**, 7516-7523 (2005).

11.   Lugade, A.A. *et al.* Radiation-induced IFN-gamma production within the tumor microenvironment influences antitumor immunity. *J Immunol* **180**, 3132-3139 (2008).

12.   Gerber, S.A. *et al.* IFN-gamma mediates the antitumor effects of radiation therapy in a murine colon tumor. *Am J Pathol* **182**, 2345-2354 (2013).

13.   Lee, Y. *et al.* Therapeutic effects of ablative radiation on local tumor require CD8+ T cells: changing strategies for cancer treatment. *Blood* **114**, 589-595 (2009).

14. Takeshima, T. *et al.* Local radiation therapy inhibits tumor growth through the generation of tumor-specific CTL: its potentiation by combination with Th1 cell therapy. *Cancer Res* **70**, 2697-2706 (2010).

15. Burnette, B.C. *et al.* The efficacy of radiotherapy relies upon induction of type i interferon-dependent innate and adaptive immunity. *Cancer Res* **71**, 2488-2496 (2011).

16. Diamond, M.S. *et al.* Type I interferon is selectively required by dendritic cells for immune rejection of tumors. *J Exp Med* **208**, 1989-2003 (2011).

17. Fuertes, M.B. *et al.* Host type I IFN signals are required for antitumor CD8+ T cell responses through CD8alpha+ dendritic cells. *J Exp Med* **208**, 2005-2016 (2011).

18. Lim, J.Y., Gerber, S.A., Murphy, S.P. & Lord, E.M. Type I interferons induced by radiation therapy mediate recruitment and effector function of CD8(+) T cells. *Cancer Immunol Immunother* **63**, 259-271 (2014).

19. Deng, L. *et al.* STING-Dependent Cytosolic DNA Sensing Promotes Radiation-Induced Type I Interferon-Dependent Antitumor Immunity in Immunogenic Tumors. *Immunity* **41**, 843-852 (2014).

20. Woo, S.R. *et al.* STING-dependent cytosolic DNA sensing mediates innate immune recognition of immunogenic tumors. *Immunity* **41**, 830-842 (2014).

21. Ablasser, A. *et al.* Cell intrinsic immunity spreads to bystander cells via the intercellular transfer of cGAMP. *Nature* **503**, 530-534 (2013).

22. Gupta, A. *et al.* Radiotherapy promotes tumor-specific effector CD8+ T cells via dendritic cell activation. *J Immunol* **189**, 558-566 (2012).

23. Yu, P. *et al.* Intratumor depletion of CD4+ cells unmasks tumor immunogenicity leading to the rejection of late-stage tumors. *J Exp Med* **201**, 779-791 (2005).

24. Bos, P.D., Plitas, G., Rudra, D., Lee, S.Y. & Rudensky, A.Y. Transient regulatory T cell ablation deters oncogene-driven breast cancer and enhances radiotherapy. *J Exp Med* **210**, 2435-2466 (2013).

25. Filatenkov, A. *et al.* Ablative Tumor Radiation Can Change the Tumor Immune Cell Microenvironment to Induce Durable Complete Remissions. *Clin Cancer Res* **21**, 3727-3739 (2015).

26. Reits, E.A. *et al.* Radiation modulates the peptide repertoire, enhances MHC class I expression, and induces successful antitumor immunotherapy. *J Exp Med* **203**, 1259-1271 (2006).

27.   Chakraborty, M. *et al.* External beam radiation of tumors alters phenotype of tumor cells to render them susceptible to vaccine-mediated T-cell killing. *Cancer Res* **64**, 4328-4337 (2004).

28.   Koshy, M., Malik, R., Weichselbaum, R.R. & Sher, D.J. Increasing radiation therapy dose is associated with improved survival in patients undergoing stereotactic body radiation therapy for stage I non-small-cell lung cancer. *Int J Radiat Oncol Biol Phys* **91**, 344-350 (2015).

29.   Darby, S. *et al.* Effect of radiotherapy after breast-conserving surgery on 10-year recurrence and 15-year breast cancer death: meta-analysis of individual patient data for 10,801 women in 17 randomised trials. *Lancet* **378**, 1707-1716 (2011).

30.   Budach, W. Radiotherapy in patients with metastatic breast cancer. *European Journal of Cancer* **47**, S23-S27 (2011).

31.   Schaue, D., Ratikan, J.A., Iwamoto, K.S. & McBride, W.H. Maximizing tumor immunity with fractionated radiation. *Int J Radiat Oncol Biol Phys* **83**, 1306-1310 (2012).

32.   Mahmoud, S.M. *et al.* Tumor-infiltrating CD8+ lymphocytes predict clinical outcome in breast cancer. *J Clin Oncol* **29**, 1949-1955 (2011).

33.   Allred, D.C. Issues and updates: evaluating estrogen receptor-alpha, progesterone receptor, and HER2 in breast cancer. *Mod Pathol* **23 Suppl 2**, S52-59 (2010).

34.   Elias, A.D. Triple-negative breast cancer: a short review. *Am J Clin Oncol* **33**, 637-645 (2010).

35.   Liedtke, C. *et al.* Response to neoadjuvant therapy and long-term survival in patients with triple-negative breast cancer. *J Clin Oncol* **26**, 1275-1281 (2008).

36.   Kao, J. *et al.* Molecular profiling of breast cancer cell lines defines relevant tumor models and provides a resource for cancer gene discovery. *PLoS One* **4**, e6146 (2009).

37.   Chiorean, R., Braicu, C. & Berindan-Neagoe, I. Another review on triple negative breast cancer. Are we on the right way towards the exit from the labyrinth? *Breast* **22**, 1026-1033 (2013).

38.   Toss, A. & Cristofanilli, M. Molecular characterization and targeted therapeutic approaches in breast cancer. *Breast Cancer Res* **17**, 60 (2015).

39.   Antoniou, A. *et al.* Average risks of breast and ovarian cancer associated with BRCA1 or BRCA2 mutations detected in case Series unselected for family history: a combined analysis of 22 studies. *Am J Hum Genet* **72**, 1117-1130 (2003).

40. Chen, S. & Parmigiani, G. Meta-analysis of BRCA1 and BRCA2 penetrance. *J Clin Oncol* **25**, 1329-1333 (2007).

41. Kean, S. Breast cancer. The 'other' breast cancer genes. *Science* **343**, 1457-1459 (2014).

42. Liu, W., Ip, M.M., Podgorsak, M.B. & Das, G.M. Disruption of estrogen receptor alpha-p53 interaction in breast tumors: a novel mechanism underlying the anti-tumor effect of radiation therapy. *Breast Cancer Res Treat* **115**, 43-50 (2009).

43. Konduri, S.D. *et al.* Mechanisms of estrogen receptor antagonism toward p53 and its implications in breast cancer therapeutic response and stem cell regulation. *Proc Natl Acad Sci U S A* **107**, 15081-15086 (2010).

44. Pajonk, F., Vlashi, E. & McBride, W.H. Radiation resistance of cancer stem cells: the 4 R's of radiobiology revisited. *Stem Cells* **28**, 639-648 (2010).

45. Holloway, C.L., Panet-Raymond, V. & Olivotto, I. Hypofractionation should be the new 'standard' for radiation therapy after breast conserving surgery. *Breast* **19**, 163-167 (2010).

46. Vaidya, J.S. *et al.* Targeted intraoperative radiotherapy versus whole breast radiotherapy for breast cancer (TARGIT-A trial): an international, prospective, randomised, non-inferiority phase 3 trial. *The Lancet* **376**, 91-102 (2010).

47. Vaidya, J.S. *et al.* Risk-adapted targeted intraoperative radiotherapy versus whole-breast radiotherapy for breast cancer: 5-year results for local control and overall survival from the TARGIT-A randomised trial. *The Lancet* **383**, 603-613 (2014).

48. Lauber, K. *et al.* Targeting the heat shock response in combination with radiotherapy: Sensitizing cancer cells to irradiation-induced cell death and heating up their immunogenicity. *Cancer letters* (2015).

49. Kroemer, G., Galluzzi, L., Kepp, O. & Zitvogel, L. Immunogenic Cell Death in Cancer Therapy. *Annual review of immunology* (2012).

50. Krysko, D.V. *et al.* Immunogenic cell death and DAMPs in cancer therapy. *Nat Rev Cancer* **12**, 860-875 (2012).

51. Ghiringhelli, F. *et al.* Activation of the NLRP3 inflammasome in dendritic cells induces IL-1beta-dependent adaptive immunity against tumors. *Nat Med* **15**, 1170-1178 (2009).

52. McDonald, B. *et al.* Intravascular danger signals guide neutrophils to sites of sterile inflammation. *Science* **330**, 362-366 (2010).

53. Iyer, S.S. *et al.* Necrotic cells trigger a sterile inflammatory response through the Nlrp3 inflammasome. *Proc Natl Acad Sci U S A* **106**, 20388-20393 (2009).

54. Elliott, M.R. *et al.* Nucleotides released by apoptotic cells act as a find-me signal to promote phagocytic clearance. *Nature* **461**, 282-286 (2009).

55. Kronlage, M. *et al.* Autocrine purinergic receptor signaling is essential for macrophage chemotaxis. *Sci Signal* **3**, ra55 (2010).

56. Chekeni, F.B. *et al.* Pannexin 1 channels mediate 'find-me' signal release and membrane permeability during apoptosis. *Nature* **467**, 863-867 (2010).

57. Schildkopf, P. *et al.* Radiation combined with hyperthermia induces HSP70-dependent maturation of dendritic cells and release of pro-inflammatory cytokines by dendritic cells and macrophages. *Radiother Oncol* **101**, 109-115 (2011).

58. Gastpar, R. *et al.* The cell surface-localized heat shock protein 70 epitope TKD induces migration and cytolytic activity selectively in human NK cells. *J Immunol* **172**, 972-980 (2004).

59. Gastpar, R. *et al.* Heat shock protein 70 surface-positive tumor exosomes stimulate migratory and cytolytic activity of natural killer cells. *Cancer Res* **65**, 5238-5247 (2005).

60. Bianchi, M.E. HMGB1 loves company. *J Leukoc Biol* **86**, 573-576 (2009).

61. Lotze, M.T. & Tracey, K.J. High-mobility group box 1 protein (HMGB1): nuclear weapon in the immune arsenal. *Nat Rev Immunol* **5**, 331-342 (2005).

62. Apetoh, L. *et al.* Toll-like receptor 4-dependent contribution of the immune system to anticancer chemotherapy and radiotherapy. *Nat Med* **13**, 1050-1059 (2007).

63. Tang, D., Billiar, T.R. & Lotze, M.T. A Janus tale of two active high mobility group box 1 (HMGB1) redox states. *Mol Med* **18**, 1360-1362 (2012).

64. Hori, O. *et al.* The receptor for advanced glycation end products (RAGE) is a cellular binding site for amphoterin. Mediation of neurite outgrowth and co-expression of rage and amphoterin in the developing nervous system. *J Biol Chem* **270**, 25752-25761 (1995).

65. Park, J.S. *et al.* High mobility group box 1 protein interacts with multiple Toll-like receptors. *Am J Physiol Cell Physiol* **290**, C917-924 (2006).

66. Bresnick, A.R., Weber, D.J. & Zimmer, D.B. S100 proteins in cancer. *Nature reviews. Cancer* **15**, 96-109 (2015).

67. Donato, R. *et al.* Functions of S100 proteins. *Curr Mol Med* **13**, 24-57 (2013).

68. Donato, R. RAGE: a single receptor for several ligands and different cellular responses: the case of certain S100 proteins. *Curr Mol Med* **7**, 711-724 (2007).

69. Vogl, T. *et al.* Mrp8 and Mrp14 are endogenous activators of Toll-like receptor 4, promoting lethal, endotoxin-induced shock. *Nat Med* **13**, 1042-1049 (2007).

70. Newton, R.A. & Hogg, N. The human S100 protein MRP-14 is a novel activator of the beta 2 integrin Mac-1 on neutrophils. *J Immunol* **160**, 1427-1435 (1998).

71. Eue, I., Pietz, B., Storck, J., Klempt, M. & Sorg, C. Transendothelial migration of 27E10+ human monocytes. *Int Immunol* **12**, 1593-1604 (2000).

72. Vandenabeele, P., Galluzzi, L., Vanden Berghe, T. & Kroemer, G. Molecular mechanisms of necroptosis: an ordered cellular explosion. *Nat Rev Mol Cell Biol* **11**, 700-714 (2010).

73. Rudner, J. *et al.* Radiation sensitivity and apoptosis in human lymphoma cells. *Int J Radiat Biol* **77**, 1-11 (2001).

74. Taylor, R.C., Cullen, S.P. & Martin, S.J. Apoptosis: controlled demolition at the cellular level. *Nat Rev Mol Cell Biol* **9**, 231-241 (2008).

75. Fadok, V.A. *et al.* Macrophages that have ingested apoptotic cells in vitro inhibit proinflammatory cytokine production through autocrine/paracrine mechanisms involving TGF-beta, PGE2, and PAF. *J Clin Invest* **101**, 890-898 (1998).

76. Silva, M.T. Secondary necrosis: the natural outcome of the complete apoptotic program. *FEBS Lett* **584**, 4491-4499 (2010).

77. Kuilman, T., Michaloglou, C., Mooi, W.J. & Peeper, D.S. The essence of senescence. *Genes Dev* **24**, 2463-2479 (2010).

78. Coppe, J.P., Desprez, P.Y., Krtolica, A. & Campisi, J. The senescence-associated secretory phenotype: the dark side of tumor suppression. *Annu Rev Pathol* **5**, 99-118 (2010).

79. Angelini, P.D. *et al.* Constitutive HER2 signaling promotes breast cancer metastasis through cellular senescence. *Cancer research* **73**, 450-458 (2013).

80. Pribluda, A. *et al.* A senescence-inflammatory switch from cancer-inhibitory to cancer-promoting mechanism. *Cancer cell* **24**, 242-256 (2013).

81. Ley, K., Laudanna, C., Cybulsky, M.I. & Nourshargh, S. Getting to the site of inflammation: the leukocyte adhesion cascade updated. *Nat Rev Immunol* **7**, 678-689 (2007).

82. McEver, R.P. & Zhu, C. Rolling cell adhesion. *Annu Rev Cell Dev Biol* **26**, 363-396 (2010).

83. Hidalgo, A., Peired, A.J., Wild, M.K., Vestweber, D. & Frenette, P.S. Complete identification of E-selectin ligands on neutrophils reveals distinct functions of PSGL-1, ESL-1, and CD44. *Immunity* **26**, 477-489 (2007).

84. Zuchtriegel, G. *et al.* Spatiotemporal expression dynamics of selectins govern the sequential extravasation of neutrophils and monocytes in the acute inflammatory response. *Arterioscler Thromb Vasc Biol* **35**, 899-910 (2015).

85. Alon, R. & Feigelson, S.W. Chemokine-triggered leukocyte arrest: force-regulated bi-directional integrin activation in quantal adhesive contacts. *Curr Opin Cell Biol* **24**, 670-676 (2012).

86. Herter, J. & Zarbock, A. Integrin Regulation during Leukocyte Recruitment. *J Immunol* **190**, 4451-4457 (2013).

87. Nourshargh, S., Hordijk, P.L. & Sixt, M. Breaching multiple barriers: leukocyte motility through venular walls and the interstitium. *Nat Rev Mol Cell Biol* **11**, 366-378 (2010).

88. Voisin, M.B. & Nourshargh, S. Neutrophil transmigration: emergence of an adhesive cascade within venular walls. *J Innate Immun* **5**, 336-347 (2013).

89. Arnaout, M.A., Mahalingam, B. & Xiong, J.P. Integrin structure, allostery, and bidirectional signaling. *Annu Rev Cell Dev Biol* **21**, 381-410 (2005).

90. Luo, B.H., Carman, C.V. & Springer, T.A. Structural basis of integrin regulation and signaling. *Annu Rev Immunol* **25**, 619-647 (2007).

91. Schenkel, A.R., Mamdouh, Z. & Muller, W.A. Locomotion of monocytes on endothelium is a critical step during extravasation. *Nat Immunol* **5**, 393-400 (2004).

92. Phillipson, M. *et al.* Intraluminal crawling of neutrophils to emigration sites: a molecularly distinct process from adhesion in the recruitment cascade. *J Exp Med* **203**, 2569-2575 (2006).

93. Sumagin, R., Prizant, H., Lomakina, E., Waugh, R.E. & Sarelius, I.H. LFA-1 and Mac-1 define characteristically different intralumenal crawling and emigration patterns for monocytes and neutrophils in situ. *J Immunol* **185**, 7057-7066 (2010).

94. Vestweber, D. How leukocytes cross the vascular endothelium. *Nat Rev Immunol* **15**, 692-704 (2015).

95. Wakelin, M.W. *et al.* An anti-platelet-endothelial cell adhesion molecule-1 antibody inhibits leukocyte extravasation from mesenteric microvessels in vivo

by blocking the passage through the basement membrane. *J Exp Med* **184**, 229-239 (1996).

96. Liao, F., Ali, J., Greene, T. & Muller, W.A. Soluble domain 1 of platelet-endothelial cell adhesion molecule (PECAM) is sufficient to block transendothelial migration in vitro and in vivo. *J Exp Med* **185**, 1349-1357 (1997).

97. Stark, K. *et al.* Capillary and arteriolar pericytes attract innate leukocytes exiting through venules and 'instruct' them with pattern-recognition and motility programs. *Nat Immunol* **14**, 41-51 (2013).

98. Rot, A. & von Andrian, U.H. Chemokines in innate and adaptive host defense: basic chemokinese grammar for immune cells. *Annu Rev Immunol* **22**, 891-928 (2004).

99. Viola, A. & Luster, A.D. Chemokines and their receptors: drug targets in immunity and inflammation. *Annu Rev Pharmacol Toxicol* **48**, 171-197 (2008).

100. Reichel, C.A. *et al.* Chemokine receptors Ccr1, Ccr2, and Ccr5 mediate neutrophil migration to postischemic tissue. *J Leukoc Biol* **79**, 114-122 (2006).

101. Reichel, C.A. *et al.* C-C motif chemokine CCL3 and canonical neutrophil attractants promote neutrophil extravasation through common and distinct mechanisms. *Blood* **120**, 880-890 (2012).

102. Foxman, E.F., Campbell, J.J. & Butcher, E.C. Multistep navigation and the combinatorial control of leukocyte chemotaxis. *J Cell Biol* **139**, 1349-1360 (1997).

103. Heit, B., Tavener, S., Raharjo, E. & Kubes, P. An intracellular signaling hierarchy determines direction of migration in opposing chemotactic gradients. *J Cell Biol* **159**, 91-102 (2002).

104. Seth, S. *et al.* CCR7 essentially contributes to the homing of plasmacytoid dendritic cells to lymph nodes under steady-state as well as inflammatory conditions. *J Immunol* **186**, 3364-3372 (2011).

105. Grakoui, A. *et al.* The immunological synapse: a molecular machine controlling T cell activation. *Science* **285**, 221-227 (1999).

106. Kikutani, H. & Kumanogoh, A. Semaphorins in interactions between T cells and antigen-presenting cells. *Nat Rev Immunol* **3**, 159-167 (2003).

107. Anton van der Merwe, P., Davis, S.J., Shaw, A.S. & Dustin, M.L. Cytoskeletal polarization and redistribution of cell-surface molecules during T cell antigen recognition. *Semin Immunol* **12**, 5-21 (2000).

108. Gunzer, M. *et al.* Antigen presentation in extracellular matrix: interactions of T cells with dendritic cells are dynamic, short lived, and sequential. *Immunity* **13**, 323-332 (2000).

109. Pardoll, D.M. The blockade of immune checkpoints in cancer immunotherapy. *Nat Rev Cancer* **12**, 252-264 (2012).

110. Ma, D.Y. & Clark, E.A. The role of CD40 and CD154/CD40L in dendritic cells. *Semin Immunol* **21**, 265-272 (2009).

111. Egen, J.G., Kuhns, M.S. & Allison, J.P. CTLA-4: new insights into its biological function and use in tumor immunotherapy. *Nat Immunol* **3**, 611-618 (2002).

112. Okazaki, T., Iwai, Y. & Honjo, T. New regulatory co-receptors: inducible co-stimulator and PD-1. *Curr Opin Immunol* **14**, 779-782 (2002).

113. Hodi, F.S. *et al.* Improved survival with ipilimumab in patients with metastatic melanoma. *N Engl J Med* **363**, 711-723 (2010).

114. Dong, H. *et al.* Tumor-associated B7-H1 promotes T-cell apoptosis: a potential mechanism of immune evasion. *Nat Med* **8**, 793-800 (2002).

115. Blank, C. *et al.* PD-L1/B7H-1 inhibits the effector phase of tumor rejection by T cell receptor (TCR) transgenic CD8+ T cells. *Cancer Res* **64**, 1140-1145 (2004).

116. Taube, J.M. *et al.* Colocalization of inflammatory response with B7-h1 expression in human melanocytic lesions supports an adaptive resistance mechanism of immune escape. *Sci Transl Med* **4**, 127ra137 (2012).

117. Ivashko, I.N. & Kolesar, J.M. Pembrolizumab and nivolumab: PD-1 inhibitors for advanced melanoma. *Am J Health Syst Pharm* **73**, 193-201 (2016).

118. Herbst, R.S. *et al.* Pembrolizumab versus docetaxel for previously treated, PD-L1-positive, advanced non-small-cell lung cancer (KEYNOTE-010): a randomised controlled trial. *Lancet* **387**, 1540-1550 (2016).

119. Debacq-Chainiaux, F., Erusalimsky, J.D., Campisi, J. & Toussaint, O. Protocols to detect senescence-associated beta-galactosidase (SA-betagal) activity, a biomarker of senescent cells in culture and in vivo. *Nat Protoc* **4**, 1798-1806 (2009).

120. Bradford, M.M. A rapid and sensitive method for the quantitation of microgram quantities of protein utilizing the principle of protein-dye binding. *Anal Biochem* **72**, 248-254 (1976).

121. Frosch, M. *et al.* Myeloid-related proteins 8 and 14 are specifically secreted during interaction of phagocytes and activated endothelium and are useful markers for monitoring disease activity in pauciarticular-onset juvenile rheumatoid arthritis. *Arthritis Rheum* **43**, 628-637 (2000).

122. Pessler, F. *et al.* Identification of novel monosodium urate crystal regulated mRNAs by transcript profiling of dissected murine air pouch membranes. *Arthritis Res Ther* **10**, R64 (2008).

123. Ernst, A. *et al.* HSP90 inhibition as a means of radiosensitizing resistant, aggressive soft tissue sarcomas. *Cancer Lett* **365**, 211-222 (2015).

124. Hennel, R. *et al.* Release of monocyte migration signals by breast cancer cell lines after ablative and fractionated gamma-irradiation. *Radiation oncology* **9**, 85 (2014).

125. Peter, C., Wesselborg, S., Herrmann, M. & Lauber, K. Dangerous attraction: phagocyte recruitment and danger signals of apoptotic and necrotic cells. *Apoptosis* **15**, 1007-1028 (2010).

126. Berger, C.E., Qian, Y., Liu, G., Chen, H. & Chen, X. p53, a target of estrogen receptor (ER) alpha, modulates DNA damage-induced growth suppression in ER-positive breast cancer cells. *J Biol Chem* **287**, 30117-30127 (2012).

127. Angeloni, S.V. *et al.* Regulation of estrogen receptor-alpha expression by the tumor suppressor gene p53 in MCF-7 cells. *J Endocrinol* **180**, 497-504 (2004).

128. Menendez, D., Inga, A. & Resnick, M.A. Estrogen receptor acting in cis enhances WT and mutant p53 transactivation at canonical and noncanonical p53 target sequences. *Proc Natl Acad Sci U S A* **107**, 1500-1505 (2010).

129. Hallahan, D.E. *et al.* c-jun and Egr-1 Participate in DNA Synthesis and Cell Survival in Response to Ionizing Radiation Exposure. *Journal of Biological Chemistry* **270**, 30303-30309 (1995).

130. Isfort, K. *et al.* Real-time imaging reveals that P2Y2 and P2Y12 receptor agonists are not chemoattractants and macrophage chemotaxis to complement C5a is phosphatidylinositol 3-kinase (PI3K)- and p38 mitogen-activated protein kinase (MAPK)-independent. *J Biol Chem* **286**, 44776-44787 (2011).

131. Tanaka, T., Narazaki, M. & Kishimoto, T. IL-6 in inflammation, immunity, and disease. *Cold Spring Harb Perspect Biol* **6**, a016295 (2014).

132. Ma, Y. *et al.* Anticancer chemotherapy-induced intratumoral recruitment and differentiation of antigen-presenting cells. *Immunity* **38**, 729-741 (2013).

133. Ma, Y. *et al.* CCL2/CCR2-dependent recruitment of functional antigen-presenting cells into tumors upon chemotherapy. *Cancer Res* **74**, 436-445 (2014).

134. Voll, R.E. *et al.* Immunosuppressive effects of apoptotic cells. *Nature* **390**, 350-351 (1997).

135. Huang, Q. *et al.* Caspase 3-mediated stimulation of tumor cell repopulation during cancer radiotherapy. *Nat Med* **17**, 860-866 (2011).

136. Ford, C.A. *et al.* Oncogenic properties of apoptotic tumor cells in aggressive B cell lymphoma. *Curr Biol* **25**, 577-588 (2015).

137. Chaurio, R. *et al.* UVB-irradiated apoptotic cells induce accelerated growth of co-implanted viable tumor cells in immune competent mice. *Autoimmunity* **46**, 317-322 (2013).

138. Willems, J.J., Arnold, B.P. & Gregory, C.D. Sinister self-sacrifice: the contribution of apoptosis to malignancy. *Front Immunol* **5**, 299 (2014).

139. Bondanza, A. *et al.* Inhibition of phosphatidylserine recognition heightens the immunogenicity of irradiated lymphoma cells in vivo. *J Exp Med* **200**, 1157-1165 (2004).

140. Frey, B. *et al.* AnnexinA5 renders dead tumor cells immunogenic--implications for multimodal cancer therapies. *J Immunotoxicol* **6**, 209-216 (2009).

141. Werthmoller, N. *et al.* Combination of ionising radiation with hyperthermia increases the immunogenic potential of B16-F10 melanoma cells in vitro and in vivo. *International journal of hyperthermia : the official journal of European Society for Hyperthermic Oncology, North American Hyperthermia Group* **32**, 23-30 (2016).

142. Ma, Y. *et al.* ATP-dependent recruitment, survival and differentiation of dendritic cell precursors in the tumor bed after anticancer chemotherapy. *Oncoimmunology* **2**, e24568 (2013).

143. Dzhandzhugazyan, K.N., Kirkin, A.F., thor Straten, P. & Zeuthen, J. Ecto-ATP diphosphohydrolase/CD39 is overexpressed in differentiated human melanomas. *FEBS Lett* **430**, 227-230 (1998).

144. Kunzli, B.M. *et al.* Upregulation of CD39/NTPDases and P2 receptors in human pancreatic disease. *Am J Physiol Gastrointest Liver Physiol* **292**, G223-230 (2007).

145. Clayton, A., Al-Taei, S., Webber, J., Mason, M.D. & Tabi, Z. Cancer exosomes express CD39 and CD73, which suppress T cells through adenosine production. *J Immunol* **187**, 676-683 (2011).

146. Ghiringhelli, F., Bruchard, M., Chalmin, F. & Rebe, C. Production of adenosine by ectonucleotidases: a key factor in tumor immunoescape. *J Biomed Biotechnol* **2012**, 473712 (2012).

147. Bastid, J. *et al.* Inhibition of CD39 enzymatic function at the surface of tumor cells alleviates their immunosuppressive activity. *Cancer Immunol Res* **3**, 254-265 (2015).

148. Antonioli, L., Pacher, P., Vizi, E.S. & Hasko, G. CD39 and CD73 in immunity and inflammation. *Trends Mol Med* **19**, 355-367 (2013).

149. Ryzhov, S.V. *et al.* Role of TGF-beta signaling in generation of CD39+CD73+ myeloid cells in tumors. *J Immunol* **193**, 3155-3164 (2014).

150. Takenaka, M.C., Robson, S. & Quintana, F.J. Regulation of the T Cell Response by CD39. *Trends Immunol* (2016).

151. Pasparakis, M. & Vandenabeele, P. Necroptosis and its role in inflammation. *Nature* **517**, 311-320 (2015).

152. Maes, H., Rubio, N., Garg, A.D. & Agostinis, P. Autophagy: shaping the tumor microenvironment and therapeutic response. *Trends Mol Med* **19**, 428-446 (2013).

153. Ko, A. *et al.* Autophagy inhibition radiosensitizes in vitro, yet reduces radioresponses in vivo due to deficient immunogenic signalling. *Cell Death Differ* **21**, 92-99 (2014).

154. Iannello, A., Thompson, T.W., Ardolino, M., Lowe, S.W. & Raulet, D.H. p53-dependent chemokine production by senescent tumor cells supports NKG2D-dependent tumor elimination by natural killer cells. *J Exp Med* **210**, 2057-2069 (2013).

155. Fiuza, C. *et al.* Inflammation-promoting activity of HMGB1 on human microvascular endothelial cells. *Blood* **101**, 2652-2660 (2003).

156. Chen, T., Guo, J., Han, C., Yang, M. & Cao, X. Heat shock protein 70, released from heat-stressed tumor cells, initiates antitumor immunity by inducing tumor cell chemokine production and activating dendritic cells via TLR4 pathway. *J Immunol* **182**, 1449-1459 (2009).

157. Okada, M. *et al.* IL-6/BSF-2 functions as a killer helper factor in the in vitro induction of cytotoxic T cells. *J Immunol* **141**, 1543-1549 (1988).

158. Bettelli, E. *et al.* Reciprocal developmental pathways for the generation of pathogenic effector TH17 and regulatory T cells. *Nature* **441**, 235-238 (2006).

159. Fioretti, F. *et al.* Reduced tumorigenicity and augmented leukocyte infiltration after monocyte chemotactic protein-3 (MCP-3) gene transfer: perivascular accumulation of dendritic cells in peritumoral tissue and neutrophil recruitment within the tumor. *J Immunol* **161**, 342-346 (1998).

160. Pittman, K. & Kubes, P. Damage-associated molecular patterns control neutrophil recruitment. *J Innate Immun* **5**, 315-323 (2013).

161. Soehnlein, O., Lindbom, L. & Weber, C. Mechanisms underlying neutrophil-mediated monocyte recruitment. *Blood* **114**, 4613-4623 (2009).

162. Shi, C. & Pamer, E.G. Monocyte recruitment during infection and inflammation. *Nat Rev Immunol* **11**, 762-774 (2011).

163. Gabrilovich, D.I., Ostrand-Rosenberg, S. & Bronte, V. Coordinated regulation of myeloid cells by tumours. *Nat Rev Immunol* **12**, 253-268 (2012).

164. Merad, M., Sathe, P., Helft, J., Miller, J. & Mortha, A. The dendritic cell lineage: ontogeny and function of dendritic cells and their subsets in the steady state and the inflamed setting. *Annu Rev Immunol* **31**, 563-604 (2013).

165. Norian, L.A. *et al.* Tumor-infiltrating regulatory dendritic cells inhibit CD8+ T cell function via L-arginine metabolism. *Cancer Res* **69**, 3086-3094 (2009).

166. Gabrilovich, D. Mechanisms and functional significance of tumour-induced dendritic-cell defects. *Nat Rev Immunol* **4**, 941-952 (2004).

167. Seliger, B. & Massa, C. The dark side of dendritic cells: development and exploitation of tolerogenic activity that favor tumor outgrowth and immune escape. *Front Immunol* **4**, 419 (2013).

168. Broz, M.L. *et al.* Dissecting the tumor myeloid compartment reveals rare activating antigen-presenting cells critical for T cell immunity. *Cancer Cell* **26**, 638-652 (2014).

169. Ruffell, B. *et al.* Macrophage IL-10 blocks CD8+ T cell-dependent responses to chemotherapy by suppressing IL-12 expression in intratumoral dendritic cells. *Cancer Cell* **26**, 623-637 (2014).

170. Hancock, W.W. *et al.* Costimulatory function and expression of CD40 ligand, CD80, and CD86 in vascularized murine cardiac allograft rejection. *Proc Natl Acad Sci U S A* **93**, 13967-13972 (1996).

171. Krahling, S., Callahan, M.K., Williamson, P. & Schlegel, R.A. Exposure of phosphatidylserine is a general feature in the phagocytosis of apoptotic lymphocytes by macrophages. *Cell Death Differ* **6**, 183-189 (1999).

172. Fadok, V.A. *et al.* Exposure of phosphatidylserine on the surface of apoptotic lymphocytes triggers specific recognition and removal by macrophages. *J Immunol* **148**, 2207-2216 (1992).

173. Fadok, V.A., de Cathelineau, A., Daleke, D.L., Henson, P.M. & Bratton, D.L. Loss of phospholipid asymmetry and surface exposure of phosphatidylserine is required for phagocytosis of apoptotic cells by macrophages and fibroblasts. *J Biol Chem* **276**, 1071-1077 (2001).

174. Park, D. *et al.* BAI1 is an engulfment receptor for apoptotic cells upstream of the ELMO/Dock180/Rac module. *Nature* **450**, 430-434 (2007).

175. Kobayashi, N. *et al.* TIM-1 and TIM-4 glycoproteins bind phosphatidylserine and mediate uptake of apoptotic cells. *Immunity* **27**, 927-940 (2007).

176. Hanayama, R., Miyasaka, K., Nakaya, M. & Nagata, S. MFG-E8-dependent clearance of apoptotic cells, and autoimmunity caused by its failure. *Curr Dir Autoimmun* **9**, 162-172 (2006).

177. Brouckaert, G. *et al.* Phagocytosis of necrotic cells by macrophages is phosphatidylserine dependent and does not induce inflammatory cytokine production. *Mol Biol Cell* **15**, 1089-1100 (2004).

178. Kagan, V.E. *et al.* A role for oxidative stress in apoptosis: oxidation and externalization of phosphatidylserine is required for macrophage clearance of cells undergoing Fas-mediated apoptosis. *J Immunol* **169**, 487-499 (2002).

179. McGaha, T.L., Chen, Y., Ravishankar, B., van Rooijen, N. & Karlsson, M.C. Marginal zone macrophages suppress innate and adaptive immunity to apoptotic cells in the spleen. *Blood* **117**, 5403-5412 (2011).

180. Xue, W. *et al.* Senescence and tumour clearance is triggered by p53 restoration in murine liver carcinomas. *Nature* **445**, 656-660 (2007).

181. Bates, G.J. *et al.* Quantification of regulatory T cells enables the identification of high-risk breast cancer patients and those at risk of late relapse. *J Clin Oncol* **24**, 5373-5380 (2006).

182. Petersen, R.P. *et al.* Tumor infiltrating Foxp3+ regulatory T-cells are associated with recurrence in pathologic stage I NSCLC patients. *Cancer* **107**, 2866-2872 (2006).

183. Hiraoka, N., Onozato, K., Kosuge, T. & Hirohashi, S. Prevalence of FOXP3+ regulatory T cells increases during the progression of pancreatic ductal adenocarcinoma and its premalignant lesions. *Clin Cancer Res* **12**, 5423-5434 (2006).

184. Bevan, M.J. Helping the CD8(+) T-cell response. *Nat Rev Immunol* **4**, 595-602 (2004).

185. Seung, S.K. *et al.* Phase 1 study of stereotactic body radiotherapy and interleukin-2--tumor and immunological responses. *Sci Transl Med* **4**, 137ra174 (2012).

186. Kroemer, G., Galluzzi, L., Kepp, O. & Zitvogel, L. Immunogenic cell death in cancer therapy. *Annu Rev Immunol* **31**, 51-72 (2013).

187. Arai, K. *et al.* S100A8 and S100A9 overexpression is associated with poor pathological parameters in invasive ductal carcinoma of the breast. *Curr Cancer Drug Targets* **8**, 243-252 (2008).

188. Viemann, D. *et al.* Myeloid-related proteins 8 and 14 induce a specific inflammatory response in human microvascular endothelial cells. *Blood* **105**, 2955-2962 (2005).

189.   Pruenster, M. *et al.* Extracellular MRP8/14 is a regulator of beta2 integrin-dependent neutrophil slow rolling and adhesion. *Nat Commun* **6**, 6915 (2015).

190.   Sinha, P. *et al.* Proinflammatory S100 Proteins Regulate the Accumulation of Myeloid-Derived Suppressor Cells. *The Journal of Immunology* **181**, 4666-4675 (2008).

191.   Yin, C. *et al.* RAGE-binding S100A8/A9 promotes the migration and invasion of human breast cancer cells through actin polymerization and epithelial-mesenchymal transition. *Breast Cancer Res Treat* **142**, 297-309 (2013).

11 List of figures and tables

12 List of publications

Kinzel L, Ernst A, Orth M, Albrecht V, **Hennel R**, Brix N, Frey B, Gaipl US, Zuchtriegel G, Reichel CA, Blutke A, Schilling D, Multhoff G, Li M, Niyazi M, Friedl AA, Winssinger N, Belka C, Lauber K (2016): A novel HSP90 inhibitor with reduced hepatotoxicity synergizes with radiotherapy to induce apoptosis, abrogate clonogenic survival, and improve tumor control in models of colorectal cancer. Oncotarget. 2016 Jun 1 [Epub ahead of print]

Harnicek D, Kampmann E, Lauber K, **Hennel R**, Cardoso Martins AS, Guo Y, Belka C, Mörtl S, Gallmeier E, Kanaar R, Mansmann U, Hucl T, Lindner LH, Hiddemann W, Issels RD (2016): Hyperthermia adds to trabectedin effectiveness and thermal enhancement is associated with BRCA2 degradation and impairment of DNA homologous recombination repair. Int J Cancer. 2016 Mar 2

Ernst A, Anders H, Kapfhammer H, Orth M, **Hennel R**, Seidl K, Winssinger N, Belka C, Unkel S, Lauber K (2015): HSP90 inhibition as a means of radiosensitizing resistant, aggressive soft tissue sarcomas. Cancer Lett. 2015 Sep 1;365(2):211-22

Lauber K, Brix N, Ernst A, **Hennel R**, Krombach J, Anders H, Belka C (2015): Targeting the heat shock response in combination with radiotherapy: Sensitizing cancer cells to irradiation-induced cell death and heating up their immunogenicity. Cancer Lett. 2015 Nov 28;368(2):209-29

Hennel R, Brix N, Seidl K, Ernst A, Scheithauer H, Belka C, Lauber K (2014): Release of monocyte migration signals by breast cancer cell lines after ablative and fractionated gamma-irradiation. Radiat Oncol 2014, 9:85

Rosenwald M, Koppe U, Keppeler H, Sauer G, **Hennel R**, Ernst A, Blume KE, Peter C, Herrmann M, Belka C, Schulze-Osthoff K, Wesselborg S, Lauber K (2012): Serum-derived plasminogen is activated by apoptotic cells and promotes their phagocytic clearance. J Immunol. 2012 Dec 15;189(12):5722-8

Becirovic E, Nakova K, Hammelmann V, **Hennel R**, Biel M, Michalakis S (2010): The retinitis pigmentosa mutation c.3444+1G>A in CNGB1 results in skipping of exon 32. PLoS One. 2010 Jan 29;5(1):e8969

13 Wissenschaftliche Beiträge

Unterstützt wurde diese Arbeit mit folgenden wissenschaftlichen Beiträgen:

- Messung der S100A8/A9-Proteine (Herr Prof. Dr. Thomas Vogl, Institute of Immunology of the University of Muenster, Muenster, Germany)
- Konfokal-Mikroskopie (Frau Dr. Gabriele Zuchtriegel, Walter Brendel Centre of Experimental Medicine, Klinikum der Universität München, Munich, Germany)

An der Durchführung von folgenden Experimenten war im Rahmen einer medizinischen Doktorarbeit (betreut von Roman Hennel) Frau Julia Krombach, Klinik und Poliklinik für Strahlentherapie und Radioonkologie, Klinikum der Universität München, Munich, Germany, beteiligt:

- Endothelzellaktivierung
- Air pouch
- Monozytendifferenzierung
- Phagozytose und Mixed-Leukocyte-Reaction

14 Acknowledgements

15 Curriculum Vitae

16 Eidesstattliche Versicherung

Hennel, Roman

Ich erkläre hiermit an Eides statt,

dass ich die vorliegende Dissertation mit dem Thema

Immune-stimulatory effects induced by radiotherapy of breast cancer

selbstständig verfasst, mich außer der angegebenen keiner weiteren Hilfsmittel bedient und alle Erkenntnisse, die aus dem Schrifttum ganz oder annähernd übernommen sind, als solche kenntlich gemacht und nach ihrer Herkunft unter Bezeichnung der Fundstelle einzeln nachgewiesen habe.

Ich erkläre des Weiteren, dass die hier vorgelegte Dissertation nicht in gleicher oder in ähnlicher Form bei einer anderen Stelle zur Erlangung eines akademischen Grades eingereicht wurde.

München, 10.07.2016   Roman Hennel
_____   _____
Ort, Datum   Unterschrift Doktorandin/Doktorand